

**Copyright**

**by**

**Xiaoyan Jiang**

**2010**

**The Dissertation Committee for Xiaoyan Jiang certifies that this is the approved  
version of the following dissertation:**

**Regional-scale Land–Climate Interactions and Their Impacts on Air  
Quality in a Changing Climate**

**Committee:**

---

**Zong-Liang Yang, Supervisor**

---

**Robert E. Dickinson**

---

**Alex Guenther**

---

**Charles Jackson**

---

**John M. Sharp, Jr.**

---

**Clark R. Wilson**

**Regional-scale Land–Climate Interactions and Their Impacts on Air  
Quality in a Changing Climate**

**by**

**Xiaoyan Jiang, B.S.; M.S.; M.S.**

**Dissertation**

Presented to the Faculty of the Graduate School of

The University of Texas at Austin

in Partial Fulfillment

of the Requirements

for the Degree of

**Doctor of Philosophy**

The University of Texas at Austin

December 2010

## **Acknowledgements**

Major funding support for my research was provided by the NASA Headquarters under the NASA Earth and Space Science Fellowship (NESSF) Program (Grant No. NNX07AO28H) and the Jackson School of Geosciences. I was also in part supported by a grant of the NOAA Climate Prediction Program for the Americas (Grant No. NA070AR4310216), a grant of the U.S. EPA STAR program (Grant No. RD83145201), and the National Center for Atmospheric Research (NCAR) Advanced Study Program. Computing resources were provided by the Texas Advanced Computing Center.

I thank Dr. Zong-Liang Yang, my adviser, for providing solid scientific mentorship and guidance, and for encouraging me to pursue my intellectual interests with a great degree of freedom. I also appreciate his willingness to accommodate the circumstances of life that can occasionally place a hurdle on the path to a Ph.D. I am grateful to the other members of my committee, Dr. Robert E. Dickinson, Dr. Alex Guenther, Dr. Charles Jackson, Dr. John M. Jr. Sharp, and Dr. Clark R. Wilson for their scientific wisdom and support. I learned a lot from Dr. Sharp and Dr. Wilson in the classroom and elsewhere. I appreciate Dr. Alex Guenther's willingness to serve as the external member of my committee and want to thank him for consistently providing me with great suggestions on my research. A special thanks goes to Dr. Christine Wiedinmyer at the National Center for Atmospheric Sciences for her supervising on my dissertation work. She always has great research ideas that helped me throughout my Ph.D. study. I also thank Dr. Hong Liao at the Institute of Atmospheric Physics, Chinese Academy of Sciences for always



being there to discuss about research questions and for giving me valuable input on my research.

The students and research staff of the LEAD group provided crucial help throughout this research. The coauthors of the papers presented here made significant contributions to both the substance and style of the published research. I thank them for their insight, time, energy, and resources. I also would like to express my thanks to a number of researchers including Fei Chen, Sarah Davidson, David Gochis, Lindsey Gulden, Keith Hutchison, Kolby Jardine, Kenneth Mitchell, Enrique Rosero, Hua Su as well as the anonymous reviewers of my papers for their insightful, constructive comments.

I also would like to take this opportunity to thank Philip Guerrero for his continuous support during the course of my study at the Jackson School of Geosciences.

Finally, I dedicate this dissertation to my parents, my husband, and my son for their love, support and encouragement.

# **Regional-scale Land–Climate Interactions and Their Impacts on Air Quality in a Changing Climate**

Xiaoyan Jiang, Ph.D.

The University of Texas at Austin, 2010

Supervisor: Zong-Liang Yang

Land surface areas, which represent approximately 30% of the Earth's surface, contribute largely to the complexity of the climate system by exchanging water, energy, momentum, and chemical materials with the overlying atmosphere. Because of the highly heterogeneous nature of the land surface and its rapid transformation due to human activities, future climate projections are less certain on regional scales than for the globe as a whole. The work presented in this dissertation is focused on a better understanding of regional-scale land–atmosphere interactions and their impacts on climate and air quality. Specifically, I concentrate my research on three typical regions in the United States (U.S.): 1) the Central U.S. (representing transition zones between arid and wet climates); 2) the Houston metropolitan region (representing a major urban area); and 3) the eastern U.S. (representing temperate forested regions). These regions are also chosen owing to the consideration of data availability.

The first study concerns the roles of vegetation phenology and groundwater dynamics in regulating evapotranspiration and precipitation over the transition zones in

summer months. It is found that the warm-season precipitation in the Central U.S. is sensitive to latent heat fluxes controlled by vegetation dynamics. Groundwater enhances the persistence of soil moisture memory from rainy periods to dry periods by transferring water to upper soil layers through capillary forces. Enhancement in soil moisture facilitates vegetation persistence in dry periods, producing more evaporation to the atmosphere and resulting in enhanced precipitation, which then increases soil moisture. The second study compares the impacts of future urbanization and climate change on regional air quality. The results show that the effect of land use change on surface ozone ( $O_3$ ) is comparable to that of climate change, but the details differ across the domain. The third study deals with the formation and distributions of secondary organic aerosols (SOA) — a largely overlooked but potentially important component in the climate system. Under future different climate scenarios, I found that biogenic emissions — an important precursor of SOA — are expected to increase everywhere over the U.S., with the largest increase found in the southeastern U.S. and the northwestern U.S., while changes in SOA do not necessarily follow those in biogenic emissions. Other factors such as partitioning coefficients, atmospheric oxidative capability, primary organic carbon, and anthropogenic emissions also play a role in SOA formation. Direct and indirect impacts from climate change complicate the future SOA formation.

## Table of Contents

<b>List of Tables</b> .....	xi
<b>List of Figures</b> .....	xii
<b>Chapter 1: Introduction</b> .....	1
1.1. BACKGROUND .....	1
1.1.1. Land–climate interactions .....	1
1.1.2. Land–climate interactions in a changing climate .....	4
1.1.3. Their impacts on air quality .....	5
1.2. RESEARCH QUESTIONS AND OBJECTIVES .....	8
1.3. RESEARCH FOCUS .....	10
<b>Chapter 2: Impacts of Vegetation and Groundwater Dynamics on Warm Season Precipitation and Land–climate Interactions over the Central United States<sup>1</sup></b> .....	13
2.1. ABSTRACT .....	13
2.2. INTRODUCTION .....	14
2. 3. MODEL DESCRIPTION AND EXPERIMENTAL DESIGN .....	19
2.3.1. Model description .....	19
2.3.2. Experimental design .....	21
2.4. RESULTS .....	24
2.4.1. Impact on precipitation .....	24
2.4.2. Impact on surface fluxes .....	29
2.4.3. Impact on vegetation greenness fraction (VGF) .....	33
2.4.4. Impact on diurnal cycles of precipitation and surface fluxes .....	35
2.4.5. Impact on the coupling between soil moisture and lifting condensation level (LCL) .....	37
2.5. SUMMARY .....	39

2.6. ACKNOWLEDGEMENTS .....	41
<b>Chapter 3: Impacts of Land–climate Interactions on Regional Air Quality in a Changing Climate.....</b>	<b>56</b>
3.1. ABSTRACT .....	56
3.2. IMPORTANCE .....	56
3.3. IMPACT ON SURFACE OZONE (O <sub>3</sub> ).....	58
3.4. IMPACT ON SECONDARY ORGANIC AEROSOLS (SOA) .....	60
<b>Chapter 4: Predicted Impacts of Climate and Land Use Change on Surface Ozone in the Houston Area<sup>2</sup> .....</b>	<b>63</b>
4.1. ABSTRACT .....	63
4.2. INTRODUCTION .....	64
4.3. METHODOLOGY.....	67
4.3.1. Regional land–atmosphere–chemistry model .....	67
4.3.2. Global and regional climate modeling.....	69
4.3.3. Land use and land cover data .....	70
4.3.4. Anthropogenic and biogenic emissions .....	72
4.3.5. Experiment design .....	74
4.4. RESULTS AND DISCUSSION.....	75
4.4.1. Evaluation of simulation results for current year conditions .....	75
4.4.2. Regional climate change .....	78
4.4.3. Impact on regional distribution of photooxidants .....	80
4.4.4. Changes in surface O <sub>3</sub> .....	81
4.4.5. Contributions of climate change and land use change to O <sub>3</sub> changes .....	83
4.4.6. Sensitivity of surface O <sub>3</sub> to future anthropogenic emissions .....	87

4.5. CONCLUSIONS.....	88
4.6. ACKNOWLEDGMENTS .....	89
<b>Chapter 5: Sensitivity of Biogenic Secondary Organic Aerosols to Future Climate Change at Regional Scales<sup>3</sup></b> .....	108
5.1. ABSTRACT .....	108
5.2. INTRODUCTION .....	109
5.3. MODEL DESCRIPTION.....	113
5.3.1. WRF/Chem model.....	113
5.3.2. Secondary organic aerosol model.....	115
5.4. EXPERIMENT DESIGN .....	118
5.5. PRESENT-DAY SIMULATION OF BIOGENIC SOA .....	121
5.5.1 Regional distributions of biogenic emissions and SOA .....	122
5.5.2. Comparison with observations .....	123
5.6. PROJECTED FUTURE CHANGES .....	127
5.6.1. Projected changes in regional climate .....	127
5.6.2. Projected changes in biogenic emissions and SOA.....	130
5.7. CONCLUSIONS.....	133
5.8. ACKNOWLEDGEMENTS .....	135
<b>Chapter 6: Conclusions and Future Work</b> .....	153
6.1. SUMMARY AND IMPLICATIONS .....	153
6.2. CONTRIBUTIONS, LIMITATIONS, AND FUTURE DIRECTIONS.....	158
<b>References</b> .....	163
<b>Vita</b> .....	184

## **List of Tables**

Table 2.1. Design of experiments .....	43
Table 2.2. Water budget over the Central United States in June, July, and August (JJA) 2002 .....	44
Table 4.1. Surface parameterizations for each land use category <sup>a</sup> .....	91
Table 4.2. List of all simulations <sup>a</sup> .....	92
Table 4.3. Correlation studies between O <sub>3</sub> concentrations and the main meteorological variables .....	93
Table 5.1. Hydrocarbon classes of reactive biogenic emissions <sup>a</sup> .....	136
Table 5.2. Parameters used in the SOA model <sup>b</sup> .....	137
Table 5.3. Description of oxidation products <sup>a</sup> .....	138
Table 5.4. Regional climate changes in seven sub-regions as shown in Figure 5.8 .....	139

## List of Figures

Figure 1.1. Schematic diagram showing the importance of land–climate interactions in the climate system and the work presented in this dissertation. ....	12
Figure 2.1. Schematic diagram of a coupled land–atmosphere modeling system. A dynamic vegetation model (DV) is incorporated into the Noah LSM and a simple groundwater model (SIMGM) is added beneath the Noah LSM. ....	45
Figure 2.2. Map showing the modeling domain in which the shaded area represents the Central United States. ....	46
Figure 2.3. Observed and simulated precipitation in June, July and August (JJA) 2002 over the contiguous United States. (a) Observed JJA precipitation from the Climate Prediction Center (CPC) unified precipitation data set, which is a gridded data set at $0.25^{\circ} \times 0.25^{\circ}$ resolution covering the United States and Mexico. (b) Simulated JJA precipitation in DEFAULT, which uses prescribed monthly mean vegetation greenness fraction (VGF). (c) Simulated JJA precipitation in DV, which includes a dynamic vegetation model, allowing the vegetation growth in response to climate conditions. (d) Simulated JJA precipitation in DVGW, which is augmented with SIMGM and DV to represent vegetation growth and water table dynamics. ....	47
Figure 2.4. Observed versus simulated cumulative precipitation over the Central United States (DEFAULT, DV and DVGW are as in Figure 2.3). ....	48
Figure 2.5. Observed and simulated JJA and monthly mean precipitation ( $\text{mm d}^{-1}$ ) over the Central United States. ....	49
Figure 2.6. Comparisons of simulated latent heat flux (a) and sensible heat flux (b) over the Central United States among three experiments. ....	50
Figure 2.7. Map of differences in monthly average latent heat flux ( $\text{W m}^{-2}$ ) and precipitation ( $\text{mm d}^{-1}$ ) between DV and DEFAULT experiments. Differences were computed from ensemble simulations of DV and DEFAULT. The domain covers the contiguous United States ( $21^{\circ}\text{N}$ – $50^{\circ}\text{N}$ , $125^{\circ}\text{W}$ – $68^{\circ}\text{W}$ ). ....	51
Figure 2.8. As in Figure 2.7, but for differences between DVGW and DV. ....	52
Figure 2.9. MODIS NDVI-derived and model simulated VGF over the Central United States in August. The MODIS NDVI data I used is a 16-day interval data set downloaded from <a href="http://glcf.umd.edu/data/modis/">http://glcf.umd.edu/data/modis/</a> . The VGF is calculated by following the method defined in the work of Gutman and Ignatov (1998). ....	53



Figure 2.10. Observed and simulated diurnal cycles of (a) sensible heat flux, (b) latent heat flux, (c) surface temperature, and (d) precipitation over the Central United States. All variables were computed using the 3-month (JJA) data.....	54
Figure 2.11. Daily averaged lifting condensation level (LCL) versus soil moisture index (SMI) for (a) soil layer 1 and (b) soil layers 1–4. Estimates of the height of the LCL in pressure coordinates were computed from the lowest model level data using the formula defined by the work of Betts (1997).....	55
Figure 4.1. The three urban land use categories, industrial or commercial (red), high-intensity residential (light green), and low-intensity residential (blue), for (a) current years (2000s) defined from the NLCD database and a total area of urban land use of 3264 km <sup>2</sup> and (b) future years (2050s) defined on the basis of projected population growth in 2030 and a total urban land use area of 5293 km <sup>2</sup> . Box A denotes the core urban area, and box B is for the suburban area. ....	94
Figure 4.2. (a) Daily average anthropogenic NO emissions in summer (mol km <sup>-2</sup> hr <sup>-1</sup> ) and (b) normalized biogenic emissions of isoprene generated by the BEIS3 (mol km <sup>-2</sup> hr <sup>-1</sup> ). The normalized isoprene emissions are estimated at standard conditions of light and temperature (30 °C and 1000 μmol photosynthetically active radiation (PAR)). ....	95
Figure 4.3. Map showing several surface observation stations used for model evaluation. ....	96
Figure 4.4. Observed and simulated (a) 2-m temperature and (b) O <sub>3</sub> concentrations during August 2001–2003. Gray lines represent the observations averaged over the sites shown in Figure 4.3 with one line representing one day, and black lines represent the simulated results for 31 days in August. ....	97
Figure 4.5. Observed (marked by circles) and simulated (shaded colors) wind speeds in Houston and surrounding areas. ....	98
Figure 4.6. Simulated differences in afternoon (1200 to 1800 LST) (a) temperature (°C), (b) 2-m water vapor mixing ratio (kg kg <sup>-1</sup> ), (c) planetary boundary layer height (PBLH) (m), and (d) 10-m wind speed (m s <sup>-1</sup> ) between CL-LU and BASE simulations for the month of August (ocean is masked out in all plots). CL-LU represents the future year simulations with the consideration of land use change, and BASE represents the present year simulations. ....	99
Figure 4.7. Simulated wind directions during the afternoon (1200 to 1800 LST) for (a) August 2001–2003 (BASE) and (b) August 2051–2053 (CL-LU).....	100

Figure 4.8. As in Figure 4.6 but for the differences in mixing ratios of (a) NO <sub>x</sub> , (b) HNO <sub>3</sub> , (c) PAN and (d) HCHO. (ppb).....	101
Figure 4.9. As in Figure 4.6 but for the differences in (a) O <sub>3</sub> concentrations (ppb) and (b) the number of days with the daily maximum 8-hr O <sub>3</sub> concentrations larger than 84 ppb. ....	102
Figure 4.10. Simulated differences in (a) afternoon (1200 to 1800 LST) O <sub>3</sub> concentrations and (b) the number of days with the daily maximum 8-h O <sub>3</sub> concentrations larger than 84 ppb between CL-LU and CL simulations for the month of August. CL represents the future year simulations using the present year land use data. ....	103
Figure 4.11. Changes in average daily maximum 8-h O <sub>3</sub> concentrations for (a) climate change effect (difference between CL and BASE simulations), (b) land use change effect (difference between CL-LU and CL simulations), and (c) combined climate change and land use change effect (difference between CL-LU and BASE simulations). ....	104
Figure 4.12. Frequency distributions of the simulated daily maximum 8-h O <sub>3</sub> concentrations averaged over zone A (dashed lines) and zone B (solid lines) during August for BASE (blue), CL (green), and CL-LU (red) simulations. ....	105
Figure 4.13. Spatially averaged contributions of climate-induced change, land use-induced change, and combined climate and land use change from the 2000s to the 2050s to changes in daily maximum 8-h O <sub>3</sub> concentrations.....	106
Figure 4.14. The percentage of the number of days with the daily maximum 8-h O <sub>3</sub> concentrations larger than 84 ppb over zone A and zone B. CL-LU-EMIS represents future year simulations with the consideration of future anthropogenic emissions change. ....	107
Figure 5.1. BVOC emissions under standard climatic condition of light and temperature (30 °C and 1000 μmol photosynthetically active radiation (PAR)). This is based on the work of Williams et al. (1992), Geron et al. (1994), and Guenther et al. (1995). ....	140
Figure 5.2. Model calculated BVOCs (a), Isoprene (b), Monoterpenes (c) and ORVOCs (d) in July 2002. (mole km <sup>-2</sup> h <sup>-1</sup> ).....	141
Figure 5.3. Model simulated concentrations of total SOA (a), SOA from monoterpenes (b) and SOA from isoprene (c) in July 2002. (μg m <sup>-3</sup> ).....	142

Figure 5.4. Aerosols optical depth (AOD): (a) MODIS derived monthly level 2 product, (b) Model simulated without SOA, and (c) Model simulated with SOA included. ....	143
Figure 5.5. AERONET measured and model simulated AOD at three sites (a) HJAndrews, (b) BSRN_BAO_Boulder and (c) Stennis. (d) is a map showing the three locations. ....	144
Figure 5.6. (a) Model simulated and measured (at IMPROVED sites) monthly mean surface layer OC (Primary OC (POC) + SOA) concentrations ( $\mu\text{g m}^{-3}$ ), (b) POC, and (c) ratio of SOA in OC in July 2002. ....	145
Figure 5.7. Differences in temperature, wind speed, PBLH, cloud fraction (CLDFRA), precipitation and net shortwave radiation in July between 2050s (2051–2053) and 2000s (2001–2003) under the A1B and A2 scenarios. ....	147
Figure 5.8. Seven sub-regions in the United States (U.S.). ....	148
Figure 5.9. As in Figure 5.7, but for isoprene, monoterpenes, ORVOCs, and total biogenic emissions. ( $\text{mol km}^{-2} \text{h}^{-1}$ ). ....	149
Figure 5.10. As in Figure 5.7, but for SOA concentrations ( $\mu\text{g m}^{-3}$ ). (a) and (d) are the contribution from isoprene, (b) and (e) are the contribution from monoterpenes, and (c) and (f) are the total concentrations. ....	150
Figure 5.11. As in Figure 5.7, but for POC. ( $\mu\text{g m}^{-3}$ ). ....	151
Figure 5.12. Percentage changes of biogenic emissions and SOA concentrations in three regions (Southwest, Texas and Southeast) under the A1B (a and b) and A2 (c and d) scenarios. ....	152

## **Chapter 1: Introduction**

This chapter explains the research background, offers an overview of the research focus, and defines the research objectives. Major research questions are also presented in this chapter.

### **1.1. BACKGROUND**

#### **1.1.1. Land–climate interactions**

Land surface areas, which represent approximately 30% of the Earth's surface, exchange water, energy, momentum, and chemical compounds with the overlying atmosphere, affect weather and climate on local, regional and global scales from seconds to millions of years, and contribute to a large extent to the complexity of the climate system. The interactions between land and climate are manifold and strongly interconnected (Figure 1.1). Despite the key role of land surface in the climate system, there are still significant uncertainties in the land–climate interactions research. The major reason is due to the lack of direct measurements at a relatively large scale, such as soil moisture, evapotranspiration, emissions from vegetation on land. This impedes our understanding of the underlying physics. Hence, coupled climate models are needed to understand their interactions on regional and global scales.

Efforts are being made to develop physical realism of land surface processes in coupled climate models. Over the past two decades or so, much progress has been made in developing advanced land surface models (LSMs) for use in climate models (e.g., Koster et al., 2000; Chen and Dudhia, 2001; Bonan et al., 2002; Ek et al., 2003; Wei et al., 2010). Advanced subsurface hydrology (e.g., Seuffert et al., 2002; York et al., 2002;

Maxwell et al., 2007; Maxwell and Kollet, 2008) and detailed vegetation and soil processes (e.g., Foley et al, 1996, 1998; Dickinson et al., 1998; Baudena et al., 2008; Grote et al, 2009) have been included in weather and climate models. More recently, biogeochemical processes are being represented in LSMs for climate modeling (e.g., Levis et al., 2003; Heald et al., 2008; Thorton et al., 2009). One example is the incorporation of biogenic volatile organic compounds (BVOCs) in LSMs (e.g., Levis et al., 2003; Gulden and Yang, 2006; Heald et al., 2008). With the utilization of advanced coupled models, land and climate interactions have been exclusively investigated on regional and global scales (e.g., Schar et al., 1999; Pal and Eltahir, 2001; Koster et al., 2002, 2004; Betts, 2004; Holt et al., 2006; Seneviratne et al., 2006; Senna et al., 2009; Steiner et al., 2009; van den Hurk et al., 2010). For example, on a global scale, Koster et al. (2004) assessed the coupling strength — the degree to which all prescribed boundary conditions affect some atmospheric quantity — through an ensemble of multi-model simulations, and they found that strong coupling occurs over the transition areas or the so called hot spots (the locations on the Earth's surface where soil moisture anomalies have a substantial impact on precipitation). At a regional scale, van den Hurk et al. (2010) used a regional climate model to understand the land–atmosphere interactions and found that atmospheric mechanisms impose a strong constraint on the effect of soil moisture on the regional hydrological cycle.

While our understanding of the coupling between land and climate has significantly improved, further investigations of the roles of processes such as vegetation (Bonan, 2008; Peñuelas, et al., 2009) and groundwater dynamics (Maxwell and Kollet, 2008) in

the climate system are still needed. Vegetation influences climate through physical, chemical, and biological processes that affect the Earth's energy, the hydrologic cycle and atmospheric composition. In turn, climate controls vegetation growth through temperature, precipitation, and other climatic variables. Very few studies have assessed vegetation–climate feedbacks using observations (Liu et al., 2006; Notaro et al., 2006; Méndez-Barroso et al., 2009), hence numerical parameterizations of vegetation processes in coupled land–atmosphere models (e.g., Dickinson and Shaikh, 1998; Bonan, 2003; Sitch et al., 2003) are often used to understand the feedbacks. Model simulations have demonstrated biogeophysical regulation of climate by vegetation through albedo, surface turbulent fluxes, and the hydrologic cycles. Recent vegetation–climate studies also considered the carbon cycle and vegetation dynamics (e.g., Foley et al., 2000; Krinner et al., 2005; Thornton and Zimmermann, 2007) for long-term climate simulations. Short-term vegetation phenology has also been shown to play an important role in regional climate (Hoffman and Jackson, 2000; Matsui et al., 2005; Baudena et al., 2008; Méndez-Barroso et al., 2009). However, most studies used either satellite derived vegetation products (Hoffman and Jackson, 2000; Matsui et al., 2005; Méndez-Barroso et al., 2009) or simple methods (e.g., Baudena et al., 2008) to understand the feedbacks between vegetation and climate, very few studies (e.g., Kim and Wang, 2005; Steiner et al., 2009) have used an interactive vegetation model (or a short-term vegetation phenology model) in their studies, thus the feedbacks between vegetation and climate may not be well represented in the models. There is a strong need to represent vegetation phenology in climate models and to understand vegetation–climate feedbacks on regional scales.

Furthermore, the interactions between the subsurface groundwater systems and climate have not been well understood. Most LSMs traditionally ignore groundwater dynamics. Several recent studies (e.g., Yeh and Eltahan, 2005; Niu et al., 2007; Maxwell et al., 2007) show that the water balance computed by LSMs with detailed subsurface processes including runoff and groundwater flow can be much improved. These studies used different approaches to incorporate groundwater systems into LSMs and demonstrated the significant impacts of groundwater dynamics in land surface modeling. A few studies (Anyah et al., 2008; Yuan et al., 2008) also demonstrated the importance of groundwater in land–atmosphere interactions on regional scales. In the context of climate change, a work by Maxwell and Kollet (2008) shows that annual mean response of the surface water and energy balance at a given location to changing climate conditions is strongly dependent on water table depth. More recently, Ferguson and Maxwell (2010) found that influence of groundwater feedbacks on sensitivity of surface fluxes to changing climate conditions depends on changes in both moisture and energy availability over the watershed. These studies suggest that groundwater feedbacks are very sensitive to changes in climate and they are important in understanding land–climate interactions, in particular on regional scales. Work is needed to incorporate groundwater dynamics in regional climate models and to further explore its roles in land–climate coupling in a changing climate.

#### **1.1.2. Land–climate interactions in a changing climate**

Human activities are changing the global climate not only directly through the emissions of trace gases and aerosols, but also indirectly through perturbations in the land

surface conditions (Figure 1.1). The 4<sup>th</sup> Assessment Report of the Intergovernmental Panel on Climate Change (IPCC) presents mean climate projections for this century based on an ensemble of several global climate models (Christensen et al, 2007). Simulations driven by increasing greenhouse gas concentrations predict a considerable increase in temperature. The trends in temperature increase are roughly linear in time. Global precipitation increases slightly due to enhanced evaporation from the warming areas of land and the oceans, but considerable regional variability does exist. Other climatic variables (e.g., humidity, cloud cover, and boundary height) also change with changing temperature and precipitation.

Land–climate interactions involve many processes, which are strongly modified in the context of climate change. For instance, under the future warming climate, climate regimes will be shifted, and the location of transitional climate zones will be modified. As a result, the current hot spots (e.g., the central Great Plains of North America, the Sahel, equatorial Africa, and India) of land–atmosphere coupling may be changed. With a coupled regional climate model, Seneviratne et al. (2006) found that the feedbacks between land and atmosphere determine the increase in summer temperature variability predicted in central and Eastern Europe. Their results highlight the crucial role of land–climate interactions in a future changing climate.

### **1.1.3. Their impacts on air quality**

Land–climate interactions are significant in predicting changes in extreme events, water resources, ecosystems, air quality for decision making in a future changing climate. In this dissertation, I mainly focus on their impacts on air quality. The two atmospheric



chemical species of most concern for public health and climate are surface ozone ( $O_3$ ) and atmospheric aerosol. Surface  $O_3$  is produced in the troposphere by photochemical oxidation of other gases such as carbon monoxide, methane, VOCs, and nitrogen oxides ( $NO_x$ ). Atmospheric aerosols include primary (emitted into the atmosphere directly from the nature and the human activities. These include sulfate, nitrate, and organic carbon) and secondary (formed in the atmosphere. These include sulfates from sulfur dioxide ( $SO_2$ ), nitrates from  $NO_x$ , and secondary organic aerosols (SOA) from VOCs) sources.

From a climate perspective (Figure 1.1), land–climate interactions affect the concentrations and distributions of chemical species through changing meteorological conditions such as temperature, boundary heights, winds, and precipitation (Jacob et al., 2009). There have been a significant number of studies that have explored the effects of climate change on  $O_3$  and aerosols (mainly primary aerosols) (e.g., Hogrefe et al., 2004; Leung and Gustafson, 2005; Forkel and Knoche, 2006; Liao et al., 2006; Tagaris et al., 2007; Nolte et al., 2008; Avise et al., 2009; Pye et al., 2009). From a biogeochemical point of view (Figure 1.1), their roles are becoming more discernable in changing atmospheric compounds. For example, they affect the amount of BVOCs emitted from vegetation on land, and thus influence the formation of secondary chemical species including surface  $O_3$  and SOA in the troposphere. The role of BVOCs in  $O_3$  formation is dependent on the level of  $NO_x$ . When the ratio of VOCs to  $NO_x$  is high, VOCs reaction for  $O_3$  formation is predominate. In this way, vegetation plays a very important role in  $O_3$  formation. Impacts on SOA are less certain (Carslaw et al., 2010). SOA have an important implication for both air quality and climate studies (Kanakidou et al., 2005).

Studies indicate the amount of SOA predicted by models severely underestimates the actual amount present in the atmosphere (de Gouw et al., 2005; Heald et al., 2005; Volkamer et al., 2006). The roles of land surface processes and land–climate interactions in SOA formation have not been well explored.

Additionally, changes in land surface conditions caused by human activities, such as urbanization could influence air quality through land–climate interactions. Urbanization affects regional air quality by changing the near-surface atmospheric conditions (Foley et al., 2005). As the world’s population continues to rise, changes in land use and land cover such as the modification of vegetated area to urban land use could lead to changes in emissions and meteorological variables that can further contribute to changes in air quality. As more natural or vegetated areas are expected to be converted for human use in the future, induced changes in climatic variables such as temperature, wind, boundary layer height can alter local or regional air quality by affecting reaction rates, transport and deposition (Taha, 1996; Taha et al., 1998; Civerolo et al., 2007; Wang et al., 2007; Chen et al., 2009). Consequently, it is important to understand how urbanization or urban land use change could influence regional air quality.

Given the importance of land–climate interactions in air quality, a quantitative assessment of the impacts in a future changing climate with a tool, which consists of the atmosphere, land, and atmospheric chemistry, is needed. Furthermore, the coarse horizontal resolution of current global climate model simulations does not permit estimation of the effects of climate change on regional air quality; regional downscaling

method is also required to assess the impacts on regional scales. Most previous studies concerning the effects of global climate change on O<sub>3</sub> and aerosols used one-way nesting approach where the global models provide physical and chemical boundary conditions to the regional models or chemical transport models. The interactions between the land, atmosphere and chemistry are not considered. Recently, models considering the interactions between the land, atmosphere, and chemistry are being developed, such as the WRF/Chem model (Grell et al., 2005). The research presented in this dissertation uses a coupled regional land–atmosphere–chemistry model to understand the impacts of land–climate interactions on air quality in a changing climate.

## **1.2. RESEARCH QUESTIONS AND OBJECTIVES**

The overarching research question of this dissertation is: What are the roles of land–climate interactions in regional climate and air quality in a changing climate? The whole picture of this dissertation work is illustrated in Figure 1.1, and below are several sub-research questions I address in this dissertation:

- To what extent do the land surface processes, particularly vegetation and groundwater dynamics contribute to land–climate interactions and at what locations are their impacts significant?
- How are the land–climate interactions affecting regional air quality under a future changing climate?
- Is global climate change affecting regional climate and air quality significantly, and if so, how?

- What aspects of climate change are most likely to affect regional air quality, in particular, O<sub>3</sub>, BVOCs and SOA?
- How will changes in urban land use due to human activities affect regional climate and air quality?
- How well does the coupled land–atmosphere–chemistry model simulate the impacts on air quality in comparison with observations?

By addressing the above research questions, the research conducted for this dissertation contributes to a broader understanding of interactions between land, climate, and air quality on regional scales. The overall objective of this research project is to understand the nature and magnitude of the interactions between land and climate, and how they would influence future air quality.

The main goals of this dissertation research are:

- To advance knowledge of the impacts of land surface processes on land–climate interactions;
- To provide a better understanding of the impacts of land, climate, and their interactions on regional O<sub>3</sub>;
- To get an insight about the effects of future climate change on regional air quality, in particular, surface O<sub>3</sub>, BVOCs, and SOA;
- To improve the coupled regional land–atmosphere–chemistry model for further understanding of the interactions among land, atmosphere, and chemistry in the climate system;
- To make contributions to the development of a regional Earth system model;

- To help policy makers to keep polluted areas in compliance with Clean Air Act standards in a warming climate.

### **1.3. RESEARCH FOCUS**

This dissertation investigates land–climate interactions and their impacts on regional air quality in a changing climate. Specifically, I investigate land–climate interactions with a focus on the impacts of vegetation and groundwater dynamics on precipitation and their roles in the land–climate coupling. Their impacts on air quality are concentrated on surface O<sub>3</sub>, BVOCs, and SOA.

In Chapter 2, I focus on the understanding of land–climate interactions, in particular, the feedbacks between vegetation, groundwater, and the atmosphere over the transition zone. The impacts of vegetation and groundwater dynamics are investigated through an application of a short-term vegetation phenology model and a groundwater model in a coupled regional climate model. A set of sensitivity experiments are conducted to understand the effects of vegetation and groundwater on precipitation and other climatic variables. The effects on the land–atmosphere coupling are also analyzed. Chapter 3 details the importance of land–climate interactions on air quality. Case studies concerning the impacts on regional air quality, in particular, surface O<sub>3</sub>, BVOCs, and SOA are presented in Chapter 4 and Chapter 5. Chapter 4 examines the impacts of land–climate interactions on surface O<sub>3</sub> air quality. Sensitivity experiments with the consideration of future land use and climate changes are conducted to examine future changes in regional climate, surface O<sub>3</sub> as well as other related chemical species at a regional scale. A coupled regional land–atmosphere–chemistry model is augmented with a detailed urban

canopy model to study the effect of future land use change on air quality. Global climate model output is dynamically downscaled to regional scales with this coupled regional model to understand future O<sub>3</sub> changes. Chapter 5 focuses on biogenic emissions and SOA. To do so, a simple two-product SOA model is incorporated into the coupled regional model. Model results are evaluated against the ground-based and satellite measurements. Global climate model output under different future climate scenarios are used to assess the potential effects of climate change on these atmospheric species. Conclusions and implications for future work are presented in Chapter 6.

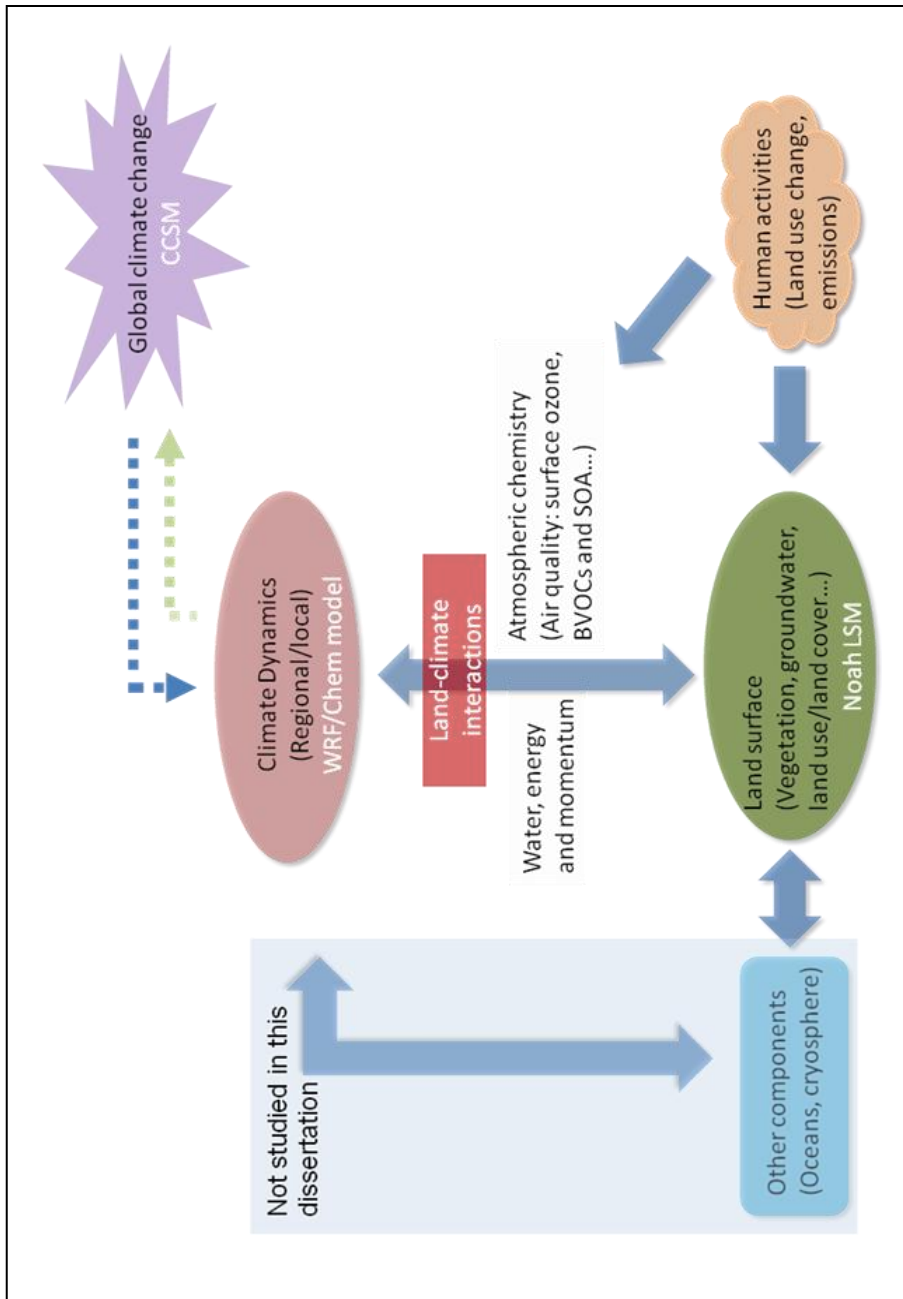


Figure 1.1. Schematic diagram showing the importance of land–climate interactions in the climate system and the work presented in this dissertation.

## **Chapter 2: Impacts of Vegetation and Groundwater Dynamics on Warm Season Precipitation and Land–climate Interactions over the Central United States<sup>1</sup>**

### **2.1. ABSTRACT**

The impacts of vegetation and groundwater dynamics on warm season precipitation were investigated by using the Weather Research and Forecasting (WRF) model coupled with a modified Noah land surface model (LSM). The modified Noah LSM was augmented with an interactive canopy model and a simple groundwater model (SIMGM). A series of experiments show that incorporating vegetation and groundwater dynamics into the WRF model can improve the simulation of summer precipitation in the Central United States. The enhanced model produces more precipitation in response to an increase in the latent heat flux. The advantage of incorporating the two components into the model becomes more discernable after one month. The model results suggest that the land–atmosphere feedback is an important mechanism for summer precipitation over the Central United States. Vegetation growth and groundwater dynamics play a significant role in enhancing the persistence of intraseasonal precipitation in regional climate models. Their combined effects act to favor a stronger land–atmosphere feedback during the summer season. The simulated diurnal cycle of precipitation is improved by the WRF model with the augmented Noah LSM. Moreover, I found that the coupling between the soil moisture and the lifting condensation level (LCL) is enhanced by adding vegetation and groundwater dynamics to the WRF model. The impact of groundwater is significant

---

<sup>1</sup>Significant portions of this chapter were first published as:

Jiang, X., G.-Y. Niu, and Z.-L. Yang (2009), Impacts of vegetation and groundwater dynamics on warm season precipitation over the Central United States, *J. Geophys. Res.*, 114, D06109, doi:10.1029/2008JD010756.

Work cited here is referenced in the **References** section of this dissertation.



when the soil moisture is relatively dry, while the influence is relatively small when soils become highly saturated. This work suggests incorporating vegetation and groundwater dynamics into a regional climate model would be especially beneficial for seasonal precipitation forecast in the transition zones.

## **2.2. INTRODUCTION**

The predictability of precipitation on timescales of days to years is largely limited by the effects of atmospheric noise, which restricts weather forecasts beyond about two weeks (e.g., Lorenz, 1963, 1969). The hope to improve intraseasonal to seasonal precipitation forecasts largely relies on simulating the atmospheric response to slowly varying states of the land surface (Beljaars et al., 1996; Koster et al., 2004) and the ocean (e.g., Wallace et al., 1998), which can be predicted weeks to months in advance. In mid-latitude and in the interior of those large continents such as the North America, oceanic impact on precipitation is small relative to that of land soil moisture as suggested by recent studies using atmospheric general circulation models (GCMs) (e.g., Koster et al., 2000, 2004; Dirmeyer et al., 2006). Understanding complex interactions between the land surface and atmosphere is central to better predicting precipitation over land.

Studies of such coupled-system problems are often conducted by using coupled land–atmosphere models. A number of studies with the use of coupled GCMs have shown that soil moisture is particularly important for maintaining long-term climate and its temporal variability (e.g., Koster et al., 2004; Dirmeyer, 2006; Guo et al., 2006). Koster et al. (2004) concluded that a strong coupling exists in the transition zones

between dry and wet regions such as the Central United States (U.S.). Dirmeyer (2006) quantified the strength of the hydrologic cycle between the land and atmosphere, and found that in the dry regions, specified precipitation anomalies can contribute to the latent heat flux anomalies immediately; while in the wet regions, precipitation is not very sensitive to soil moisture anomalies. In the transition zones, the soil moisture–precipitation coupling can be best preserved, which is consistent with the work of Koster et al. (2004). Guo et al. (2006) revealed that differences in the coupling strengths exist among different models, and that these differences are related to different values of evapotranspiration (ET) simulated over land. These studies suggest that there remain uncertainties in representing soil moisture processes and their coupling with other physical processes in land surface models (LSMs).

Most LSMs used in the abovementioned studies did not include an interactive vegetation canopy and a dynamic water table. Neglecting short-term response of vegetation greenness and leaf amounts to precipitation and temperature may yield an underestimate or overestimate of latent heat flux. Several studies have shown that changes in vegetation phenology can have a strong influence on regional climate through partitioning sensible and latent heat fluxes (Chase et al., 1996, 2000; Hoffmann et al., 2000; Matsui et al., 2005; Liu et al., 2006; Wang et al., 2006a, b; Xue et al., 2006; Dekker et al., 2007; Dong et al., 2007; Natoro et al., 2007). Matsui et al. (2005) applied satellite-derived vegetation greenness fraction (VGF) in a regional climate model to account for the temporal and spatial variations of vegetation distribution. Their results showed that there was a strong link among the evaporative fraction, surface temperature,

and relative humidity in the boundary layer. However, their results did not reveal that a higher VGF could lead to more precipitation. By adding a sophisticated photosynthesis scheme in a coupled mesoscale model, Holt et al. (2006) found that the atmospheric model is able to respond to the detailed representation of soil moisture and temperature, and the model performance is improved. Kim and Wang (2007) examined the positive soil moisture–precipitation feedback over North America on a seasonal timescale. Their results showed that soil moisture–induced precipitation increase is enhanced under wet summer soil moisture anomalies when vegetation phenology is included in their model. To investigate the impact of the vegetation growth on precipitation, a better representation of vegetation growth response to climate conditions in coupled land–atmosphere models is needed.

Like vegetation, which in turn, can feed back to precipitation, groundwater also can respond to precipitation rapidly. However, most LSMs traditionally ignored groundwater dynamics. In recent years, different approaches to incorporating groundwater dynamics into land surface processes have been developed (e.g., Gutowski et al., 2002; Liang et al., 2003; Yeh and Eltahir, 2005; Maxwell and Miller, 2005; Niu et al., 2007; Fan et al., 2007; Maxwell et al., 2007; Kollet and Maxwell, 2008; Anyah et al., 2008). These studies incorporated groundwater processes into LSMs and demonstrated the significant impacts of considering surface and ground water dynamic interactions on surface fluxes and soil moisture in land surface modeling. Some of the approaches used in these studies (e.g., Yeh and Eltahir, 2005; Niu et al., 2007) use the water table as the lower boundary, while others do not (Liang et al., 2003). Moreover, some studies even included detailed lateral

flow. Famiglietti and Wood (1994) parameterized groundwater dynamics in a LSM using a TOPMODEL concept (Beven and Kirkby, 1979) and found the lateral redistribution of surface and subsurface soil water in a small-scale model is critical in controlling both runoff production and energy balance. Seuffert et al. (2002) examined how the incorporation of a land surface hydrologic model in a mesoscale weather prediction model affects surface energy fluxes, structure of the atmospheric boundary layer, and precipitation. They found that a better representation of soil hydrologic processes improves the predicted energy fluxes and rainfall. York et al. (2002) developed a coupled aquifer–land surface–atmosphere model, and found that the physically based model was able to reproduce monthly and yearly trends in precipitation, stream discharge, and ET, for a catchment.

More recently, Maxwell et al. (2007) and Maxwell and Kollet (2008) coupled a groundwater flow model with an atmospheric model to examine the effects of soil moisture heterogeneity on atmospheric boundary layer processes. Their studies showed that the fully coupled model was able to capture a realistic soil moisture distribution. The study of Maxwell and Kollet (2008) also revealed that groundwater is key to understanding processes of recharge and drought under a changing climate, especially in the critical zones where the water table depth is neither very shallow nor very deep. They found a strong correlation between the water table depth and land surface energy. These studies all suggest the need for a better understanding of the role of subsurface processes in the overlying atmosphere. However, most of these studies have been focused on relatively small (e.g., catchment or watershed) scales. The exceptions are Anyah et al.

(2007) and Yuan et al. (2008), who studied the influences of groundwater on land–atmosphere coupling on a continental scale. Despite a large number of research studies, it remains unanswered that how the inclusion of groundwater dynamics affects precipitation in the transition zones, as these regions are very sensitive to soil moisture.

The goal of this research is to examine the impacts of vegetation and groundwater dynamics on warm season precipitation on a continental scale. The study area is focused on the Central U.S., which has been identified by Koster et al. (2004) as a hot spot where soil moisture anomalies have a substantial impact on precipitation. The study is aimed at understanding the influences of vegetation and groundwater dynamics on intraseasonal precipitation in the warm season. The impacts of the two components are investigated through application of a short-term vegetation phenology model and a groundwater model. In this work, I hypothesize that including vegetation growth and groundwater dynamics in a coupled land–atmosphere model can improve intraseasonal to seasonal predictions of precipitation and have a strong effect on the coupling between the land and atmosphere over the Central U.S. I begin in section 2.3 with a brief description of the coupled land–atmosphere model and experiments. The role of initialization in seasonal forecasting is taken into account through ensemble simulations. In section 2.4, I evaluate the model results against available observations and examine the roles of vegetation growth and groundwater dynamics in precipitation and surface fluxes. Furthermore, the impacts of these processes on diurnal cycles of climate variables are investigated. Finally, the effects of the new components on the relationship between soil moisture and lifting condensation level (LCL) are examined.

## **2. 3. MODEL DESCRIPTION AND EXPERIMENTAL DESIGN**

### **2.3.1. Model description**

A non-hydrostatic (considering frictional and Coriolis forces in addition to pressure and gravity forces), fully compressible (density of air is not constant) model, the Weather Research and Forecasting (WRF) model, is used as an investigative tool in this study (Skamarock et al., 2005). The model: 1) includes interactive nested grid capabilities; 2) supports various cumulus schemes, microphysics, shortwave and longwave radiation schemes; and 3) includes two options of LSMs. The WRF model 2.1.2, which contains all of the above features plus time-varying sea surface temperature (SST) and prescribed monthly changing VGF, was used. These time-varying lower boundary conditions are important for monthly to seasonal climate simulations.

To assess the impacts of vegetation phenology on warm season precipitation over the Central U.S., an interactive canopy model (Dickinson et al., 1998; Yang and Niu, 2003) has been coupled to the WRF model (Figure 2.1). The interactive canopy model (or called dynamic vegetation model) has two major parts: a stomatal conductance–photosynthesis part, and a dynamic leaf part. The first part computes carbon assimilation through photosynthesis of both sunlit and shaded leaves following Collatz et al. (1991). The second part describes carbon allocation to different vegetation components (leaf, stem, root etc.), respiration, and vegetation phenology. A more detailed description of this canopy model can be found in Dickinson et al. (1998). This canopy model was added to the Noah LSM (Chen and Dudhia, 2001) by converting the predicted leaf area index (LAI) to VGF using the following exponential function:

$$VGF = 1 - \exp\left(-\frac{2.5}{6.5}LAI\right). \quad (2.1)$$

Following the methods used in Dickinson et al. (1998), water stress was parameterized on conductance as a function of soil water matric potential rather than a function of soil moisture in the Noah LSM.

I also included a simple groundwater model (SIMGM) developed by Niu et al. (2007) in the Noah LSM to investigate the influences of groundwater dynamics on precipitation. As aforementioned, several previous studies have incorporated groundwater models into LSMs, and some of them even included lateral flow (e.g., Seuffert et al., 2002; Maxwell et al., 2007). In this work, I did not explicitly include the effects of lateral flow between grid cells, because our model grid spacing is coarse (~32 km). At such a coarse grid, the vertical water exchange between soil and its underlying unconfined aquifer is considered to be more important than the horizontal water exchange. The soil in the Noah LSM has four layers with a total depth of 2 m. In the present study, SIMGM is added beneath the fourth soil layer of Noah LSM, allowing the interaction between soil moisture and groundwater (Figure 2.1). SIMGM represents the vertical exchange of water between the bottom soil layer and the unconfined aquifer by parameterizing the recharging rate to the aquifer that has been added as a single integration element below the bottom soil layer. Therefore, it takes into account not only gravitational drainage from the soil to the aquifer when soil is relatively wet (the total water head at the bottom soil layer is greater than that at the water table), but also upward diffusion of water from the aquifer driven by capillary forces when the soil is dry (the water head at the water table is greater than that

at the bottom soil layer). The water table depth was solved by converting the water storage in the aquifer through specific yield (Niu et al., 2007). In SIMGM, a simple TOPMODEL-based subsurface runoff scheme, expressed as an exponential function of the water table depth, was used to parameterize groundwater discharge. To be consistent with the subsurface runoff scheme, the surface runoff scheme was also replaced with a simple TOPMODEL-based surface runoff scheme, which used an exponential function of the water table depth to represent the fractional saturated fraction (Niu et al., 2005). The lateral transport of groundwater between grid cells and to rivers is considered implicitly through the TOPMODEL base flow formulation.

### **2.3.2. Experimental design**

To understand the effects of vegetation and groundwater dynamics on precipitation and their impacts on land and atmosphere interactions, a series of ensemble numerical experiments with each lasting three months were performed. In all simulations, the following physical schemes were used: the Lin et al. (1983) Microphysics scheme, the Kain-Fritsch Cumulus Parameterization scheme (Kain and Fritsch, 1990), the Yonsei University Planetary Boundary Layer (PBL) scheme (Hong and Pan, 1996), the Simple Cloud Interactive Radiation scheme (Dudhia, 1989), the Rapid Radiative Transfer Model Longwave Radiation scheme (Mlawer et al., 1997), and the Noah LSM. The modeling domain covers the entire contiguous U.S. on a 32-km horizontal grid (Figure 2.2). The initial and lateral boundary conditions were derived from the NCEP's North American Regional Reanalysis (NARR) data set, which has a domain covering the configured computational area (Mesinger et al., 2006). The NARR data were generated at a 3-hourly



interval with the use of the NCEP Eta model, its data assimilation system, and a recent version of the Noah LSM at 32 km/45 layer resolution. The system used to generate the NARR data also includes hourly assimilation of precipitation, which means the observed precipitation from the past is combined in the system to predict future precipitation with some mathematical method. Since the focus of this study is on summer season, I selected June, July and August (JJA) 2002 as the simulation period. This period was also associated with less-than-normal precipitation in June over the western U.S. and adjacent High Plains, and more-than-normal precipitation in July and August over part of Texas and the northern Great Plains. As June is relatively dry, soil moisture may dry out in the default modeling system, resulting in poor model performance in the ensuing months because of the lack of the detailed subsurface processes (e.g., groundwater system). In this case, I expect that new improvements in the LSM could lead to better simulations of precipitation, in particular in the months of July and August.

To test the impacts of new components, three different experiments were performed (Table 2.1). The first one, called DEFAULT, is a control run without any changes to the Noah LSM. The Noah LSM in this modeling system uses prescribed climatological VGF data derived from the Normalized Difference Vegetation Index (NDVI) collected by the NOAA-Advanced Very High Resolution Radiometer (AVHRR) sensor. Although recent NDVI data acquired from the Moderate Resolution Imaging Spectroradiometer (MODIS) sensor appear to be more accurate than the AVHRR-derived NDVI data, Gallo et al. (2004) found 16-day composite values of the two data sets over the same time periods and a variety of land cover classes within the contiguous U.S. are quite similar over the

23 intervals of 2001 that were analyzed. Since the purpose of incorporating dynamic vegetation into the model is to make the model capable of predicting vegetation growth and its interaction with atmosphere, I used AVHRR derived climatological VGF as experimental data in DEFAULT. Thus, DEFAULT does not allow vegetation to grow in response to climate change. By incorporating the dynamic vegetation model into the default Noah LSM, the second experiment (DV) allows vegetation growth to respond to climate change. DV investigates whether considering the vegetation–precipitation feedback in the coupled model improves the forecast. The third experiment (DVGW) implemented SIMGM to DV to simultaneously represent vegetation growth and water table dynamics. For each experiment, five-member ensemble simulations for three months (JJA) were constructed starting from different initial dates: 00Z May 31, 2002, 06Z May 31, 2002, 12Z May 31, 2002, 18 May 31, 2002, and 00Z June 1 2002. The five members for each experiment only differ in their starting times. While the three modeling systems utilize the same combinations of physical parameterization schemes such as cumulus parameterization scheme, they differ in the use of dynamic vegetation and groundwater models in the Noah LSM. SSTs were updated every six hours during the model integration.

The initial values of land surface variables, especially soil moisture exert a strong control on seasonal forecast in regional climate models (Pielke et al., 1999). In order to minimize the effects of initial conditions, the same sets of land surface variables were used in all three experiments, with the same starting dates having the same initial conditions. All initial values of land surface variables, except for the water table depth

and VGF, are from the NARR data set. It should be pointed out that the modeling system employed to produce NARR data also utilizes the Noah LSM. The initial values of VGF required to initialize DV and DVGW are the same as those used in DEFAULT. I also prepared initial values of water table depth needed by the groundwater component in the coupled model by running the offline Noah LSM coupled with SIMGM. To do so, offline runs driven by the same NARR data were conducted from January of 2000 to December of 2002 and the spin-up enabled the model to reach an equilibrium state (Yang et al., 1995). Then, the values of water table level on June 1 2002 were used to initialize the water table depth and water storage for SIMGM in the coupled model.

These designed experiments allow us to identify the key mechanisms and processes involved in the land–atmosphere feedback. Consequently, the differences between DEFAULT and DV were used to evaluate the impacts of vegetation dynamics on surface heat fluxes and precipitation. Similarly, differences between DV and DVGW were used to reveal the contribution of groundwater variations to vegetation phenology, surface heat fluxes, and precipitation.

## **2.4. RESULTS**

### **2.4.1. Impact on precipitation**

To reiterate, the objective of this work is to assess how seasonal and intraseasonal evolution and patterns of precipitation are influenced by the improvements in the LSM. Although the ensemble spread of simulated variables is small at the beginning, it becomes large afterwards. To reduce the uncertainties associated with initial conditions, the results presented below are based on the five-member ensemble means of different

experiments. The results of the days before June 1 have been discarded to reduce possible spin-up effects. The model-simulated precipitation is evaluated against observed precipitation data set (a gridded data set at  $0.25^\circ \times 0.25^\circ$  resolution covering U.S. and Mexico downloaded from the Climate Prediction Center (CPC) (Higgins et al., 2000)).

Figure 2.3 plots the spatial patterns of observed and simulated seasonal precipitation (JJA) over the modeling domain. In general, all three modeling systems reproduce the spatial distribution of precipitation. The observed precipitation pattern for JJA (Figure 2.3a) is characterized by less precipitation in the western U.S. and more precipitation in the eastern U.S. The Central U.S., where the JJA mean precipitation is about  $1\text{--}4 \text{ mm d}^{-1}$ , exhibits a feature of transition zones from the dry western U.S. to the wet eastern U.S. Overall, DEFAULT captures the main patterns and (for the most part) magnitudes of continental precipitation (Figure 2.3b). It overestimates precipitation in much of the eastern states (e.g., Ohio, Pennsylvania, Kentucky, Tennessee and South Carolina), and underestimates precipitation in the Central U.S. Comparing precipitation simulated by DV against DEFAULT and observations, I found that DV produces somewhat increased precipitation over the Central U.S. and northern parts of North American Monsoon regions such as New Mexico and West Texas, where rainfall increases by nearly  $1 \text{ mm d}^{-1}$  (Figure 2.3c). The majority of the increase in precipitation occurs over the Central U.S. However, it should be noted that the increase in precipitation in parts of the eastern U.S. is not expected, and needs further investigation. Furthermore, as expected the impact of inclusion of groundwater component in DV on JJA average precipitation is extensive, covering most parts of the continent (Figure 2.3d).

Incorporating groundwater dynamics into the model accounts for 1–2 mm d<sup>-1</sup> increase in JJA average precipitation over the Central U.S. The overestimated precipitation in the eastern U.S. is slightly reduced, which I ascribe to the improved TOPMODEL-based runoff scheme. Thus one can conclude that adding the two new components to the model tends to result in a substantial increase in precipitation over the Central U.S., and improved model performance. DEFAULT strongly underestimates precipitation in this area by approximately 1 mm d<sup>-1</sup>, while DV and DVGW yield more reasonable estimates as compared to observations. The overestimated precipitation over the eastern U.S. is reduced by the modeling system with the inclusion of new runoff schemes. Future work with the consideration of the effects of lateral flow may further improve model performance.

A comparison of the modeled and measured cumulative precipitation over the Central U.S. is shown in Figure 2.4. In general, the temporal development of precipitation is fairly reproduced in all three experiments. I also noticed that the three modeling systems have similar performances in June. However, the precipitation amounts simulated by the three modeling systems differ significantly from each other in July and August, and all three modeling systems underestimate precipitation when compared with measurements. The performance of DEFAULT decreased dramatically as the integration time becomes longer. DEFAULT underestimates the JJA precipitation over the Central U.S. by a factor of two. Lo et al. (2008) investigated different dynamical downscaling methods and found that the model with continuous integration tends to have a relatively low skill in simulating long-term climate. In the simulations, DEFAULT shows a

decreasing performance in simulating seasonal precipitation. As I incorporated the vegetation effect into the model, the model performance in simulating JJA precipitation is improved. Furthermore, DVGW with the consideration of groundwater effect exhibits the best performance, and the difference in cumulative precipitation between DVGW and the observations is the smallest, suggesting that SIMGM is capable of maintaining a reasonable amount of soil moisture and ET in dry seasons by extracting water from the underlying aquifers. When the soil is drying because of ET, the soil can draw water through capillary suction from the underlying groundwater system, which has a longer memory of the past precipitation events than the soil. This suggests that the new processes in the coupled model help to maintain reasonable soil moisture. The influences of subsurface processes on precipitation have been examined by other studies (e.g., Seuffert et al., 2002; Bierkens et al., 2007; Anyah et al., 2008). In the study of Seuffert et al. (2002), the authors found that their model with the inclusion of lateral water transport from one soil column to its neighbors reduces simulated precipitation. Without the effects of lateral runoff, their model tends to overestimate precipitation. The current work differs from their study in several aspects including the runoff scheme, the simulation time, and the horizontal spatial resolution. Besides, depending on the status of available soil moisture, the impacts of groundwater could be different in different regions. In the current study, I did not consider the lateral water transport. In future studies, this needs to be considered to investigate the evolution of precipitation. As discussed here, the effect of groundwater is more significant over the transition zone (the Central U.S.) than over

other regions. Over the eastern U.S., the groundwater tends to reduce overestimated precipitation to some extent to improve the model performance over that region.

Figure 2.5 shows that the three modeling systems have distinct behaviors in terms of simulating intraseasonal variations of precipitation over the Central U.S. The observed precipitation maintains approximately  $2.4 \text{ mm d}^{-1}$ , varying slightly from  $2.2 \text{ mm d}^{-1}$  in June,  $2.6 \text{ mm d}^{-1}$  in July, to  $2.4 \text{ mm d}^{-1}$  in August. Although June precipitation is reproduced in the three experiments, there is a pronounced decreasing trend toward the end of the summer season. Compared to observations in JJA, all three modeling systems produce less precipitation, exhibiting an excessive summer drydown. This drydown may in part be due to the lack of the lateral water transport in the subsurface. As demonstrated in Bierkens and van den Hurk (2007), the groundwater convergence (i.e. the confluence of groundwater to discharge zones that remain wet throughout the year to sustain evaporation for longer periods) is a possible mechanism for persistence in rainfall. Therefore, I expect that when the lateral water transport is included, the model performance may be further enhanced. Additional work is needed to investigate the mechanisms of these feedbacks. Further analysis shows that the largest drying pattern (from  $2.4 \text{ mm d}^{-1}$  in June to  $0.6 \text{ mm d}^{-1}$  in August) occurs in DEFAULT. As I introduced vegetation phenology to the default model, the drying trend seen in DEFAULT is significantly ameliorated, with July rainfall at  $1.7 \text{ mm d}^{-1}$  and August rainfall at  $0.98 \text{ mm d}^{-1}$ . Combined with the implementation of groundwater model, the results are further improved, with July rainfall at  $2.1 \text{ mm d}^{-1}$  and August rainfall at  $1.5 \text{ mm d}^{-1}$ . Clearly, including vegetation and groundwater dynamics in the coupled land–atmosphere model

improves the intraseasonal (JJA) precipitation simulations (from  $1.3 \text{ mm d}^{-1}$  in DEFAULT,  $1.7 \text{ mm d}^{-1}$  in DV, to  $2.1 \text{ mm d}^{-1}$  in DVGW). The model dry bias in simulating intraseasonal precipitation is reduced most in DVGW. It is worth mentioning that if I just focus on precipitation prediction at one-month lead, the advantages of adding the vegetation growth and groundwater dynamics are not so evident. However, if I extend the lead-time to two or three months, the advantages of using DV or DVGW become increasingly apparent. This suggests that incorporating vegetation and groundwater dynamics into the model can prolong the soil moisture memory and hence maintain ET in dry seasons, which will be discussed later.

In summary, the model with the two augments performs better in reproducing summer precipitation over the Central U.S. in 2002. The results of precipitation illustrate that the vegetation–atmosphere interaction can occur on monthly timescales. The groundwater system, which is often ignored in most climate models, does impact precipitation over the Central U.S. DEFAULT has trouble simulating the overall magnitude of precipitation over the Central U.S. Of significant note, the augmented model with the new components is capable of capturing the intraseasonal variability of precipitation.

#### **2.4.2. Impact on surface fluxes**

To gain insight into the mechanism responsible for precipitation differences among different experiments, I plot the time series of latent heat and sensible heat fluxes over the Central U.S. (Figure 2.6). Clearly, simulated latent heat flux is lower in DEFALUT than those in DV and DVGW. The opposite is true for sensible heat flux. This is because soil



moisture is relatively dry in the absence of feedbacks among vegetation, groundwater and precipitation. I also noticed that the variations in DEFALUT are less pronounced than those in DV and DVGW owing to the lack of response to land–vegetation interactions. When the effects of vegetation phenology are included in the model, the partitioning between the sensible and latent heat fluxes is affected, resulting in a changed Bowen ratio (Mölders and Rütger, 2002). The decrease in the Bowen ratio induced by the vegetation dynamics could potentially increase convection. The increase in convection could bring out more precipitation, and the increased precipitation can further promote the growth of vegetation. Therefore, introducing vegetation–precipitation feedback into the model helps to maintain an appropriate amount of ET and precipitation over the study area. As I included groundwater component in DV, the Bowen ratio further decreased. This can be explained that groundwater adds more water to the dry soil, increasing the latent heat flux. Seuffert et al. (2002) also found that their model when incorporated with a sophisticated hydrological model could increase latent heat flux and reduce sensible heat flux correspondingly. Moreover, an analysis of the results indicates that higher latent heat flux in DV and DVGW corresponds to more precipitation, as described above (Figure 2.4).

Figure 2.7 plots the differences in monthly average latent heat flux and precipitation between DV and DEFAULT. A relatively large impact of vegetation growth on latent heat flux and precipitation is particularly seen over the Central U.S. For the most part, the plot shows that the increase in precipitation is consistent with the increase in latent heat flux. On average, a  $20 \text{ W m}^{-2}$  increase in latent heat flux corresponds to a  $0.5\text{--}1 \text{ mm d}^{-1}$  increase in precipitation. As described in Mölders and Rütger (2002), changes in latent

heat flux (or ET) can alter surface moisture distribution and water availability, which can affect vertical mixing, heating, cloud formation and precipitation. As a result, the modeling system with vegetation–precipitation feedback included to some extent improves precipitation simulation through changing latent heat flux. When I added groundwater component to the second modeling system, again, I see a  $30 \text{ W m}^{-2}$  increase in latent heat flux between DVGW and DV (Figure 2.8), which corresponds to  $1 \text{ mm d}^{-1}$  increase in precipitation over this area. The effects of vegetation and groundwater are most pronounced in July and August over the Central U.S., and the impacts of the two new components become more discernible after one month.

In addition to directly examining the evolution and distribution of latent heat flux and sensible heat flux, moisture budget calculation is another way to examine the causes of the increase in precipitation over the Central U.S. I calculated moisture flux convergence, which is a term in the conservation of water vapor equation, over the Central U.S. using specific humidity and wind fields on the basis of the following equations:

$$Q_u = -\frac{1}{g} \int_{P_s}^{P_t} q u dp, \text{ and} \quad (2.2)$$

$$Q_v = -\frac{1}{g} \int_{P_s}^{P_t} q v dp, \quad (2.3)$$

where  $Q_u$  is the horizontal (east-west) component of moisture flux in  $(\text{kg m}^{-1} \text{ s}^{-1})$ ,  $Q_v$  is the meridional (north-south) component of moisture vapor flux in  $(\text{kg m}^{-1} \text{ s}^{-1})$ ,  $q$  is the

specific humidity ( $\text{kg kg}^{-1}$ ),  $u$  is the horizontal component of wind velocity ( $\text{m s}^{-1}$ ),  $v$  is the meridional component of wind velocity ( $\text{m s}^{-1}$ ),  $p$  is the pressure (hPa), and  $g$  is the gravitational constant ( $9.81 \text{ m s}^{-2}$ ). The negative sign arises due to the fact that the hydrostatic assumption is used to convert from elevation to pressure. The limits of integration are the surface pressure ( $p_s$ ) and the pressure at the "top" of the atmosphere ( $p_t$ ). Here I define 100 hPa as the pressure at the top of the atmosphere in these computations. The moisture flux convergence is calculated using the following equation:

$$-\nabla \bullet Q = -\left(\frac{\partial Q_u}{\partial x} + \frac{\partial Q_v}{\partial y}\right). \quad (2.4)$$

The negative sign changes divergence to convergence, which means when the value is negative, it is divergence; and when it is positive, it is convergence. NARR and CPC gauged precipitation data are used as reference data sets.

Again, the calculated results (Table 2.2) show that DEFAULT largely underestimates the JJA precipitation by a factor of two. DV increases the JJA precipitation by  $0.5 \text{ mm d}^{-1}$ . The difference between DVGW and the observations is the smallest, with about  $0.3 \text{ mm d}^{-1}$ . The calculated ET shows that the amount of increased precipitation comes from increased ET. In summer, ET is larger than precipitation in the Central U.S., suggesting moisture flows out of this area. This result is consistent with several previous studies (Ropelewski and Yarosh, 1998; Ruiz-Barradas and Nigam, 2006), in which the authors found that the Central U.S. acts as a net moisture source during the summer months and mean evaporation exceeds mean precipitation with largest

evaporation in July and August. As I discuss here, in the results, the Central U.S. does act as a net moisture source. The increased precipitation by DVGW is almost 65%, corresponding to 34% increase in latent heat flux. The summer precipitation in the Central U.S. mostly comes from local ET showing a strong land–atmosphere coupling in this region. The role of vegetation accounts for almost 37% increase in precipitation in summer and the contribution of groundwater to summer precipitation is about 16%. I also performed one sensitivity experiment called GW, which only accounts for groundwater effect, to examine the contribution of groundwater dynamics. The result shows that groundwater alone only contributes to  $0.2 \text{ mm d}^{-1}$  increase in the JJA precipitation. Apparently, when I include vegetation and groundwater together in the model, there is an interaction between them, which can enhance the model performance.

#### **2.4.3. Impact on vegetation greenness fraction (VGF)**

Variability of vegetation can modulate surface energy fluxes and alter the partitioning of available energy into sensible and latent heat fluxes via the closing or opening of stomata, VGF, LAI, and vegetation types (e.g., Sud et al., 1993; Eastman et al., 2001). The change of wet or dry season is tightly linked to vegetation variability. One variable often used to represent vegetation variability and condition is VGF. Thus, one way to examine the role that dynamic vegetation and groundwater play is to compare the simulated VGF with observations.

Because the variation of VGF is highly correlated to NDVI, I followed the method defined by Gutman and Ignatov (1998) to derive VGF from the MODIS NDVI data. The MODIS NDVI data I used is a 16-day interval data set downloaded from

<http://glcf.umiacs.umd.edu/data/ndvi/> (NASA, 2007). The spatial resolution of this data set is 250 m and ArcGIS software is used to upscale the data to model spatial resolution. The VGF is calculated according to the following equation (Gutman and Ignatov, 1998):

$$VGF = \frac{NDVI_i - NDVI_{min}}{NDVI_{max} - NDVI_{min}}, \quad (2.5)$$

where  $NDVI_{min} = 0.04$  and  $NDVI_{max} = 0.52$  are prescribed as global constants. The analysis above illustrated the effects of vegetation and groundwater are most pronounced in August, I thus compared simulated August VGF over the Central U.S. with MODIS NDVI-derived data (Figure 2.9). In August, the prescribed AVHRR-derived VGF over the Central U.S. is lower than MODIS-derived one. Incorporation of vegetation growth and groundwater dynamics in the model increases VGF by 9%–11%, resulting in a 0.5–1.0 mm d<sup>-1</sup> increase in precipitation as indicated in Figure 2.5. This suggests that the long-term averaged VGF may not well represent actual vegetation conditions in the simulation period. With the vegetation phenology included, the modeling system is capable of maintaining ET through vegetation–precipitation feedback. As mentioned in Section 2.2, the year I selected to do these experiments is wetter than normal, corresponding to higher VGF. The default climatological VGF data used in the models do not reflect the vegetation conditions in the simulation period. With the additional consideration of upward water flux from the groundwater, plants tend to grow much better, resulting in higher VGF. Without this effect, during the dry period, plants cannot get enough water to generate more ET and greenness fraction. It is very intriguing that the impacts of vegetation and groundwater dynamics on VGF are consistent with the

impacts on latent heat flux and precipitation. Although, most previous work shows it is very difficult to find the positive correlation between vegetation and precipitation at local scales (Matsui et al., 2005; Liu et al., 2006). In the results, the impacts of vegetation and groundwater on vegetation condition lie in the region where there is an increase in precipitation.

#### **2.4.4. Impact on diurnal cycles of precipitation and surface fluxes**

It is of interest to explore the possible effects of vegetation growth and groundwater dynamics on diurnal cycles of precipitation and surface fluxes. A motivation to look at the impacts on diurnal cycles is because most climate and weather models cannot get diurnal cycle of precipitation right due to the uncertainties in the convective parameterizations, cloud physics and other land surface parameterizations, in which the uncertainties in the land surface model has a potential impact on this issue (Dai and Trenberth, 2003).

The diurnal cycles of surface heat fluxes, surface temperature, and precipitation simulated by three modeling systems over the Central U.S. are evaluated against the NARR data set. As shown on Figure 2.10, the effects of vegetation and groundwater on diurnal cycles of surface fluxes are typically from noon to early evening (local time). When compared to the NARR data, DEFALUT overestimates sensible heat flux, but underestimates latent heat flux. When vegetation phenology considered, the model produces somewhat higher latent heat flux and lower sensible heat flux. Changes in the surface fluxes in DV, because of changes in vegetation conditions, further improves the capability of the model to simulate diurnal cycles of surface temperature and precipitation

(Figures 2.10c and 2.10d). This analysis supports the findings presented in Holt et al. (2006) that including vegetation phenology in a coupled model enhances the coupling between the surface and the overlying atmosphere. As I incorporated groundwater into DV, the modeling system further reduces sensible heat flux and increases latent heat flux. This feature has also been reported in other studies (e.g., Seuffert et al., 2002), where the authors found that the model with the inclusion of groundwater and lateral water transport increases latent heat flux by increasing soil moisture content. It was thus concluded that DVGW makes better estimates of surface heat fluxes, and improves the simulations of surface temperature and precipitation. In addition, the model when enhanced with vegetation and groundwater dynamics is capable of simulating the later afternoon rainfall peak, which is not well captured in the default model.

The results presented here imply that when considering variation in vegetation phenology, the capability of the model to simulate the diurnal peak is improved. Moreover, if there is an impact of groundwater included in the model, during the dry period, the upward recharge from groundwater can increase precipitation throughout the whole day and the impacts are most significant from the late afternoon to the early morning. However, the nighttime precipitation peak (Figure 2.10d), which is clearly shown in the NARR data set, cannot be well simulated in all experiments. The reason can be explained that in the early morning, the dominant factor controlling the precipitation is not mainly from the local ET, the large-scale moisture transport might play an important role in producing precipitation. Still, the models with these two augments cannot improve the capability of the overall performance of the climate model. Other improvements such

as more appropriate cloud microphysics, convective schemes are required in regional climate models to simulate precipitation more accurately.

#### **2.4.5. Impact on the coupling between soil moisture and lifting condensation level (LCL)**

Land–atmosphere system is a highly coupled one, and the relationship between LCL and soil moisture index (*SMI*) is suggestive of important coupling within the system (Betts, 2007). Some studies (Betts, 2004, 2007; Betts and Viterbo, 2005) have found a strong link between soil moisture and LCL in reanalysis data.

To examine the coupling between the land and atmosphere, I examined the relationship between soil moisture and LCL using the method defined by Betts (1997, 2007). Estimates of the mean heights of the cloud base and LCL in pressure coordinates were computed from the lowest model level data using the formula below (Betts, 1997):

$$P_{LCL}/p = (1-RH)/(A+(A-1)RH), \quad (2.6)$$

where  $p$  is the pressure at the lowest model level (about 1hPa from the surface) and the thermodynamic coefficient  $A = (0.622L/2C_pT)$  is a weak function of Kelvin temperature,  $T$ , with  $L$  being the latent heat of vaporization and  $C_p$  the specific heat of air at constant pressure. *SMI* for the first soil layer and all soil layers is defined as:

$$SMI = (SM - SWP) / (SMC - SWP), \quad (2.7)$$

where  $SM$  is the model soil water fraction,  $SWP$  and  $SMC$  are the model soil permanent wilting and the soil porosity, which depend on different types of soil texture (Betts, 2007). As a result, *SMI* is not only a useful index on the daily timescale for the availability of



water for evaporation, but it also responds to precipitation on the intraseasonal scale. Thus, the two-way interaction of soil moisture–atmosphere coupling can be representing LCL as a function of *SMI*.

Figure 2.11 illustrates the relationship between daily averaged LCL and *SMI*, in which the NARR data are used as the reference. It is known that soil moisture, especially in the upper layer responds directly to precipitation. The evaporation from the land surface increases relative humidity and lowers the LCL (Betts, 2007). So lower value of LCL is corresponding to higher soil moisture index. Increased soil moisture due to the two augments is associated with a lower LCL and an increase in precipitation. Consistent with the results of Mölders and R ühaak (2002), Figure 2.11 shows that when vegetation phenology included in the model, the modeled ET is affected because of redistribution of vegetation conditions or VGF. As a consequence of the altered ET, the surface moisture distribution and water availability differ. This can further alter vertical mixing and affect cloud and precipitation formation. The changed pattern and amount of precipitation can in turn influence vegetation conditions (i.e., greenness fraction) through affecting soil water content. As seen here, the feedback between vegetation and atmosphere is enhanced when vegetation dynamics is included in the model (Holt et al., 2006). As I added groundwater to the model in addition to vegetation, the LCL is further lowered for the same level of *SMI*. Maxwell et al. (2007) investigated the relationship between soil moisture and the boundary layer evolution by adding a coupled groundwater model to an atmospheric model. Their modeling results show a spatial correlation between water table depth and boundary layer height. In general, a shallower water table tends to lead to

wetter soil moisture, cooler surface temperature and hence a lower boundary layer height. These features are also consistent with the aforementioned impacts of groundwater on surface fluxes. The impact of groundwater on soil moisture and LCL is more significant when a soil is drier, while the influence is relatively small when a soil becomes highly saturated. By examining the two plots in Figure 2.11, one can find that the impact of groundwater on the bottom soil layer is more distinctive, suggesting the direct interaction between the bottom soil layer and the groundwater system. Over the region I am interested in, the groundwater tends to increase soil moisture and lower LCL, resulting in an increase in precipitation. Thus by incorporating vegetation and groundwater dynamics in the model, the coupling between soil moisture and precipitation is enhanced. The result agrees well with what I found above that an increase in precipitation over the Central U.S. is due to local ET. The relationship between the LCL and the *SMI* exhibits an improvement as I incorporated dynamic vegetation and groundwater in the model, which is much closer to the NARR data.

## **2.5. SUMMARY**

This paper described the applications of vegetation and groundwater dynamics in a coupled land–atmosphere model over the Central U.S. Several sensitivity experiments with and without the two augments are designed to examine the impacts of vegetation and groundwater dynamics on warm season forecasts of precipitation. The results show that the model with the considerations of vegetation growth and groundwater dynamics improves the simulations of summer precipitation over the Central U.S. In this region, the default model produces less precipitation in comparison to observations. When

vegetation growth is included in the model, more precipitation is predicted, as perhaps induced by vegetation–atmosphere feedback. When I added a groundwater component to the model in addition to vegetation growth, the performance of the model in simulating summer precipitation is further enhanced, which is attributed to the interactions among soil moisture, vegetation, and groundwater. These results also suggest that vegetation growth and groundwater dynamics play an important role in enhancing the persistence of seasonal precipitation in the regional climate model. Through the analysis of the relationship between surface fluxes and precipitation, more precipitation generated by DV and DVGW corresponds to higher latent heat flux and lower sensible heat flux.

It is evident from the discussed Figures 2.1–2.11 and Tables 2.1 and 2.2 that local ET is an important water vapor source for summer precipitation over the Central U.S., suggesting a strong land–atmosphere coupling in this region. Vegetation and groundwater over the Central U.S. act to favor a stronger land–atmosphere feedback during summer season. Detailed analyses of the simulations suggest that the impacts of vegetation and groundwater on both energy and water budgets are critical in determining the strength of the feedback. It is also found that the two components have pronounced impacts on the diurnal cycles of surface fluxes and precipitation. The simulated diurnal cycle of precipitation is improved by the augmented model with the two components. This result may have broad implications for the development of climate models.

Finally, the coupling between soil moisture and lifting condensation level is examined by scatterplots of the two variables. The impact of groundwater is significant when the soil moisture is relatively dry. This is not surprising since groundwater systems

have a long ‘memory’ of past rainfall and recharge because of its slow flow. In addition, it appears that groundwater dynamics has a larger impact on the bottom soil layer. This result emphasizes the possible role groundwater systems play in climate prediction. If land surface models used in climate models lack groundwater systems, the performance of the models might be reduced.

The results presented in this study demonstrate the feasibility of coupling climate models with dynamic representations of vegetation growth and groundwater recharge. However, in this work, I did not include the effects of lateral flow, but only considered the vertical water exchange between soil and its underlying unconfined aquifer. In future studies, a more sophisticated physically based three-dimension groundwater model is needed in the coupled land–atmosphere model to study the feedbacks. This study only discussed the impacts of the two components on one summer season. Additional simulations of different years using these two components in the coupled model are required to gain a better sense of how the timing of the soil moisture affected by vegetation and groundwater influences seasonal precipitation. Continued development of fully coupled climate–vegetation–groundwater models will facilitate the exploration of a broad range of global change issues, including the potential roles of vegetation and groundwater feedbacks within the climate system.

## **2.6. ACKNOWLEDGEMENTS**

This research is supported by NOAA grant NA070AR4310216 and NASA Headquarters under the NASA Earth and Space Science Fellowship Program (grant

NNX07AO28H). I would like to express my thanks to David Gochis, Kenneth Mitchell, Lindsey Gulden, Enrique Rosero as well as the anonymous reviewers for their insightful, constructive comments. The computing resources are provided by the Texas Advanced Computing Center (TACC).

Table 2.1. Design of experiments

Experiment	Description
DEFAULT	prescribed VGF
DV	predicted VGF (or dynamic vegetation)
DVGW	predicted VGF and water table depth

Table 2.2. Water budget over the Central United States in June, July, and August (JJA) 2002

Variables→	Precipitation (mm d <sup>-1</sup> )	Evapotranspiration (mm d <sup>-1</sup> )	Moisture Flux Convergence (mm d <sup>-1</sup> )
NARR	2.3642 <sup>a</sup> /2.5186	2.9907	-0.4912
DEFAULT	1.2575	2.3181	-0.8660
DV	1.7215	2.9624	-1.0313
DVGW	2.0825	3.1033	-1.2663
GW	1.4614	2.2931	-1.4180
<sup>a</sup> CPC precipitation data.			

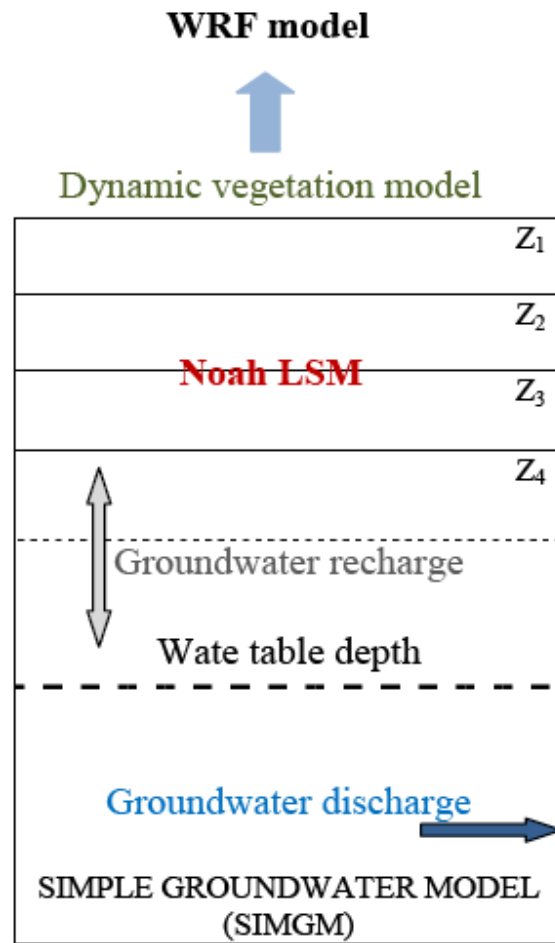


Figure 2.1. Schematic diagram of a coupled land–atmosphere modeling system. A dynamic vegetation model (DV) is incorporated into the Noah LSM and a simple groundwater model (SIMGM) is added beneath the Noah LSM.



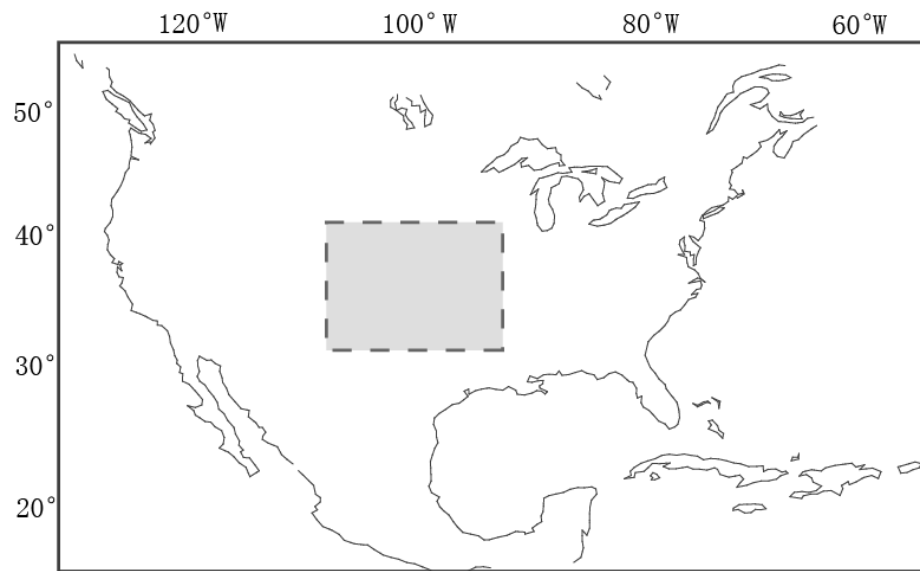


Figure 2.2. Map showing the modeling domain in which the shaded area represents the Central United States.

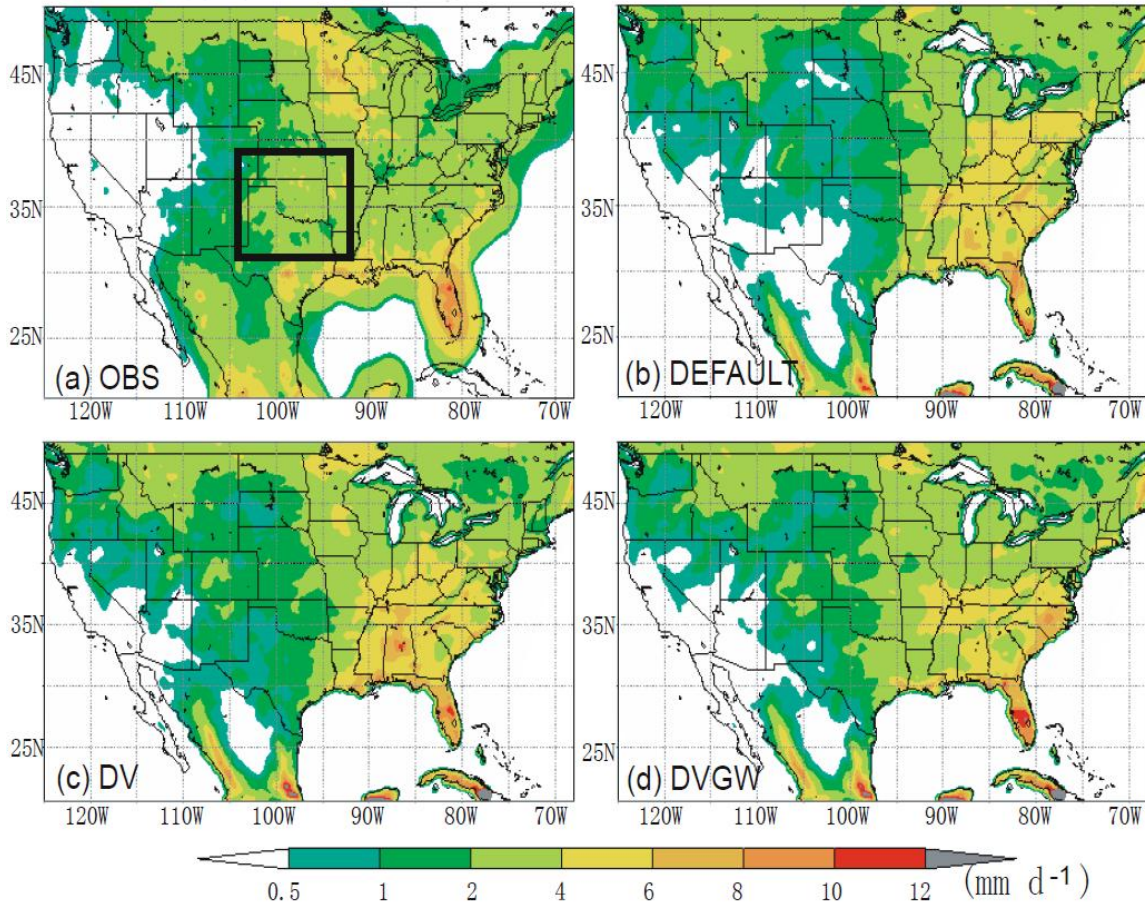


Figure 2.3. Observed and simulated precipitation in June, July and August (JJA) 2002 over the contiguous United States. (a) Observed JJA precipitation from the Climate Prediction Center (CPC) unified precipitation data set, which is a gridded data set at  $0.25^\circ \times 0.25^\circ$  resolution covering the United States and Mexico. (b) Simulated JJA precipitation in DEFAULT, which uses prescribed monthly mean vegetation greenness fraction (VGF). (c) Simulated JJA precipitation in DV, which includes a dynamic vegetation model, allowing the vegetation growth in response to climate conditions. (d) Simulated JJA precipitation in DVGW, which is augmented with SIMGM and DV to represent vegetation growth and water table dynamics.

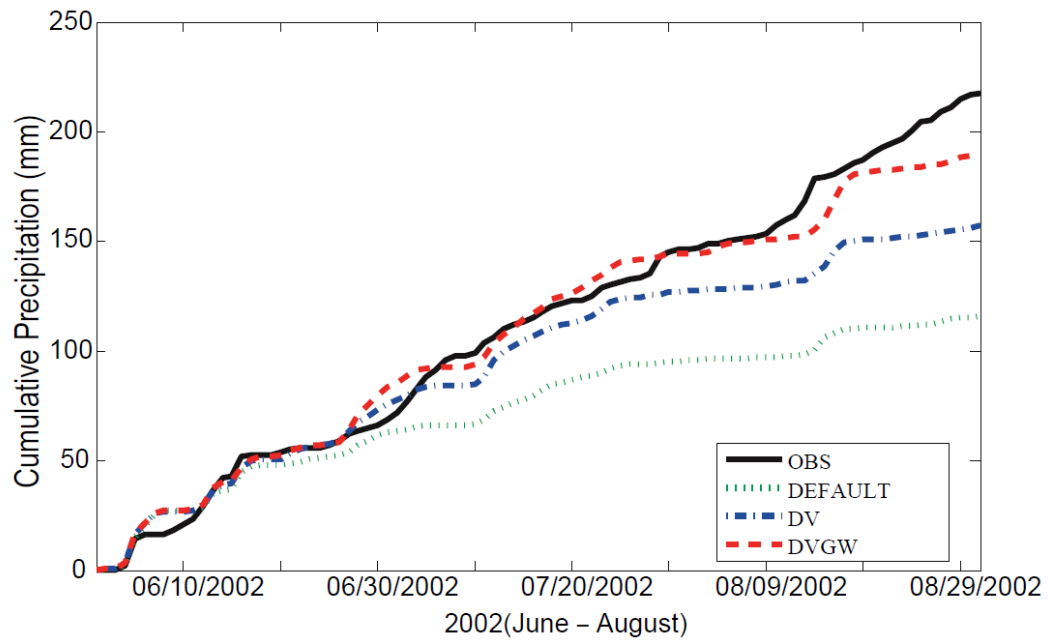


Figure 2.4. Observed versus simulated cumulative precipitation over the Central United States (DEFAULT, DV and DVGW are as in Figure 2.3).

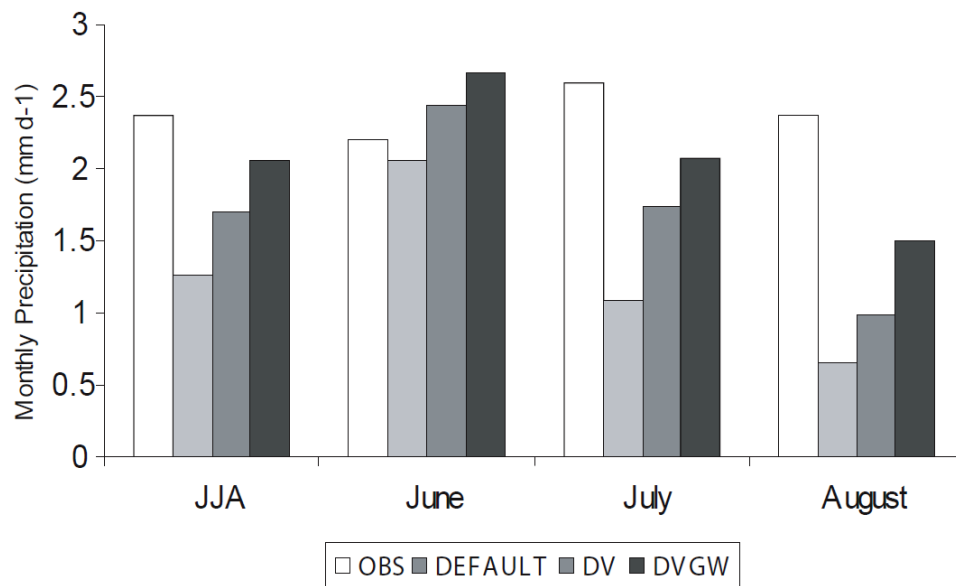


Figure 2.5. Observed and simulated JJA and monthly mean precipitation (mm d<sup>-1</sup>) over the Central United States.

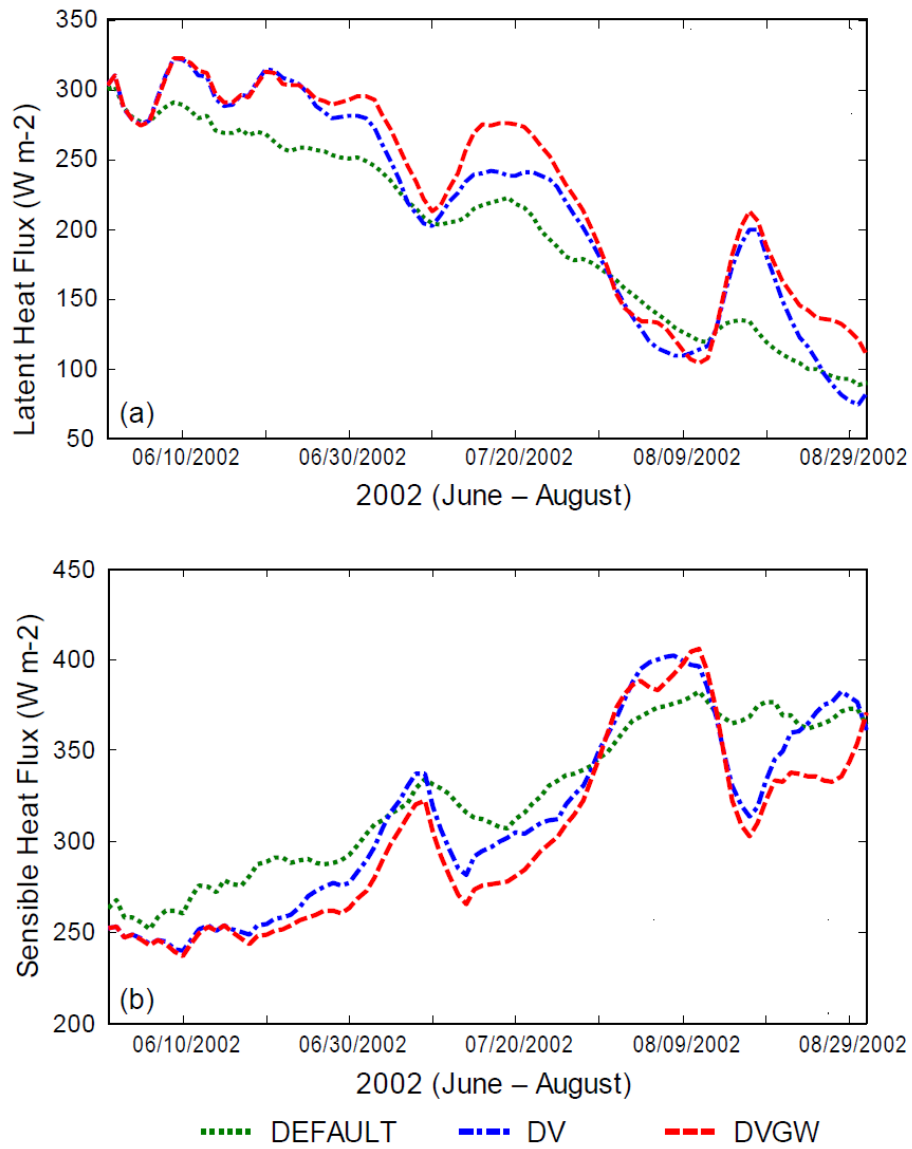


Figure 2.6. Comparisons of simulated latent heat flux (a) and sensible heat flux (b) over the Central United States among three experiments.

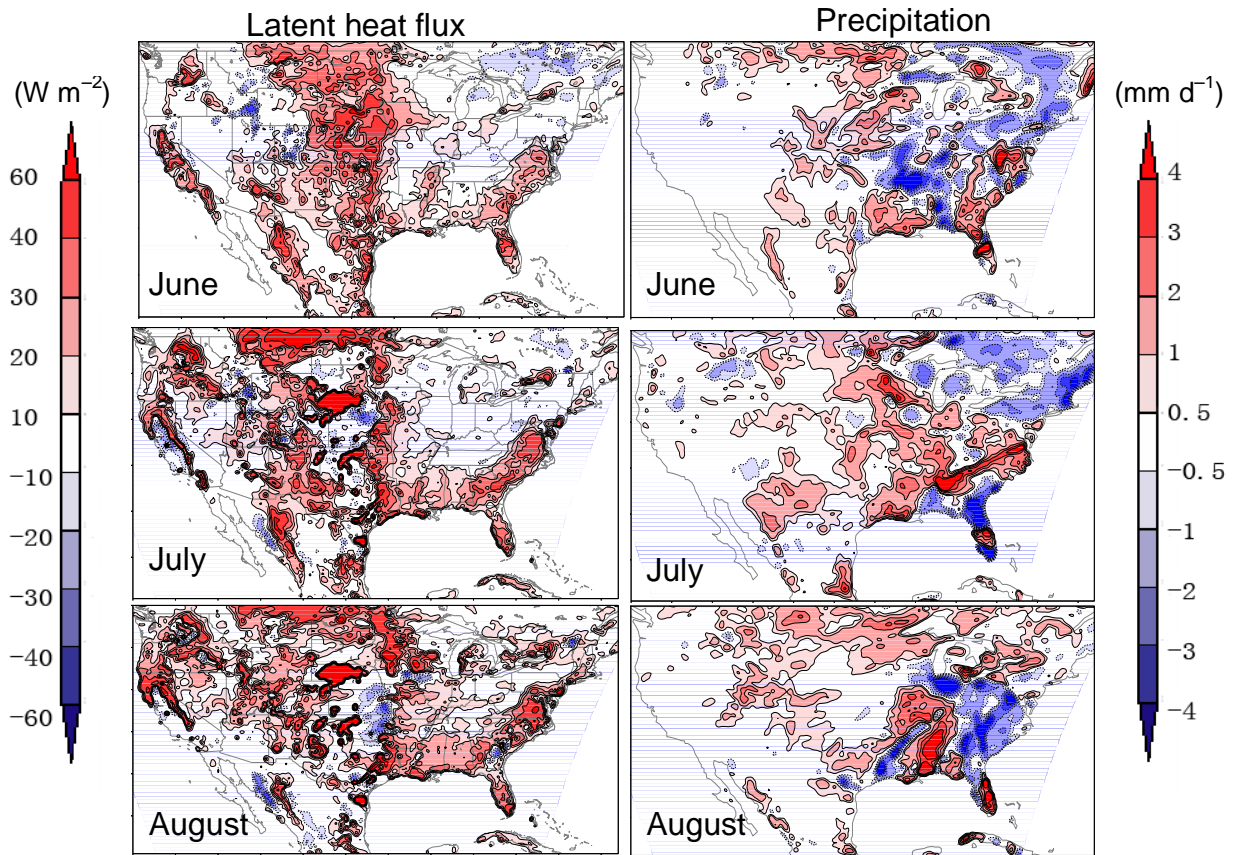


Figure 2.7. Map of differences in monthly average latent heat flux ( $\text{W m}^{-2}$ ) and precipitation ( $\text{mm d}^{-1}$ ) between DV and DEFAULT experiments. Differences were computed from ensemble simulations of DV and DEFAULT. The domain covers the contiguous United States (21°N–50°N, 125°W–68°W).

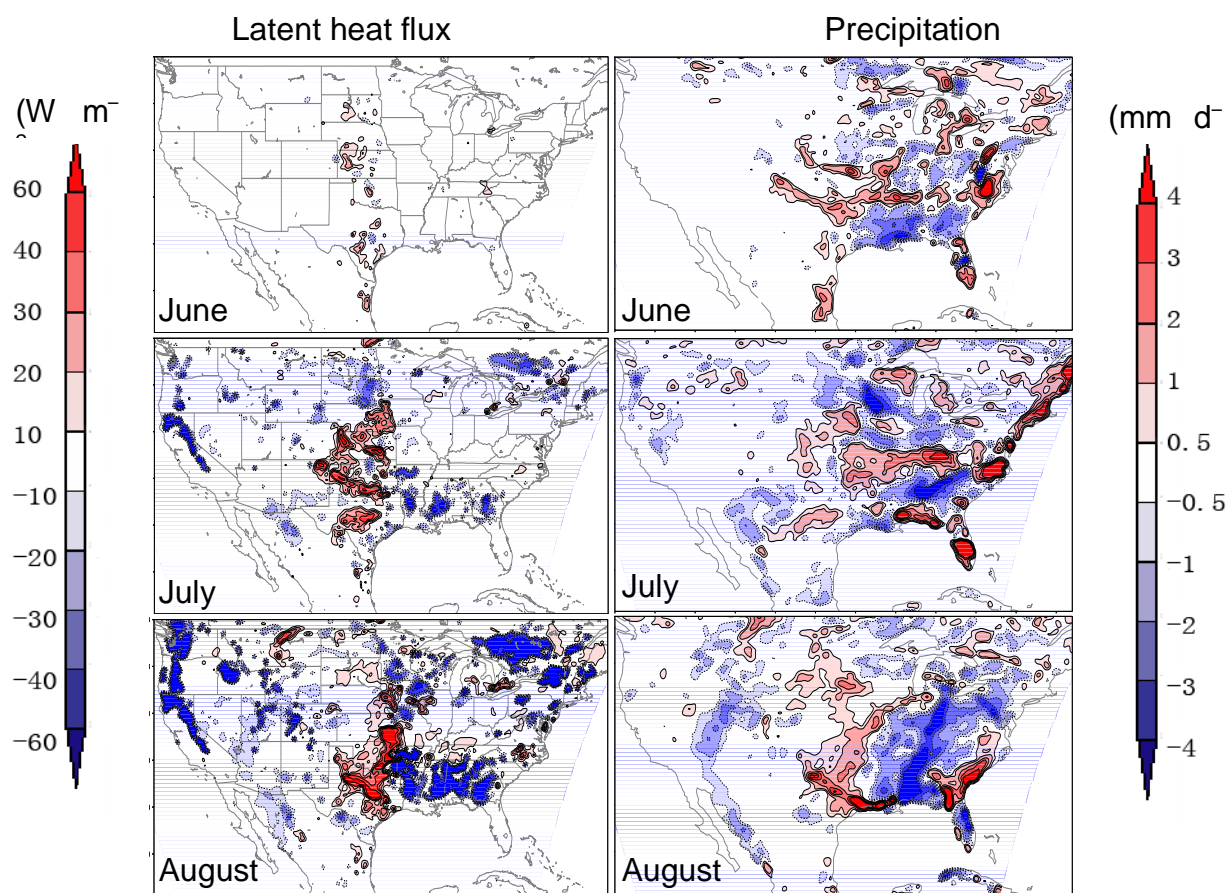


Figure 2.8. As in Figure 2.7, but for differences between DVGW and DV.

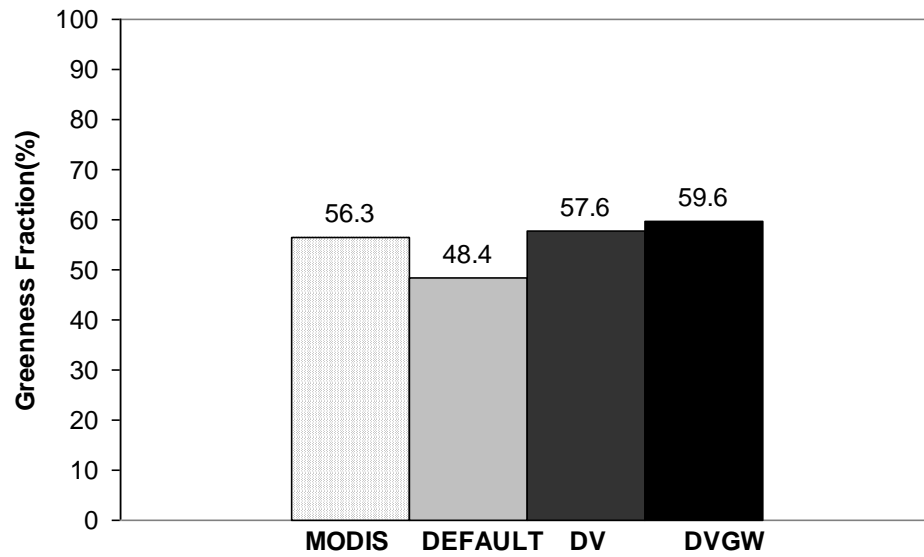


Figure 2.9. MODIS NDVI-derived and model simulated VGF over the Central United States in August. The MODIS NDVI data I used is a 16-day interval data set downloaded from <http://glcf.umd.edu/data/modis/>. The VGF is calculated by following the method defined in the work of Gutman and Ignatov (1998).



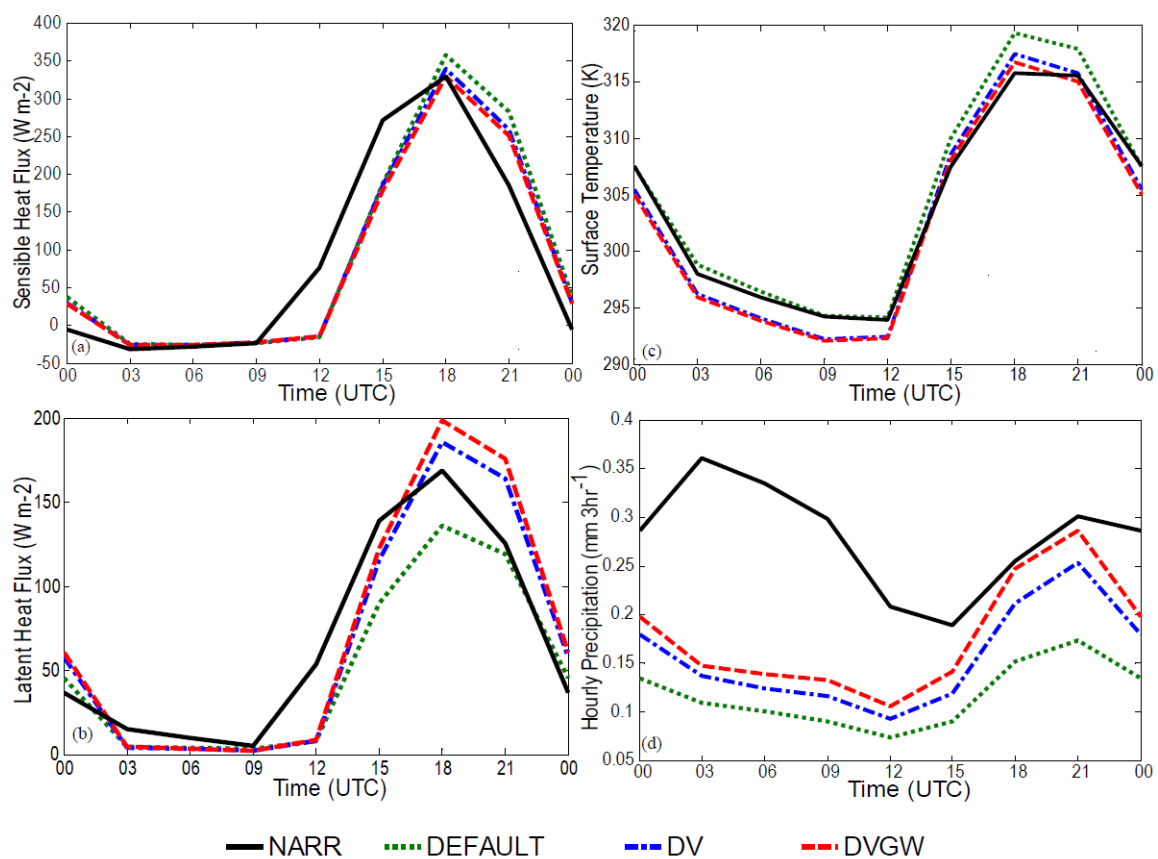


Figure 2.10. Observed and simulated diurnal cycles of (a) sensible heat flux, (b) latent heat flux, (c) surface temperature, and (d) precipitation over the Central United States. All variables were computed using the 3-month (JJA) data.

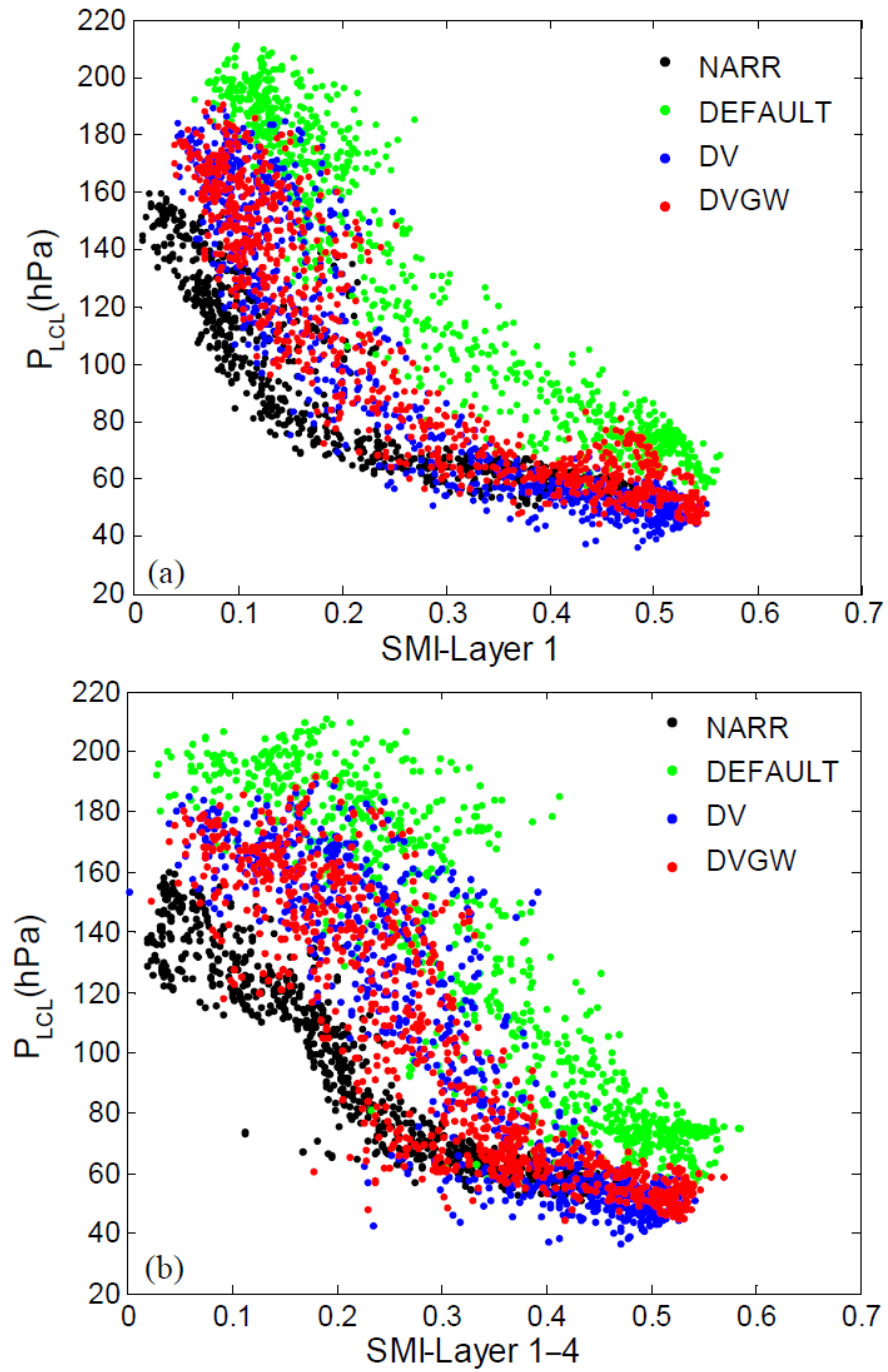


Figure 2.11. Daily averaged lifting condensation level (LCL) versus soil moisture index (SMI) for (a) soil layer 1 and (b) soil layers 1–4. Estimates of the height of the LCL in pressure coordinates were computed from the lowest model level data using the formula defined by the work of Betts (1997).

## **Chapter 3: Impacts of Land–climate Interactions on Regional Air Quality in a Changing Climate**

### **3.1. ABSTRACT**

This chapter provides an overview of the roles land–climate interactions might play in projecting future air quality. It mainly describes the importance of land–climate interactions in air quality study and how they would affect future air quality projections in both direct and in-direct ways. The two atmospheric chemical species of interest are surface ozone (O<sub>3</sub>) and secondary organic aerosols. It is followed by two chapters (Chapters 4 and 5), in which methodologies and findings are presented.

### **3.2. IMPORTANCE**

Air quality is strongly dependent on weather and is, therefore, sensitive to climate change. Climate change induced by greenhouse gases not only influences the behavior of the atmosphere and weather systems, but also brings with it modifications of a number of physical, chemical, and biological processes within the ecosystems. Many of these processes directly or indirectly affect the atmospheric composition and air quality. In response to increasing greenhouse gases, Earth's temperature will continue rising in the coming decades. A warming climate is likely to change the concentrations and distributions of air pollutants through a variety of direct and indirect processes, including the change of land cover, the modification of biogenic emissions, the change of chemical reaction rates, changes in meteorological variables and modifications of synoptic flow pattern that govern pollutant transport. Our understanding of these processes and their

roles in air quality are still at an early stage, and assessing their impacts in a changing climate is very important for policy making.

It was recognized that the relationship between climate change and air quality was not a simple one of “higher temperatures equals worse air quality”. The interactions between and among the components of the climate system could complicate the impacts of climate change on air quality. For example, the land surface of the climate system affects climate by exchanging water, energy, momentum, and chemical materials with the overlying atmosphere. Processes on land can accentuate or mitigate climate changes through feedbacks among water, energy, and biogeochemical cycles, such as vegetation–climate feedback. Climate controls the growth of vegetation on land through climatic variables including temperature, radiation and precipitation, and in turn, vegetation feeds back to climate through biogeochemical and biogeophysical processes. Thereby, interactions between land and climate can regulate the conditions of air quality. In addition, changes in the land surface conditions caused by human activities, such as urbanization may further contribute to changes in air quality by significantly altering the land surface characteristics and atmospheric composition. In order to make accurate estimates of future changes in climate and air quality, particularly at regional scales, the role of land surface processes and their interactions with climate and air quality need to be considered.

Because of the heterogeneous nature of the land surface and its rapid transformation caused by human activities, future climate projections used for policymaking are less

certain on regional scales. Simulations of climate change for the twenty-first century forced with greenhouse gas concentrations and other atmospheric constituents derived from the Intergovernmental Panel on Climate Change (IPCC) Special Report on Emission Scenarios (SRES) (Meehl et al, 2007) showed a warming of about 0.2 °C per decade for a range of SRES emission scenarios over the next two decades. These results only represent the changes in global average temperature. At local to regional scales, changes in temperature are expected to be more variable. For regional air quality assessment that requires much finer resolution of climate information, the spatial resolutions of climate models are not adequate. In the following chapters, the assessment of the impacts of future climate change on regional air quality is provided by dynamically downscaling global climate projections with a coupled regional land–atmosphere–chemistry model, which also takes into consideration of interactions between land and atmosphere.

### **3.3. IMPACT ON SURFACE OZONE (O<sub>3</sub>)**

Surface O<sub>3</sub> is formed in the troposphere by photochemical oxidation of carbon monoxide, methane, and non-methane volatile organic compounds (NMVOCs), such as isoprene, with the hydroxyl radical (OH) in the presence of reactive nitrogen oxides (NO<sub>x</sub>). O<sub>3</sub> pollution is mainly a summer problem because of the photochemical nature of the source. High levels of surface O<sub>3</sub> in the lower troposphere have detrimental effects on human health and plants. They can be strongly affected by land and atmospheric processes in direct or in-direct ways. In a direct way, land–climate interactions affect regional meteorological patterns that are related to air pollution. It was known that

meteorological conditions play an essential role in whether or not a metropolitan area meets the National Ambient Air Quality Standards (NAAQS) for air pollutants considered harmful to public health and the environment. The conditions conducive to high O<sub>3</sub> concentrations near the surface generally include warm weather, high solar radiation, and high-pressure systems (e.g., Hogrefe et al., 2004; Leung et al., 2005; Dawson et al., 2009).

In addition to the direct way through which land–climate interactions affect air quality, studies have shown that they indirectly influence the formation of O<sub>3</sub> by changing NMVOCs of O<sub>3</sub> precursors. NMVOCs can be anthropogenic or biogenic in origins. Vegetation is a large source for NMVOCs (Guenther et al., 1995, 2006), and they are often called BVOCs. Therefore, processes related to vegetation including vegetation–climate interactions have a significant impact on O<sub>3</sub> formation indirectly. As shown in the previous chapter, the feedback between vegetation phenology and climate is profound over some regions in summer time. Therefore, vegetation phenology has the potential to affect O<sub>3</sub> formation. In this way, land–climate interactions impact on O<sub>3</sub> air quality. Because of the essential role of land–climate interactions play in climate change, their impacts need to be explored when projecting future air quality. Moreover, human activities are changing climate through emitting anthropogenic emissions into the atmosphere and altering the natural land surface for human use (Foley et al. 2005). Urbanization — the change of vegetated area to human land use — can affect air quality through influencing land and atmospheric conditions. Urban land use change by itself can contribute to changes in regional weather patterns and long-term changes in climate

through surface fluxes. Then, changes induced by urban land use change may further worsen the regional O<sub>3</sub> air quality. A better understanding of the individual effects (e.g., land use change effect and climate change effect) is critical for future air quality management.

### **3.4. IMPACT ON SECONDARY ORGANIC AEROSOLS (SOA)**

Atmospheric aerosol is a term used to describe airborne particles emitted directly from natural and anthropogenic sources or produced in the atmosphere through the condensation of low-volatile trace gases. Previous work has shown that concentrations of atmospheric aerosols are strongly influenced by meteorology. Therefore, SOA concentrations are very sensitive to climate change. Modeling studies (e.g., Avise et al, 2009; Dawson et al, 2009) have examined the sensitivity of aerosol to a suite of meteorological variables including temperature, humidity, wind speed, mixing height, and precipitation. Changes in climate involving land–climate interactions are expected to result in changes in atmospheric concentrations of aerosol, which could have important impacts on air quality and climate.

Atmospheric aerosol includes as principal components sulfate, nitrate, organic carbon, elemental carbon, soil dust, and sea salt. Organic aerosol significantly contributes ~20–50% to the total fine aerosol mass at continental mid-latitudes (Putaud et al., 2004) and as high as 90% in tropical forested areas (Andreae and Crutzen, 1997; Roberts et al., 2001). Organic aerosols can be emitted directly in particulate form from natural and anthropogenic sources, and are referred to as primary organic aerosols (POA). They can

be formed in the atmosphere through the oxidation of VOCs, and are referred to Secondary Organic Aerosols (SOA). Due to the source of VOCs, SOA can be anthropogenic or biogenic. Recently, there is a growing realization that BVOCs play an important role in the formation of SOA when reacted with the principle atmospheric oxidizing agents (e.g.,  $O_3$ ) (Griffin et al., 1999; Andersson-Sköld et al., 2001; Chung and Seinfeld, 2002; Sotiropoulou et al., 2004; Lack et al., 2004; Clayes et al., 2004; Henze and Seinfeld, 2006; Liao et al., 2007). Current estimates suggest biogenic SOA sources (8 to 40 Tg/yr) are much larger than anthropogenic sources (0.3 to 1.8 Tg/yr), but the number is still underestimated (IPCC, 2001). The estimated contribution of SOA by a three-dimensional global chemistry transport model to the total organic carbon aerosol, which comprises 20–90% of the fine particulate matter over the continents (Kanakidou et al., 2005), can be more than 80% in July (Tsigaridis, 2003). As aforementioned, terrestrial vegetation controls the amount of BVOCs emitted to the atmosphere along with other climatic variables such as temperature and radiation (Guenther et al., 2006). Biogenic emissions and SOA are strongly dependent on climatic conditions. Thus, land–climate interactions could modulate biogenic SOA formation through influencing vegetation and other climatic variables (e.g., temperature, precipitation). Because of the roles SOA play in the environment, radiative forcing, and the hydrologic cycle, it is of great significance to understand SOA levels and the effects of other factors controlling SOA formation in the atmosphere (e.g., Chung and Seinfeld, 2002; Kanakidou et al., 2005; Barth et al., 2005; Hoyle et al., 2009) in a changing climate.



The research presented in the following two chapters seeks to understand the implications of land–climate interactions on regional air quality ( $O_3$  and SOA) in a future changing climate by making use of a coupled land–atmosphere–chemistry model. The effects of land use change that could affect land–climate interactions are also explored. In order to simulate SOA levels in the current and future climates, an SOA model is incorporated into the coupled land–atmosphere–chemistry model. Sensitivity experiments are designed to understand their changes in the future changing climate.

## Chapter 4: Predicted Impacts of Climate and Land Use Change on Surface Ozone in the Houston Area<sup>2</sup>

### 4.1. ABSTRACT

This chapter studies the effects of climate change under future A1B scenario, which is a midline scenario for carbon dioxide output and economic and the predicted carbon dioxide emissions increase until around 2050 and then decrease after that, and land use change on surface ozone (O<sub>3</sub>) in the greater Houston area. I applied the Weather Research and Forecasting model with Chemistry (WRF/Chem) to the Houston area for August 2001–2003 and future (2051–2053) years. The model was forced by downscaled 6-hourly Community Climate System Model (CCSM) version 3 outputs. High-resolution current year land use data from National Land Cover Database (NLCD) and future year land use distribution based on projected population density for the Houston area were used in the WRF/Chem model coupled with an Urban Canopy Model (UCM). The simulation results show that there is generally a 2°C increase in near-surface temperature over much of the modeling domain due to future climate and land use changes. In the urban area, the effect of climate change alone accounts for an increase of 2.6 ppb in daily maximum 8-hr O<sub>3</sub> concentrations and a 62% increase of urban land use area exerts more influence than does climate change. The combined effect of the two factors on O<sub>3</sub> concentrations can be up to 6.2 ppb. The impacts of climate and land use change on O<sub>3</sub> concentrations differ across the various areas of the domain. The increase in extreme O<sub>3</sub> days can be up to 4–5 days in

---

<sup>2</sup>Significant portions of this chapter were first published as:

Jiang, X., C. Wiedinmyer, F. Chen, Z.-L. Yang, and J. C.-F. Lo (2008), Predicted impacts of climate and land use change on surface ozone in the Houston, Texas, area, *J. Geophys. Res.*, 113, D20312, doi:10.1029/2008JD009820.

Work cited here is referenced in the **References** section of this dissertation.

August, in which land use contributes to 2–3 days increase. Additional sensitivity experiments show that the effect of future anthropogenic emissions change is on the same order of those induced by climate and land use change on extreme O<sub>3</sub> days.

## **4.2. INTRODUCTION**

High levels of surface ozone (O<sub>3</sub>), one of major air pollutants in the lower troposphere, have detrimental effects on human health and plants. The conditions conducive to high O<sub>3</sub> concentrations near the surface generally include warm weather, high solar radiation, and high-pressure systems. Future increases in the average global temperature as predicted by most climate models, together with future land use change induced by human activities (IPCC, 2007) may exert a strong influence on future surface O<sub>3</sub> air quality. It is of primary interest to examine future air quality change in response to future changes in climate and land use in order to help policy makers set future national air quality standards such as the National Ambient Air Quality Standard (NAAQS) in the United States (U.S.).

In recent years, efforts have been put into estimating future changes in surface O<sub>3</sub> concentrations due to changes in future anthropogenic emissions and climate change on global and regional scales (e.g., Prather et al., 2003; Hogrefe et al., 2004; Mickley et al., 2004; Leung and Gustafson, 2005; Forkel and Knoche, 2006; Murazaki and Hess, 2006; Racherla and Adams, 2006; Tao et al., 2007; Tagaris et al., 2007). Prather et al. (2003) summarized the projected future changes in O<sub>3</sub> on a global scale based on 10 global models. Yet their study only considers changes in O<sub>3</sub> due to changes in anthropogenic

emissions. Hogrefe et al. (2004) was the first study that applied a modeling system consisting of a global climate model, a regional climate model, and an air quality model to estimate the potential effects of future climate change on surface O<sub>3</sub> over the eastern U.S. More recently, Tagaris et al. (2007) estimated the impacts of future global climate change and emissions change on U.S. O<sub>3</sub> concentrations. Their results revealed that climate change, alone, with no emissions change had a small effect on the maximum 8-hr O<sub>3</sub> concentrations. Tao et al. (2007) investigated the relative contributions of projected future emissions change and climate change to surface O<sub>3</sub> concentrations in the U.S. The results of their study showed that the magnitude of changes in surface O<sub>3</sub> concentrations differed in metropolitan and rural areas. However, in these studies, future urban land use change in metropolitan areas is not included.

As more land area in metropolitan regions is expected to be converted from natural and vegetated land cover to human-dominated uses in the future, resulting changes in air temperature, wind field, humidity, and height of the atmosphere boundary layer induced by land use change (Civerolo et al., 2000; Grossman-Clarke et al., 2005; Liu et al., 2006; Lo et al., 2008) can affect the production and distribution of air pollutants (Taha, 1996; Taha et al., 1998; Civerolo et al., 2007; Wang et al., 2007). It has been demonstrated that the spatial patterns of air pollutants were positively correlated with urban built-up density (Weng et al., 2006), indicating the requirement of better treatments of urban features in the numerical models. By refining a land use classification for the arid Phoenix metropolitan area and introducing a bulk approach to a mesoscale atmospheric model, Grossman-Clarke et al. (2005) found that the model with the new features can better

simulate the daytime part of the diurnal temperature cycle in the urban area, which can improve the simulation of surface O<sub>3</sub> levels in air quality models.

Despite the recognition that land use change can have significant impacts on modeled meteorology and air quality, most previous studies generated future regional climate variables to drive the air quality models without any adjustments to the land use patterns (e.g., Hogorefe et al., 2004; Tao et al., 2007). The exception of work includes Civerolo et al. (2007), who applied future land use data estimated by a land use change model to one climate scenario to explore the effects of increased urbanization on surface O<sub>3</sub>. However, in their work, they used global climate model outputs, a regional climate model along with an offline photochemical model. The treatment for urban land use categories in their study was very simple, through assigning several new parameters for three urban land use types, which were classified based on vegetation fraction. As detailed Urban Canopy Models (UCMs) have been developed (e.g., Kusaka et al., 2001; Kusaka and Kimura, 2004a, b; Holt and Pullen, 2007), it is possible to better understand the contribution of urbanization to changes in near-surface O<sub>3</sub> from the modeling perspective.

Under the Clean Air Act, the Houston–Galveston–Brazoria (HGB) area is classified as an O<sub>3</sub> nonattainment area, which could be attributed to its rapid urban development, extensive sources of anthropogenic emissions, unique land use and land cover patterns, and complex coastal zones. Most of the previous studies have been focused on the impacts of anthropogenic (e.g., Jiang and Fast, 2004; Tao et al., 2004; Fast and Heilman, 2005; Nam et al., 2006) and biogenic emissions (e.g., Byun et al., 2005; Li et al., 2007)

and meteorological conditions (e.g., Dabberdt et al., 2004; Zhang et al., 2007) on O<sub>3</sub> formation (Jimenez et al., 2006; Bossioli et al., 2007). To date, no work has been done to assess the impacts of future climate change and land use change on the surface O<sub>3</sub> over the Houston area. The recent development of a fully coupled land–atmosphere–chemistry model with a detailed UCM allows us to assess the impacts of both climate change and land use change on air quality on regional scales simultaneously. In this study, results are presented for a modeling study aimed at predicting future changes in surface O<sub>3</sub> concentrations over the greater Houston area, taking into account the effects of climate change and land use change. I begin in Section 4.3 with a brief description of the methods used in this study. In Section 4.4, I compare model results with observations for present-day conditions and discuss the contributions of future climate change and land use change to surface O<sub>3</sub> changes in the Houston area. Additionally, the results of sensitivity simulations concerning the contribution of anthropogenic emissions change to changed surface O<sub>3</sub> over the Houston area are presented.

## **4.3. METHODOLOGY**

### **4.3.1. Regional land–atmosphere–chemistry model**

The physically-based Weather Research and Forecasting model (Skamarock et al., 2005) with Chemistry (WRF/Chem) is a new-generation atmosphere–chemistry model developed collaboratively among several groups including the National Center for Atmospheric Research (NCAR) and the National Oceanic and Atmospheric Administration (NOAA) (Grell et al., 2005). The computations of meteorology and atmospheric chemistry in the WRF/Chem model share the same land surface schemes,

time transport schemes, vertical mixing parameterizations, and time steps for transport and vertical mixing. It has been successfully applied for regional air quality studies (e.g., Fast et al., 2006).

Similar to the WRF model, the WRF/Chem model permits the choice between different physics and chemistry options. The following options were applied for the simulations presented here: Grell et al (1994) cumulus scheme, WSM 5-class microphysics scheme (Hong et al., 2004), Yonsei University Planetary Boundary Layer (PBL) scheme (Hong and Pan., 1996), Simple Cloud Interactive Radiation scheme (Dudhia et al., 1989) and Rapid Radiative Transfer Model longwave radiation scheme (Mlawer et al., 1997). The Regional Acid Deposition Model version 2 (RADM2) chemical mechanism (Stockwell et al., 1990) was used to simulate gas phase chemistry. Several previous studies (e.g., Tie et al., 2001; Martin et al., 2003) suggest that the net effect of aerosols over the U.S. results in only a small decrease in O<sub>3</sub>. Therefore, I did not include aerosol-induced changes in photolysis rates. The photolysis frequencies for the 21 photochemical reactions of the gas phase chemistry model are calculated at each grid point according to Madronich (1987).

I used the Noah land surface model (LSM) (Chen and Dudhia, 2001; Ek et al., 2003) coupled with an UCM in the WRF/Chem model. The Noah LSM calculates surface sensible heat flux, latent heat flux, and skin temperature for natural surfaces. The UCM is coupled to the Noah LSM through urban surface fractions (Kusaka et al., 2001; Kusaka and Kimura, 2004a, b). This WRF/Noah/UCM coupled modeling system (Chen et al., 2004, 2006) calculates the surface fluxes from man-made surface and includes the

following: 1) 2-D street canyons that are parameterized to represent the effects of urban geometry on urban canyon heat distribution; 2) shadowing from buildings and reflection of radiation in the canopy layer; 3) the canyon orientation and diurnal cycle of solar azimuth angle; 4) man-made surface consisting of eight canyons with different orientation; 5) Inoue's model for canopy flows (Inoue, 1963); 6) the multilayer heat equation for the roof, wall, and road interior temperatures; and 7) a very thin bucket model for evaporation and runoff from road surface. To run the UCM within the Noah LSM for the Houston area, additional parameters such as building height, roughness length, sky view factor, and anthropogenic heat for three land use categories (industrial or commercial, low-intensity residential, and high-intensity residential) are included in an additional lookup table. In general, the industry or commercial land use category has higher building height, roughness length, and anthropogenic heat, and a lower sky view factor than residential land use category. The parameters for the three different urban land use types in the UCM are presented in Table 4.1. To conduct future year simulations, one problem is the specification of anthropogenic heating in cities. Because of the steady increase in energy consumption and the growth of cities, anthropogenic heating would change significantly in the future. One sensitivity experiment shows that the effect of anthropogenic heating only leads to a 0.6 ppb increase in  $O_3$ , which is not very significant. So in the future year simulations, I applied the same set of anthropogenic heating rate shown in Table 4.1 as in current year simulations.

#### **4.3.2. Global and regional climate modeling**

Current and future year regional climate fields were obtained by downscaling the



NCAR Community Climate System Model version 3 (CCSM3) outputs, which have been used for the Intergovernmental Panel on Climate Change (IPCC) Fourth Assessment Report (AR4) (Collins et al., 2006), to the regional scale. The horizontal resolution of CCSM3 is T85, which is a 256 by 128 regular longitude/latitude global horizontal grid ( $\sim 1.41^\circ$ ). The greenhouse gas concentrations during the CCSM3 simulation period used in this study follow the IPCC Special Report on Emission Scenarios (SRES) A1B (IPCC, 2001), with increasing trace gases and aerosol concentrations from 2001 until 2050. The A1B scenario is a midline scenario for carbon dioxide output and economic growth; the predicted carbon dioxide emissions increase until around 2050 and then decrease after that. A full analysis of the CCSM3 future climate simulation is described by Meehl et al. (2006). In this study, I simulated a control period (2001–2003, denoted as “current”) and a future period (2051–2053, denoted as “future”). I prepared high-resolution initial and boundary meteorological conditions by running the WRF model at 12-km modeling domain driven by 6-hourly CCSM outputs with time-varying sea surface temperature and vegetation fraction. Then, the outputs from 12-km runs were used as the inputs for the 4-km WRF/Chem model domain covering southeastern Texas and centered on the Houston metropolitan area. The simulations were performed for August of 2001–2003 and 2051–2053. To minimize the effect of initial conditions, the initial two-day period (July 30 and July 31) of each simulation was considered as a spin-up period to establish the initial conditions for several atmospheric concentrations of different emission species.

#### **4.3.3. Land use and land cover data**

The default land use and land cover data used in the WRF/Chem model is based on

1992–1993 USGS data and does not exactly reflect the land surface conditions of 2000s. I thus replaced this USGS data with the new data derived from 2000 Moderate Resolution Imaging Spectroradiometer (MODIS) data (Friedl et al., 2002). The 1-km MODIS land use and land cover types were classified by the International Geosphere–Biosphere Programme (IGBP), but excluded the permanent wetland and cropland and natural vegetation types. Three new classes of tundra and inland water bodies have been added by the Land Team at the National Centers for Environmental Prediction (NCEP) as an experimental product used here. Hence, there are 21 types of land use and land cover in the MODIS data set. A comparison of the USGS and MODIS data shows that land cover characteristics are different over the southeastern and surrounding areas of the Houston urban center. However, the dominant land cover types over these regions are relatively similar: “Dryland Cropland and Pasture” in the USGS data set, and “Cropland/Grassland Mosaic” in the MODIS data set. The largest difference occurs in the urban areas because of urban expansion. Moreover, to characterize the present-day urban land use pattern, I incorporated high-resolution (30-m) USGS 2001 National Land Cover Database (NLCD) urban land use data with detailed urban land use classifications (low-intensity residential, high-intensity residential, and the industrial or commercial) for the Houston area (Figure 4.1a).

Future changes in land use patterns induced by human activities represent an important and highly uncertain control on near-surface meteorological conditions. I prepared the Houston urban land use data on the basis of future patterns of population density. The future patterns of population density were generated by the Spatially

Explicit Regional Growth Model, which related population growth patterns with accessibility to urban and protected lands (Theobald, 2005). The classification of different land use categories (high-density and low-density residential land use) needed for the UCM was processed according to the projected population density. I artificially treated the regions with population density larger than a certain value as the high-density residential areas. Low-density residential areas were characterized by a certain range of population density. As I did not have information about the future development of industry-commercial areas, I kept the industry or commercial land use the same as the current. I used the predicted urban land use distribution to the Houston urban area on the basis of the projected population growth to 2030. In 2030, the U.S. population is projected to grow 29%. I was limited to data projected to 2030, since projections to 2050 were unavailable. In fact, by 2050, if population continues to grow, the Houston urban area would expand, which may amplify the impacts of land use change. Although it is important to accurately represent all factors in the model, all model results are subject to uncertainty. Nevertheless, the future land use data used in the simulations at least provides us one possible scenario to study the impacts of future land use change on O<sub>3</sub>. It should be noted that changes in land surface conditions in other regions are not considered in this study. Figures 4.1a and 1b show that urban land use area in the modeling domain increases almost by 62% in the future.

#### **4.3.4. Anthropogenic and biogenic emissions**

Anthropogenic emissions of gas species for the years 2000 and 2050 are taken from the U.S. EPA's 1999 National Emissions Inventory (NEI-99, version 3) released in 2003

at a 4-km horizontal resolution (<http://www.epa.gov/air/data/neidb.html>). The emissions are representative of a typical summer day, as derived by temporal allocation factors specific to each source classification code provided by the EPA (Frost et al., 2006). This inventory is designed for regional-scale photochemical models of North America that require hourly emissions data for oxides of nitrogen ( $\text{NO}_x$ ), volatile organic compounds (VOC), carbon monoxide (CO), sulfur dioxide ( $\text{SO}_2$ ), and ammonia ( $\text{NH}_3$ ). The emissions are speciated into 41 VOCs categories and are assigned a diurnal profile. The distribution of daily averaged nitrogen oxide (NO) emissions over the Houston area highlights the spatial correlation of the NO emissions and the urban land use (Figure 4.2a). In order to isolate effects of climate change and land use change from effects of anthropogenic emissions on surface  $\text{O}_3$ , the same anthropogenic emissions were applied for current and future year simulations.

To examine the sensitivity of future change in surface  $\text{O}_3$  to future changes in climate, land use change, and anthropogenic emissions, future anthropogenic emissions are estimated by multiplying the present emissions by the growth factors for 2050s according to the SRES A1B scenario (Wigley et al., 2002). I multiplied CO,  $\text{NO}_x$ , VOC, and  $\text{CH}_4$  by factors of 1.38, 1.55, 2.01 and 1.46, respectively for the year 2053. A globally uniform  $\text{CH}_4$  concentration for current year simulations is 1700 ppb and is projected to rise to 2480 ppb by 2050 in the A1B scenario. Concentrations of CO,  $\text{NO}_x$  and VOC, which are treated on the basis of NEI-99 for current years, are various across the modeling domain in the future scenario. Initial and boundary conditions for the gas-phase variables were based on those of McKeen et al. (2002), and the laterally invariant

vertical profiles representing clean background were created from measurements collected onboard previous NASA-sponsored aircraft missions. Adjustments for boundary conditions are applied to the Houston area. In all simulations, the same chemical boundary conditions are used, which could give rise to some uncertainty in the model results.

Biogenic emissions including isoprene, other biogenic volatile organic compounds (BVOCs), and NO, are very sensitive to changes in temperature and radiation. Emission rates of biogenic compounds at standard temperature and light conditions (Figure 4.2b) have been assigned to the model grid on the basis of the Biogenic Emissions Inventory System, version 3 (BEIS3), and the Biogenic Emissions Land use Database, version 3 (BELD3), which provides distributions of 230 vegetation classes at 1-km resolution over North America (Kinnee et al., 1997). Then, biogenic emissions in all simulations are calculated online using the temperature and light-dependence algorithms from the BEIS3 (Guenther et al., 1995; Geron et al., 1994; Williams et al., 1992).

#### **4.3.5. Experiment design**

To thoroughly evaluate the impacts, multiyear ensemble simulations would be preferred. However, to run multiyear simulations with this fully coupled atmosphere–chemistry model demands huge amounts of computing time. Under this circumstance, I carefully designed the experiments on the basis of a review of literature and examination of historical O<sub>3</sub> data over the Houston. Analysis of twenty-year O<sub>3</sub> data shows that high O<sub>3</sub> episodes frequently occurred in August. Thus, an alternative way to study the impacts

on O<sub>3</sub> is to select August to represent summer season in order to avoid the limitation of computer resources. In previous studies of the impacts of anthropogenic emissions change and climate change on O<sub>3</sub> (Hogrefe et al., 2004; Liao et al., 2006; Civerolo et al., 2007; Tao et al., 2007), authors used either one summer season or five consecutive summer seasons for the present and future years to study the impacts. Thereby, I designed the experiments for three consecutive Augusts to represent the present and future scenarios respectively. In future studies, with increasingly available computational resources, multiyear runs would be the optimal way to assess the statistical significance of changes in O<sub>3</sub> caused by climate and land use change. Five experiments with different combinations of meteorological conditions, land use, and anthropogenic emissions are listed in Table 4.2. The BASE simulation, which utilized current year land use data, climate conditions, and anthropogenic emissions, is used to assess the model performance and to calculate the predicted changes in the future. Simulations CL, CL-LU, CL-EMIS, and CL-EMIS-LU, with different combinations of future climate, land use, and future anthropogenic emissions, represent future year simulations. Simulations CL-EMIS and CL-EMIS-LU were carried out to understand the potential contribution of future change in anthropogenic emissions to O<sub>3</sub> formation in the Houston area in comparison with those of climate change and land use change.

## **4.4. RESULTS AND DISCUSSION**

### **4.4.1. Evaluation of simulation results for current year conditions**

The success of the WRF/Chem model simulations was evaluated with a comparison of the model results with surface observations. The WRF/Chem simulations were driven by meteorological boundary conditions indirectly from a global climate simulation rather than a simulation of current weather and thus a direct comparison of the model output with hourly observations is not effective. Instead, the following analysis mainly focuses on an evaluation of the diurnal cycles of simulated monthly averaged daily temperature and O<sub>3</sub> concentrations and monthly averaged wind speed, which are very important to correctly simulating air quality sensitivity to climate change or land use change.

Dawson et al. (2006) have examined the sensitivity of O<sub>3</sub> concentrations to summertime climate and found that temperature had the largest effect on air-quality standard exceedances, with a 2.5 °C temperature increase leading to a 30% increase in the area exceeding the EPA standard. I evaluated the diurnal cycles of monthly averaged 2-m temperature and O<sub>3</sub> concentrations in ten major sites maintained by the Texas Commission on Environmental Quality (TCEQ) over the Houston urban area (Figure 4.3). The data sets are downloaded from

[http://www.tceq.state.tx.us/compliance/monitoring/air/monops/historical\\_data.html](http://www.tceq.state.tx.us/compliance/monitoring/air/monops/historical_data.html).

Figure 4.4a shows the diurnal evolutions of modeled and measured average 2-m temperature for August 2001–2003. The major pattern of simulated diurnal evolution of temperature is fairly similar to observations, especially during the daytime. The simulated higher nighttime temperature could be related to the uncertainties associated with parameters used in the UCM. As Tokairin et al. (2006) discussed in their work, the urban

canopy model with the inclusion of buildings tends to overestimate nighttime temperature over the urban area. Thus, I speculate that the inappropriate building-height parameters used in the UCM might lead to this overestimation. The agreement between simulations and measurements in the daytime O<sub>3</sub> concentrations is noteworthy (Figure 4.4b). However, the model clearly shows a distinct tendency to overpredict O<sub>3</sub> concentrations at night. This discrepancy is a common feature of other three-dimensional chemical transport models (Lamb, 1988; Schere and Wayland, 1989). Several possible reasons are available to explain the high O<sub>3</sub> bias during the nighttime in the WRF/Chem model. Inaccuracies in the boundary layer dynamics could lead to higher O<sub>3</sub> concentrations. One possibility could be that the bottom model layer is too thick to allow efficient deposition at night. However, there are 30 vertical model layers, with finer vertical resolution in the lower troposphere to allow the model to simulate boundary-layer processes more realistically. The bottom model layer is 17 m in all simulations. The depth of the bottom layer does not seem to be a reason causing higher nighttime O<sub>3</sub>. As a result, I do not focus on nighttime O<sub>3</sub> concentrations in the further analysis, but on the daytime and maximum 8-hr O<sub>3</sub> concentrations.

Comparison between the simulated and observed wind speeds (Figure 4.5) implies that the model has a relatively good performance in terms of simulating surface wind fields over the urban and surrounding regions. The average wind speed over the Houston urban center is around 1.8–2.1 m/s, which is quite close to observations. High wind speed in the south of the urban center is also well captured by the model. I also noticed that the model was able to capture the afternoon sea breeze over the Houston area as reflected by



the wind rose pattern for the BASE simulation (Figure 4.7a). The evaluation of the model performance gives us confidence to examine the future air quality using this coupled model.

#### **4.4.2. Regional climate change**

The occurrence of high O<sub>3</sub> concentrations during the summer is strongly determined by meteorological processes within the PBL. I briefly summarize the changes in the meteorological fields over the period between 2000s and 2050s on the basis of two simulations: CL-LU, which considers changes in both climate and land use, and BASE. In these simulations, anthropogenic emissions and chemical boundary conditions were fixed at the levels used for the current years, while the calculation of biogenic emissions took into account the effects of temperature and radiation changes under different climates. Meteorological conditions that are known to be associated with high O<sub>3</sub> concentrations are high mixing heights (Rao et al., 2003), low wind speeds, and high temperatures (Ordonez et al., 2005). Here I discuss details of climate change, particularly those climate variables that are pertinent to O<sub>3</sub> chemistry.

Modeling studies by Sillman and Samson (1995) and Aw and Kleeman (2003) have shown that summertime O<sub>3</sub> concentrations increase as temperature increases. The model simulates a significant surface temperature rise between 2050s and 2000s. The highest increase in surface temperature during 12–18 LST occurs over the Houston urban area, as indicated by Box A (here, I call it “zone A”), with an average increase of 3.3°C (Figure 4.6a). On average, the surface temperature is predicted to increase by about 2 °C. This increase is also clearly apparent in CCSM3 outputs with an increase of 1.5 °C in 2-m

temperature in most parts of Texas. This is not unexpected, because incorporating a detailed UCM into the regional model at a high spatial resolution can result in an increase in surface temperature which is somewhat higher than 2-m air temperature during the daytime. Figure 4.6b also shows that under projected future conditions considering changes in climate and land use, the Houston urban area tends to become drier (Figure 4.6b). Lin et al. (2007) have shown that urban growth tends to decrease the relative humidity because of the increase in urban land surface which has less moisture than vegetated surfaces. Conversely, more water vapor coming from the warming ocean is responsible for higher water vapor mixing ratio along coastal regions. I also noticed that an increase in Planetary Boundary Layer Height (PBLH) occurs in the urban areas, with a maximum increase of 250 m and an average increase of 135 m (Figure 4.6c). Civerolo et al. (2007) suggest that extensive urban growth in the metropolitan area has the potential to increase afternoon near-surface temperature by 0.6 °C and increase PBLH by more than 150 m. Here, the patterns in the differences of PBLH and surface temperature are identical. Moreover, under future climate conditions, I also see a daytime decrease in wind speeds with more reduction in the urban center (Figure 4.6d). The latter is attributed to the increase in roughness length associated with urbanization. The largest decrease of near-surface wind speeds is seen over the urban area (zone A) and southwest of the urban center as indicated by Box B (here, I call it “zone B”). The wind direction also changes in response to changes in the distribution of temperature, relative humidity, and surface roughness length. An evaluation of the wind rose patterns (Figure 4.7) indicates that the Houston area has more easterly winds in the afternoon because of future changes in

climate and land use for the 2050s. It can be explained that as wind passes through the urban area, the speed is slowed down because of high roughness length over the extended urban area. More urban land use leads to a decrease of near-surface wind speed in zone B. However, it should be pointed out that there is no significant difference in wind speeds in the northwest and northeast of the modeling domain.

#### **4.4.3. Impact on regional distribution of photooxidants**

Future meteorological conditions observed in the simulations are favorable for  $O_3$  formation. Increases in surface temperatures, reductions in wind speeds, and changes in boundary layer depths act to change  $O_3$  levels through affecting the regional distribution of  $O_3$  precursors such as  $NO_x$  and VOCs from anthropogenic and biogenic sources.

Figure 4.8a displays the difference in simulated  $NO_x$  mixing ratios between the future and current years (assuming that anthropogenic emissions remain constant). A decrease in near-surface  $NO_x$  mixing ratios in the northern part of the Houston urban area and the northwest of the urban center can be attributed to increased PBLH. An increase in  $NO_x$  mixing ratio occurs over the southern part of the urban area and along the Bay area, associated with emission sources and decreased PBLH. The oxidation products of  $NO_x$ , such as nitric acid ( $HNO_3$ ), are dependent on the  $NO_x$  concentrations. Figure 4.8b illustrates an increase in  $HNO_3$  in the regions with high  $NO_x$  levels, and the highest increase of  $HNO_3$  is mainly found along the Bay area and some parts of the urban area. The mixing ratio of peroxyacetyl nitrate (PAN) decreases in the northwest of the modeling domain (Figure 4.8c), which is mainly due to the increase in temperature that

results in an enhanced thermal decomposition of PAN. Apart from the increased temperature, the presence of higher NO<sub>x</sub> levels along coastal regions due to emission sources and reduced near-surface wind speeds as shown in Figure 4.6d, favors PAN formation via chemical reactions.

Carbonyl compounds can undergo photochemical reactions that will result in additional production of organic and hydrogen radicals, and produce more O<sub>3</sub>. As seen in Figure 4.8d, over much of the modeling domain, formaldehyde (HCHO) increases as temperature increases in the future. This can be explained that the distribution of HCHO strongly depends on isoprene emissions, of which biogenic sources are predominant (Wert et al., 2003). Under future warm climate conditions, biogenic emissions are expected to increase. The model predicts a 20% increase in biogenic emissions of isoprene in response to future changes in temperature and radiation. It can be seen that the highest increase in HCHO concentrations mostly lies in rural regions, in particular, in the east of the Houston area, where the land surface is mostly covered by forests (Gulden and Yang, 2006). Therefore, the significant increase in HCHO is expected to promote additional production of O<sub>3</sub> in the areas far from the urban center. However, it should be noted that future change in vegetation types is not considered in this study.

#### **4.4.4. Changes in surface O<sub>3</sub>**

The analysis presented in section 4.4.3 implies that climate and land use change can cause significant changes in predicted concentrations of NO<sub>x</sub>, HCHO, HNO<sub>3</sub>, and PAN, which can further affect O<sub>3</sub> formation in the Houston area. Figure 4.9a depicts a spatial

map of the difference in  $O_3$  concentrations during the afternoon (12 to 18 LST) between the future and current year simulations. In the future year simulations, the anthropogenic emissions were fixed at the current level, while the urban land use change was considered (Table 4.2). For the 2050s, changes in summertime average daytime  $O_3$  concentrations range from -2 to 8 ppb. The largest increases of 4–8 ppb are found over the surrounding regions of the urban center and zone B. However,  $O_3$  concentrations are predicted to decrease in the northwest modeling domain. Analysis of model results suggests that this decrease is caused by the decreased water vapor mixing ratio, changed near-surface wind direction (discussed in Subsection 4.4.2), and the low levels of  $NO_x$ . Because of more easterly winds in the future, fewer emissions are transported to northwest Houston area from the emission sources. The increased water vapor mixing ratio and decreased wind speeds along the coast which is closer to the VOC and  $NO_x$  source regions, act to favor the formation of  $O_3$ . In the areas with high PAN levels, the  $O_3$  concentrations are still high (Singh et al., 1985).

I also find increasing isoprene emissions in response to future climate change tend to promote more  $O_3$  formation in the modeling domain. In fact, this result is very sensitive to whether the reaction products of isoprene, isoprene nitrates, represent a terminal or temporary sink for  $NO_x$  (Horowitz et al., 2007). Wu et al. (2008) found little climate-driven  $O_3$  change in the southeast of U.S. and they attributed this to the role isoprene nitrates play as a terminal sink for  $NO_x$ . In this study, I used the RADM2 chemical mechanism, which only includes a very simple scheme of isoprene. Thus, the reaction

products of isoprene, organic nitrates, are more likely to be a temporary sink for NO<sub>x</sub> in the simulations.

Because the U.S. NAAQS for 8-hr O<sub>3</sub> concentration is set at 84 ppb, model-predicted exceedances of this threshold are of particular importance when assessing the effects of climate change and land use change on O<sub>3</sub> air quality. To analyze the changes in the frequency of predicted days with unhealthy O<sub>3</sub> concentrations (referred to as extreme O<sub>3</sub> days hereafter), the number of days for which the predicted daily maximum 8-hr O<sub>3</sub> concentrations exceeded 84 ppb was plotted in Figure 4.9b. The predicted distribution of the number of days with the maximum daily 8-hr O<sub>3</sub> concentrations larger than 84 ppb matches the pattern of increased O<sub>3</sub> over the modeling domain. There is a predicted increase of 4–5 days in the number of days with elevated O<sub>3</sub> with the largest increase over the surrounding regions of the urban center and zone B. Overall, the WRF/Chem simulations of O<sub>3</sub> concentrations utilizing the WRF downscaled 2050s A1B regional climate fields show an increase in summer average daily maximum 8-hr O<sub>3</sub> concentrations and an increase in the number of extreme O<sub>3</sub> days over the Houston area due to future changes in climate and land use.

#### **4.4.5. Contributions of climate change and land use change to O<sub>3</sub> changes**

Sensitivity simulations with the utilization of current and future land use data (CL and CL-LU) are used to discern the contribution of climate change and that of urban land use change to O<sub>3</sub> formation. Figure 4.10a shows that urban land use change promotes an

increase of 1–4 ppb in average afternoon (12 to 18 LST) O<sub>3</sub> concentrations over much of the modeling domain in addition to climate change. Moreover, the higher O<sub>3</sub> caused by the land use change is associated with an increase of 1–3 days per month (August) in the number of extreme O<sub>3</sub> days (Figure 4.10b). The effects of land use change on both O<sub>3</sub> concentrations and extreme O<sub>3</sub> days are the most significant over the surrounding regions of the urban center, but not exactly over the urban center, which is consistent with Civerolo et al.'s (2007) results. In the core urban areas, NO<sub>x</sub> emissions do not contribute to a significant increase in O<sub>3</sub> concentrations, but they do lead to increased O<sub>3</sub> formation in downwind areas. I attribute this increase in the spatial extent of VOC-limited regions to increasing urbanization. To be consistent with the future expansion of urban land use, the VOC-limited regions would be extended correspondingly.

Figure 4.11 depicts the changes in average daily maximum 8-hr O<sub>3</sub> concentrations due to climate change, land use change, and combined change. It can be seen that climate change alone causes –6–6 ppb change in O<sub>3</sub> (Figure 4.11a), and significant increases are found along the coast because of high NO<sub>x</sub> emissions and warm temperature. However, climate change alone does lead to a decrease in surface O<sub>3</sub> concentrations in areas further from the urban center (e.g., the northwest of the urban area or the rural areas). I ascribe this to the decreased water vapor mixing ratio and changed wind direction. When only considering the effects of future land use change (Figure 4.11b), a 2–6 ppb increase in daily maximum 8-hr O<sub>3</sub> concentrations is found over much of the modeling domain with the largest increase located in the surrounding areas of the urban center. Furthermore, additional analysis indicates that land use change induces more O<sub>3</sub> formation over the

areas (e.g., northwest of the domain) where climate change alone decreased O<sub>3</sub> concentrations. As the effects of both climate and land use changes are taken into account in the simulations, daily maximum 8-hr O<sub>3</sub> concentrations can increase up to 12 ppb in the 2050s (Figure 4.11c).

I also plotted the frequency distributions of the simulated daily O<sub>3</sub> maxima during August over zones A and B. As I expected, because of the future changes in climate and land use, the frequency is shifted toward higher values (Figure 4.12). It seems that zone B is more likely to be affected by climate change, while zone A displays a pattern highly correlated with the land use change. Climate change alone leads to an increase in days with daily maximum 8-hr O<sub>3</sub> at 65 ppb in zone B. This results in a significant increase of the number of days with near-surface O<sub>3</sub> concentrations higher than 84 ppb in this regions, as was discussed above.

The above analysis reveals that the impacts of climate change and land use change on O<sub>3</sub> differ across the modeling domain. The contributions of climate change and land use change are illustrated in a bar chart of changes in summertime average daily maximum 8-hr O<sub>3</sub> concentrations for zones A and B (Figure 4.13). It can be seen that the effects of climate change alone account for an increase of 2.6 ppb in daily maximum 8-hr O<sub>3</sub> concentrations in zone A. The land use change has more influence near the urban area than the climate change, with an additional increase of 1ppb in daily maximum 8-hr O<sub>3</sub> concentrations. The combined effects of climate and land use change on daily maximum 8-hr O<sub>3</sub> concentrations can be up to 6.2 ppb. However, in zone B, which is more likely



affected by the increased water vapor mixing ratio, reduced wind field, changed wind direction, and increased temperature, the impacts of climate change are stronger than those of future urban land use change.

As discussed above, changes in meteorological variables have different impacts in different locations. To further quantify these impacts, a statistical correlation technique is applied to identify the contributions of different meteorological variables to  $O_3$  formation due to climate change and land use change, respectively. A simple regression test was conducted and the correlation coefficients between  $O_3$  concentration and these meteorological variables are summarized in Table 4.3. It is clear that near-surface temperature, wind speed, and humidity are very important meteorological factors influencing the variation in  $O_3$  levels in the Houston area. I observed that temperature and water vapor mixing ratio have more influence on  $O_3$  concentrations in zone B under future A1B climate scenario, notwithstanding the correlation between  $O_3$  concentration and water vapor mixing ratio is negative. When the future land use change is considered in the simulations, the correlation between  $O_3$  concentration and PBLH increases indicating the important impact of land use change on the air quality over the urban areas. To a large extent, the correlation coefficients between temperature or water vapor mixing ratio and  $O_3$  concentration are not affected in zone A. However, the coefficients are somewhat different in zone B. This further indicates that zone B is affected by meteorological variables to a larger degree than is zone A.

The analysis above suggests that climate change and land use change have different

impacts in different regions. Therefore, while many previous studies have pointed out the potentially important contribution of future climate change and anthropogenic emissions to O<sub>3</sub> air quality for future decades, the results presented here imply that the effects of land use change may be at least equally important to the changing climate when planning for the future attainment of the NAAQS.

#### **4.4.6. Sensitivity of surface O<sub>3</sub> to future anthropogenic emissions**

The analysis presented in the previous subsections focused on determining the effects of climate and land use change on summertime O<sub>3</sub> concentrations over the Houston area in the absence of changes in anthropogenic emissions within the modeling domain. Several studies have investigated the effects of increasing global and regional emissions on O<sub>3</sub> air quality using regional climate and air quality models (Fiore et al. 2002, 2005; Tagaris et al., 2007; Tao et al., 2007). It is of particular interest to compare the effects of climate and land use change to those caused by change in anthropogenic emissions. For brevity, I only did sensitivity simulations for the year 2053 using the current and future land use data (CL-EMIS and CL-LU-EMIS).

Figure 4.14 displays the percentage of the number of days in August with the daily maximum 8-hr O<sub>3</sub> concentrations larger than 84 ppb over the Houston urban area. It can be seen that climate change induces around an 8% increase in the extreme O<sub>3</sub> days over the urban area. When combined with the land use change, there is an additional 4% increase over the Houston urban area. There are more extreme O<sub>3</sub> days under future conditions with the consideration of climate and land use change in zone A than those in

zone B. In zone B where the increased O<sub>3</sub> concentrations are relatively large, the increase in extreme O<sub>3</sub> days is not as significant as that in zone A. The anthropogenic emissions sensitivity experiment shows that the impacts of future change in anthropogenic emissions on extreme O<sub>3</sub> days are on the same order of those induced by climate and land use change. Still, zone A is more affected by changes in anthropogenic emissions than zone B, since the former is a source area for anthropogenic emissions. Therefore the findings presented above may have potentially important implications for policy making concerning population health.

#### **4.5. CONCLUSIONS**

This paper described the application of a coupled land–atmosphere–chemistry modeling system to understand air quality in future decades over the Houston area. The effects on surface O<sub>3</sub> caused by future climate change under future A1B scenario and land use change are at least equally important in the Houston area. An increase in spatially and temporally average summertime daily maximum 8-hr O<sub>3</sub> is found over most parts of the modeling domain, with a 6.2 ppb increase over the Houston area in the absence of changes in anthropogenic emissions. Climate change induces about an 8% increase in the extreme O<sub>3</sub> days and land use change adds an additional 4% increase over the Houston area. I also found that impacts of climate change and land use change on O<sub>3</sub> concentrations differ across the various areas of the domain. While the core urban area (zone A) is highly influenced by predicted land use change, suburban areas (e.g., zone B) are more likely affected by predicted climate change. An increase in the number of

extreme high O<sub>3</sub> days is found near the urban area, but not exactly in the urban center. This might be expected since O<sub>3</sub> is formed downwind of anthropogenic emission sources (except when weather is stagnant).

Additional sensitivity simulations for the year 2053 investigating the relative impacts of changes in regional climate, anthropogenic emissions, and land use on extreme O<sub>3</sub> days suggest that future anthropogenic emissions change also plays an important role as the climate and land use change does. In this study, I did not specifically address the effects of biogenic emissions on future changes in O<sub>3</sub> formation. It should also be pointed out here that the land use projections used in this study are relatively conservative, since they extend only as far as 2030, while the future climate conditions are from 2050. As both the population and the urban areas are expected to continue growing from 2030 to 2050, the urbanization impacts on O<sub>3</sub> are likely to be greater than reported in this study. Future studies that utilize a wide range of scenarios for climate, land use, and emissions to quantify the relative impacts of different factors on regional-scale air quality in a more comprehensive manner are needed.

#### **4.6. ACKNOWLEDGMENTS**

This work is supported by the U.S. EPA STAR program (Grant No. RD83145201), the National Center for Atmospheric Research (NCAR) Advanced Study Program, the NCAR FY07 Director Opportunity Fund, and NASA Headquarters under the NASA Earth and Space Science Fellowship Program (Grant No. NNX07AO28H). The NCAR is operated by the University Corporation for Atmospheric Research under sponsorship of the National Science Foundation. I am indebted to the land team at the NCEP for

providing us the MODIS land cover data set and to Mukul Tewari for making the current land use data available to us. Shiguang Miao is thanked for helping set up the UCM in the WRF/Chem model. I thank Mary Barth, Xuexi Tie, Alex Guenther, Jerome Fast, William Vizuete, Gregory Frost, Steven Peckham, George Grell, Jonathan Pleim, Alma Hodzic, Peggy Lemone and Susanne Grossman-Clarke for their valuable discussions during the course of this work. The computing resources are provided by the Texas Advanced Computing Center.

Table 4.1. Surface parameterizations for each land use category<sup>a</sup>

Urban Type	Urban Fraction	Building Height (m)	Roughness Length (m)	Sky View Factor	Building Volumetric Parameter ( $\text{m}^{-1}$ )	Normalized Building Height (m)	Anthropogenic Heat ( $\text{cal cm}^{-1} \text{cm}^{-1}$ )
Industrial or commercial	0.95	10.	1.0	0.48	0.4	0.50	90.0
High-intensity residential	0.9	7.5	0.75	0.56	0.3	0.40	50.0
Low-intensity residential	0.5	5.	0.5	0.62	0.2	0.30	20.0
<sup>a</sup> Based on work of Chen et al. (2004)							

Table 4.2. List of all simulations<sup>a</sup>

Simulation	Simulation Period	Emissions	Land Use and Land Cover
Base	August 2001–2003	NEI-99 plus BEIS3	MODIS land cover plus NLCD land use
CL	August 2051–2053	NEI-99 plus BEIS3	MODIS land cover plus NLCD land use
CL-LU	August 2051–2053	NEI-99 plus BEIS3	MODIS land cover plus future land use
CL-EMIS	August 2053	future emissions plus BEIS3	MODIS land cover plus NLCD land use
CL-LU-EMIS	August 2053	future emissions plus BEIS3	MODIS land cover plus future land use

<sup>a</sup>NEI-99, U.S. EPA's 1999 National Emissions Inventory; BEIS3, Biogenic Emissions Inventory System, version 3; MODIS, Moderate Resolution Imaging Spectroradiometer; NLCD, National Land Cover Database.

Table 4.3. Correlation studies between O<sub>3</sub> concentrations and the main meteorological variables

O <sub>3</sub>	Zone	2-m Temperature	2-m Water Vapor Mixing Ratio	10-m Wind Speed	PBLH <sup>a</sup>
CL simulations	zone A	0.53	−0.63	−0.79	0.19
CL simulations	zone B	0.83	−0.89	−0.62	0.79
CL-LU simulations	zone A	0.51	−0.64	−0.60	0.59
CL-LU simulations	zone B	0.74	−0.92	−0.65	0.78
<sup>a</sup> Planetary boundary layer height.					



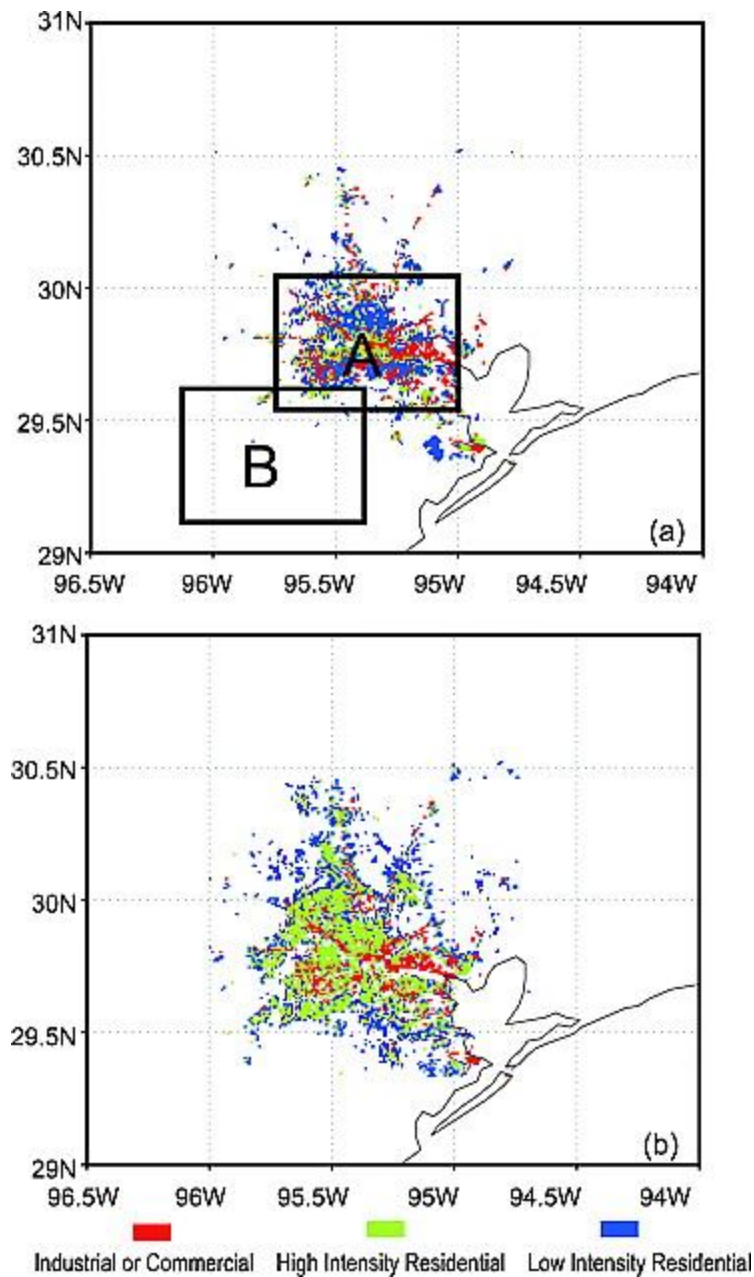


Figure 4.1. The three urban land use categories, industrial or commercial (red), high-intensity residential (light green), and low-intensity residential (blue), for (a) current years (2000s) defined from the NLCD database and a total area of urban land use of 3264 km<sup>2</sup> and (b) future years (2050s) defined on the basis of projected population growth in 2030 and a total urban land use area of 5293 km<sup>2</sup>. Box A denotes the core urban area, and box B is for the suburban area.

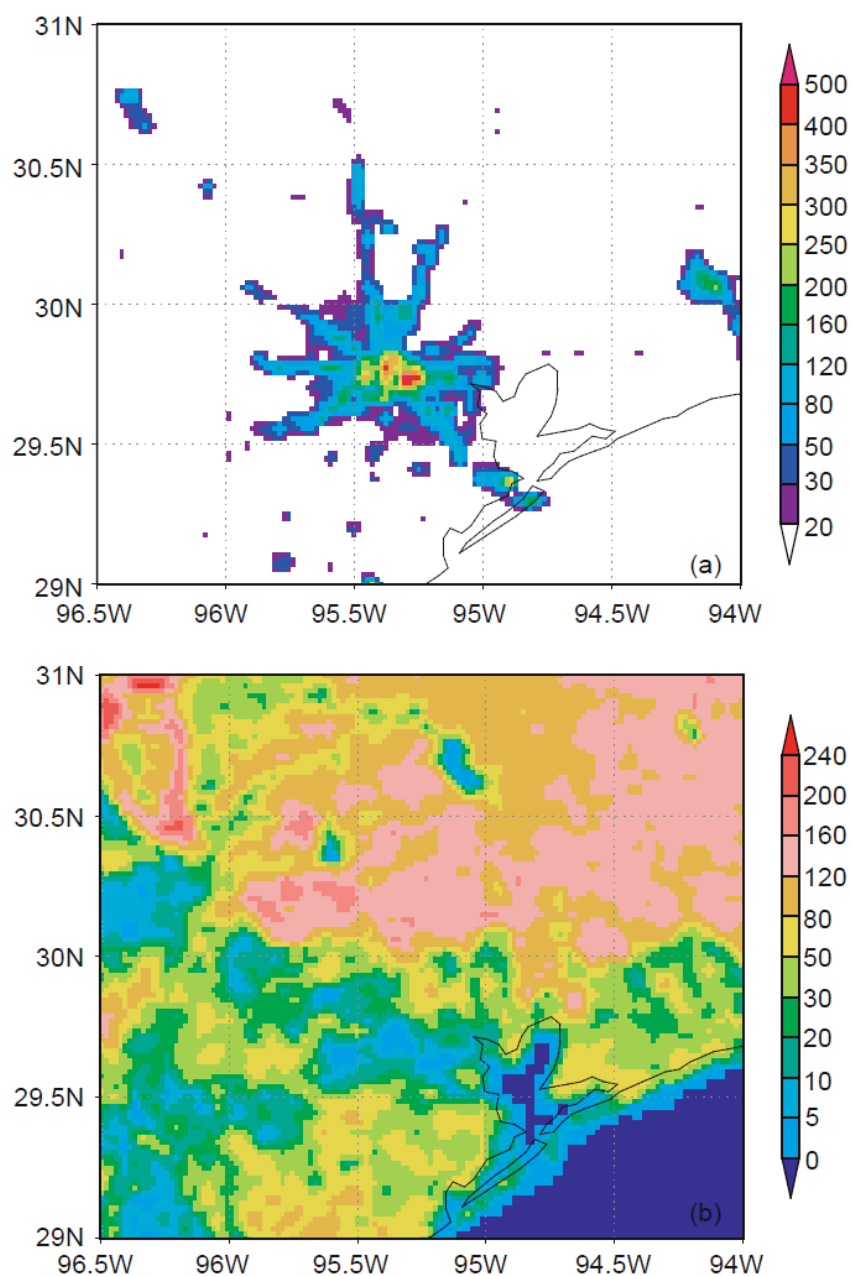


Figure 4.2. (a) Daily average anthropogenic NO emissions in summer ( $\text{mol km}^{-2} \text{hr}^{-1}$ ) and (b) normalized biogenic emissions of isoprene generated by the BEIS3 ( $\text{mol km}^{-2} \text{hr}^{-1}$ ). The normalized isoprene emissions are estimated at standard conditions of light and temperature ( $30^\circ \text{C}$  and  $1000 \mu\text{mol}$  photosynthetically active radiation (PAR)).

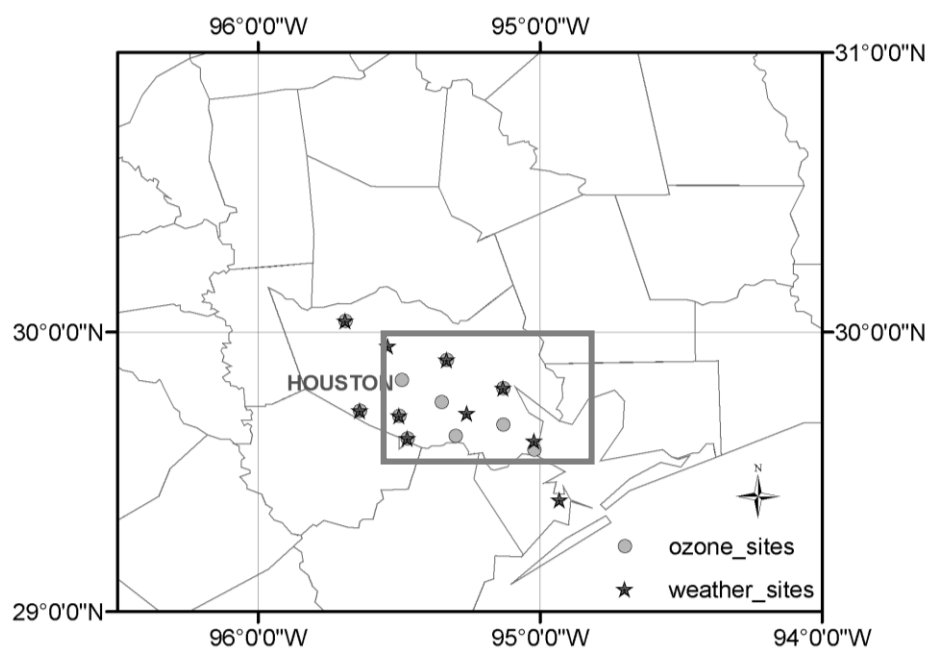


Figure 4.3. Map showing several surface observation stations used for model evaluation.

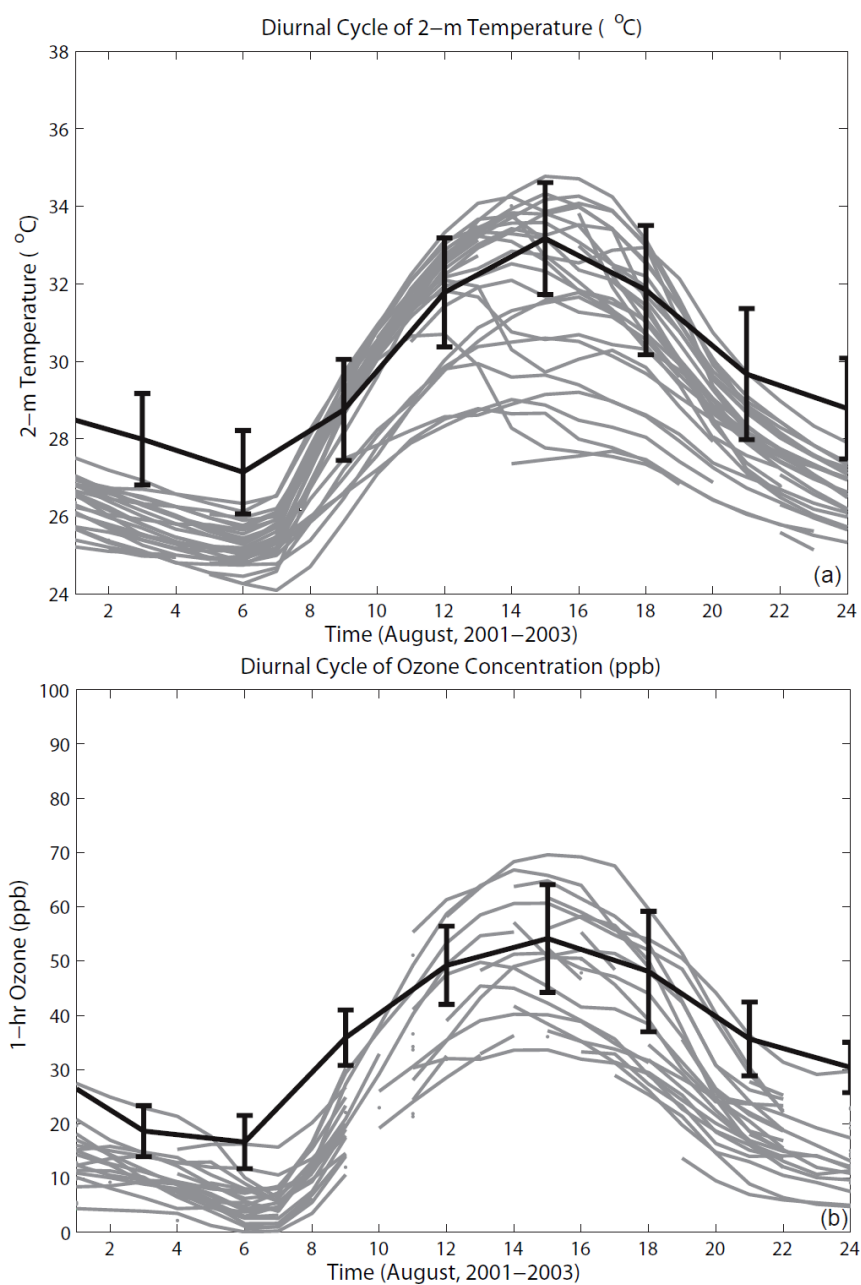


Figure 4.4. Observed and simulated (a) 2-m temperature and (b) O<sub>3</sub> concentrations during August 2001–2003. Gray lines represent the observations averaged over the sites shown in Figure 4.3 with one line representing one day, and black lines represent the simulated results for 31 days in August.

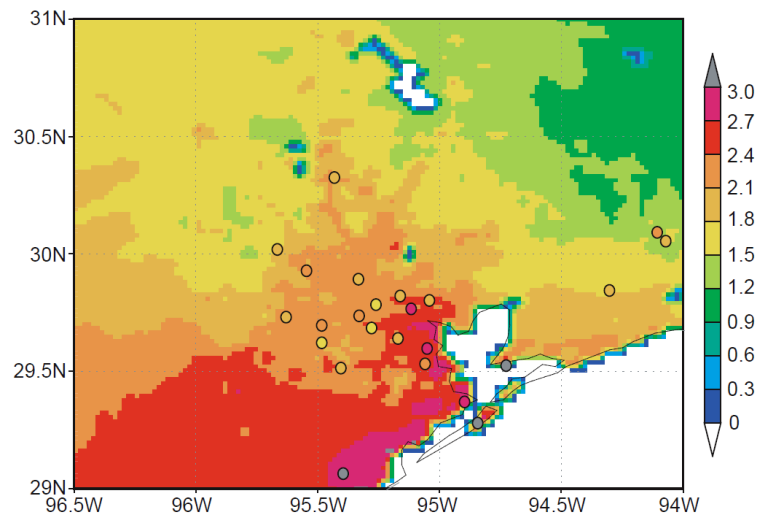


Figure 4.5. Observed (marked by circles) and simulated (shaded colors) wind speeds in Houston and surrounding areas.

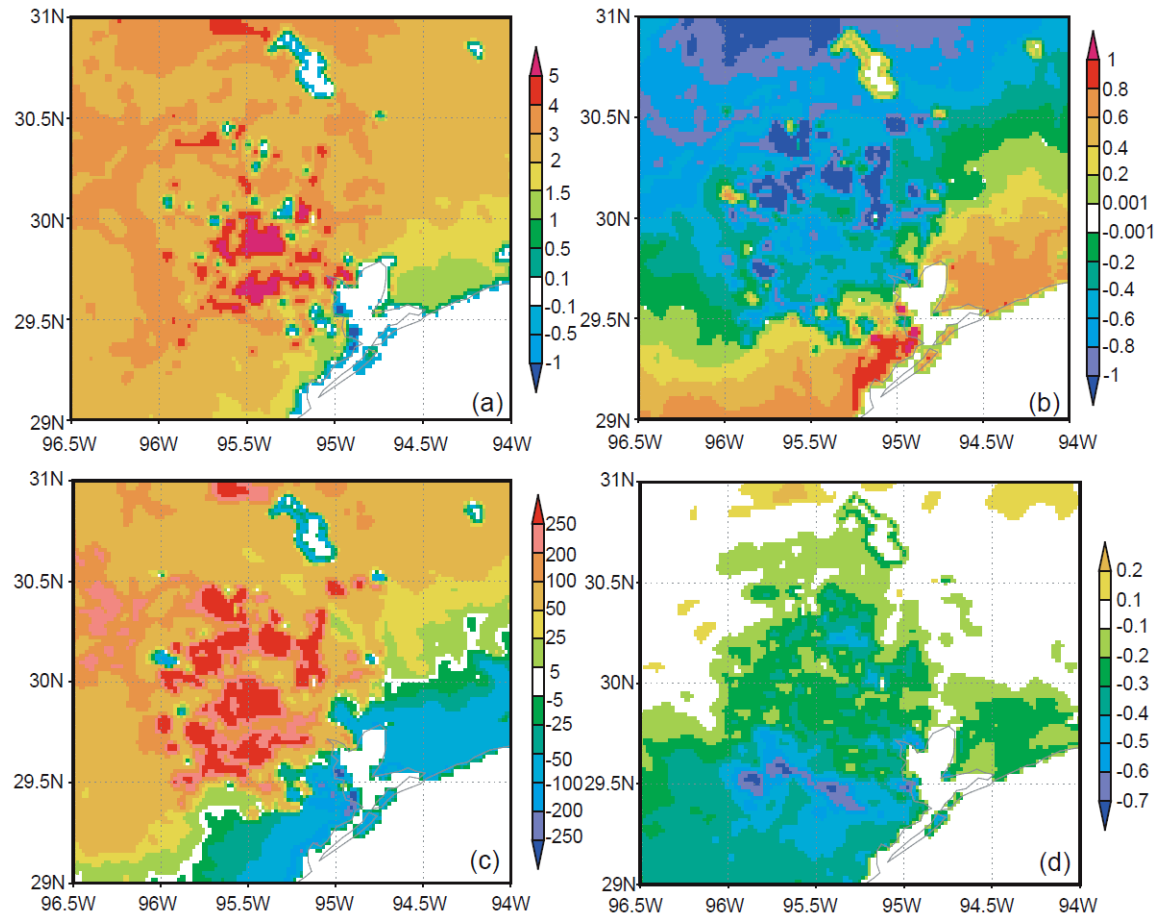


Figure 4.6. Simulated differences in afternoon (1200 to 1800 LST) (a) temperature ( $^{\circ}\text{C}$ ), (b) 2-m water vapor mixing ratio ( $\text{kg kg}^{-1}$ ), (c) planetary boundary layer height (PBLH) (m), and (d) 10-m wind speed ( $\text{m s}^{-1}$ ) between CL-LU and BASE simulations for the month of August (ocean is masked out in all plots). CL-LU represents the future year simulations with the consideration of land use change, and BASE represents the present year simulations.

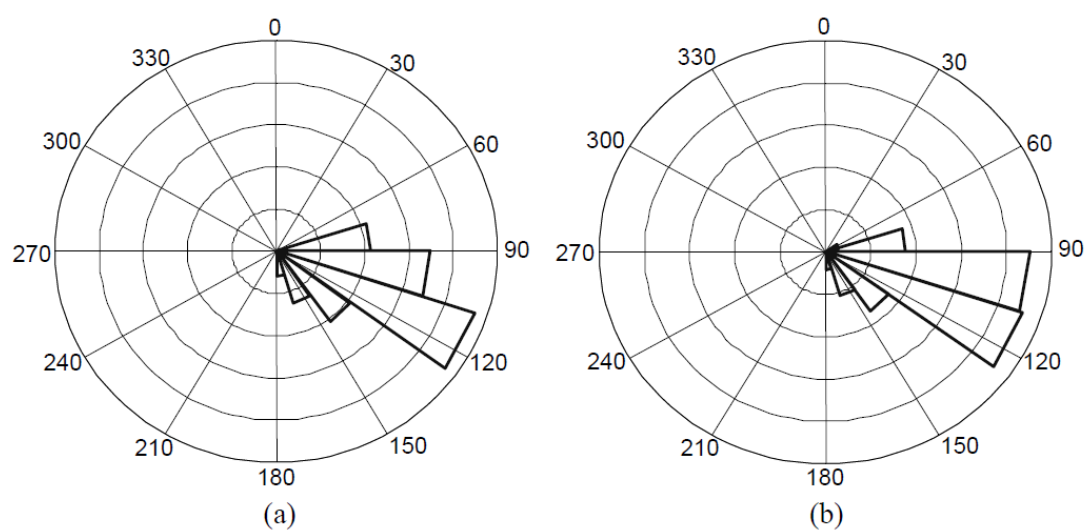


Figure 4.7. Simulated wind directions during the afternoon (1200 to 1800 LST) for (a) August 2001–2003 (BASE) and (b) August 2051–2053 (CL-LU).

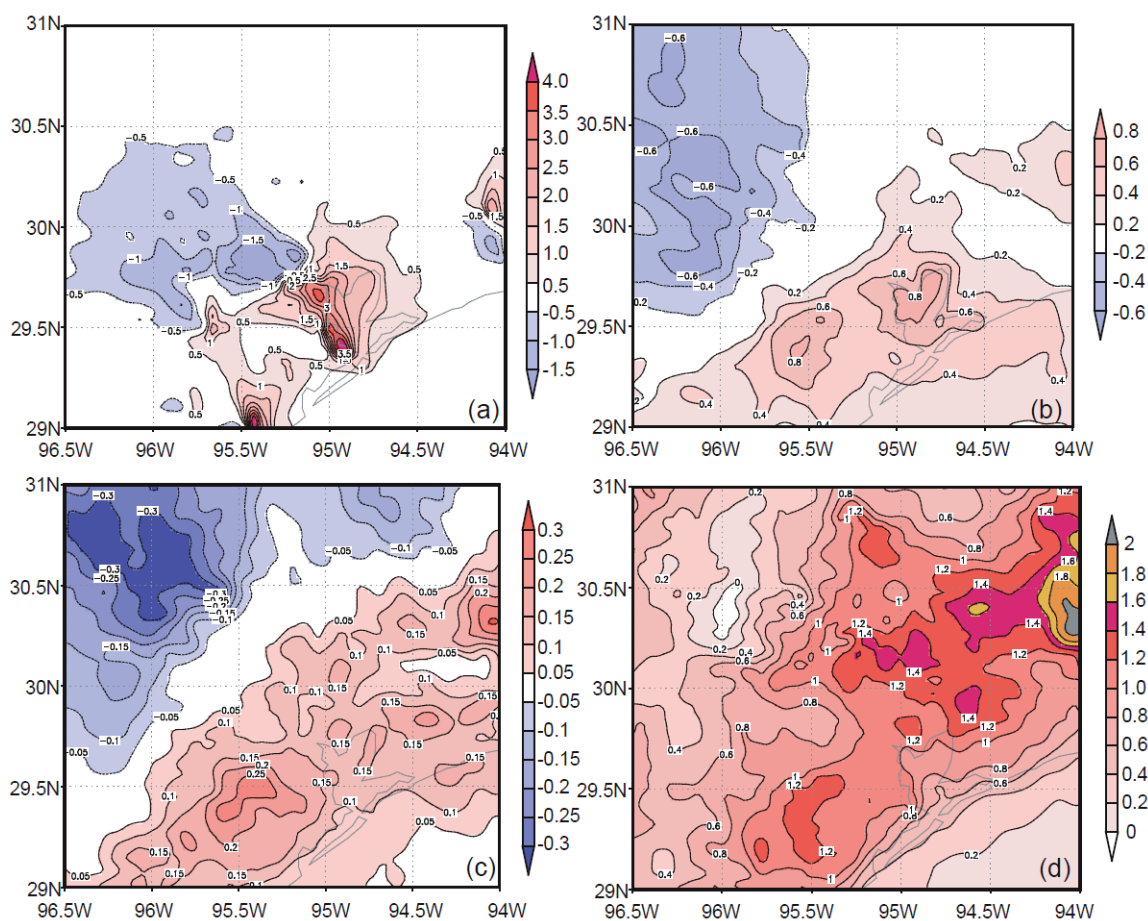


Figure 4.8. As in Figure 4.6 but for the differences in mixing ratios of (a) NO<sub>x</sub>, (b) HNO<sub>3</sub>, (c) PAN and (d) HCHO. (ppb).



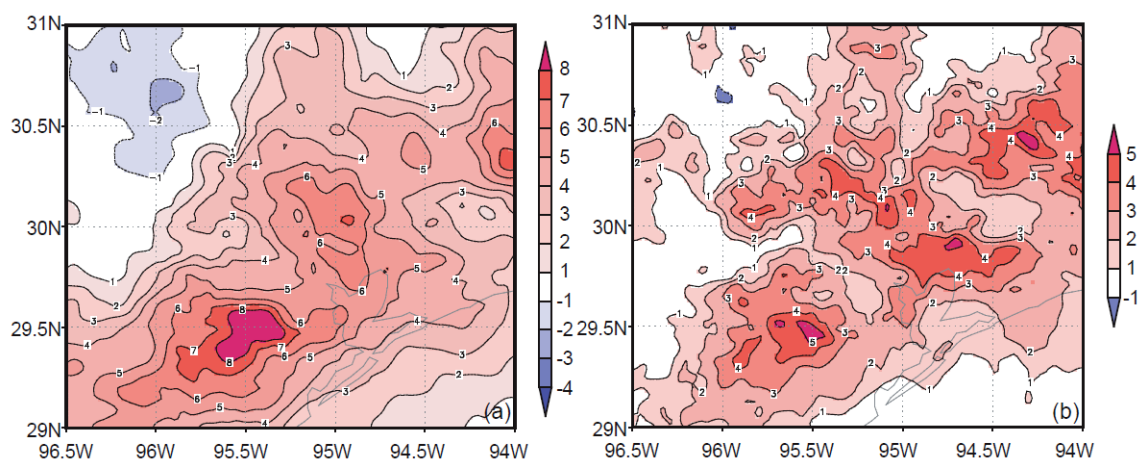


Figure 4.9. As in Figure 4.6 but for the differences in (a)  $O_3$  concentrations (ppb) and (b) the number of days with the daily maximum 8-hr  $O_3$  concentrations larger than 84 ppb.

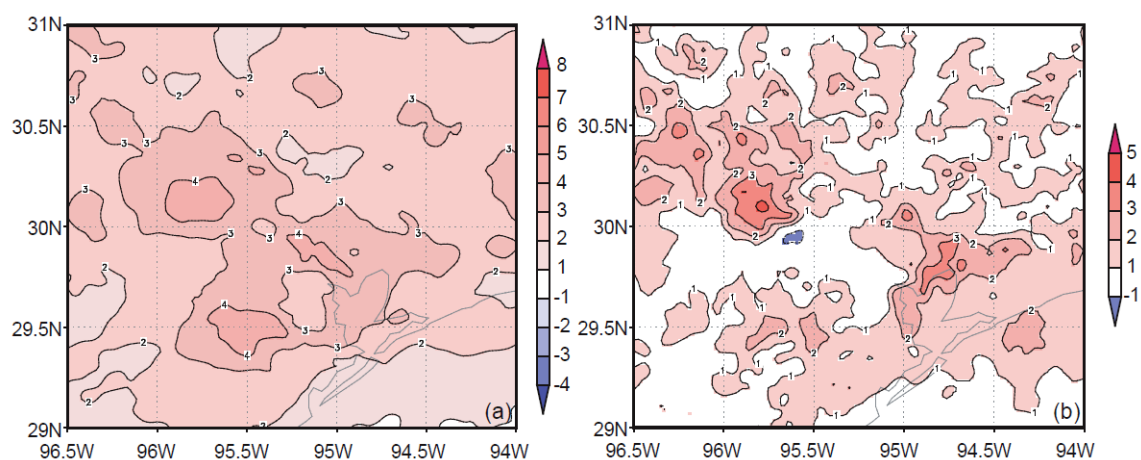


Figure 4.10. Simulated differences in (a) afternoon (1200 to 1800 LST) O<sub>3</sub> concentrations and (b) the number of days with the daily maximum 8-h O<sub>3</sub> concentrations larger than 84 ppb between CL-LU and CL simulations for the month of August. CL represents the future year simulations using the present year land use data.

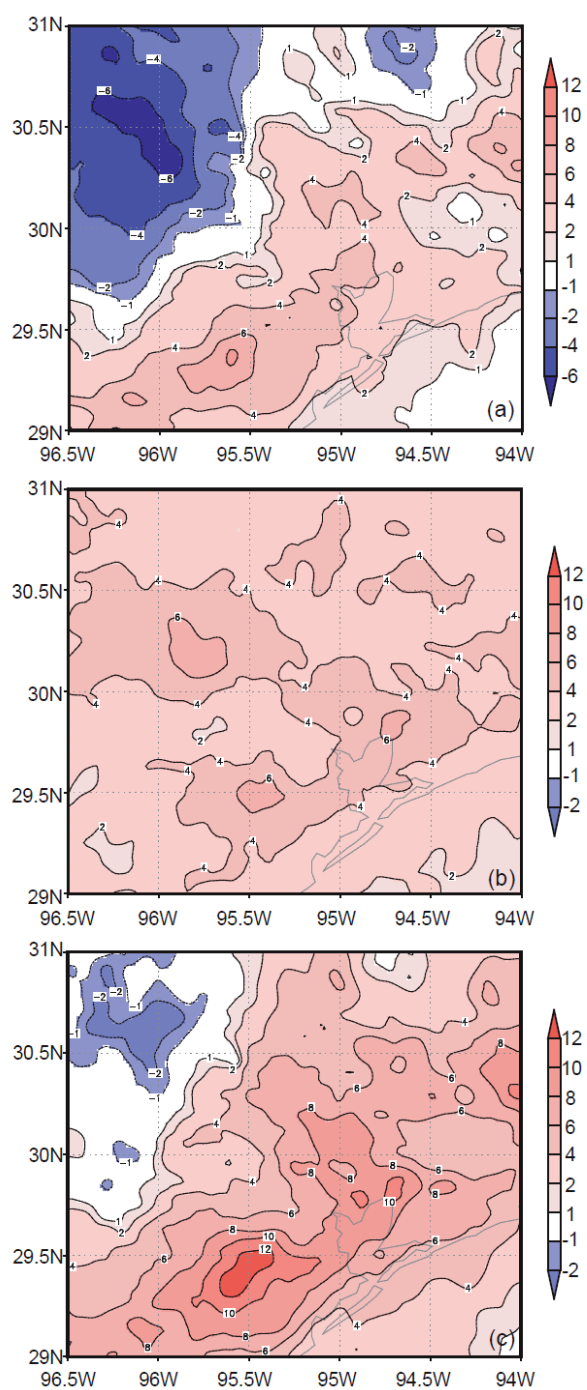


Figure 4.11. Changes in average daily maximum 8-h  $O_3$  concentrations for (a) climate change effect (difference between CL and BASE simulations), (b) land use change effect (difference between CL-LU and CL simulations), and (c) combined climate change and land use change effect (difference between CL-LU and BASE simulations).

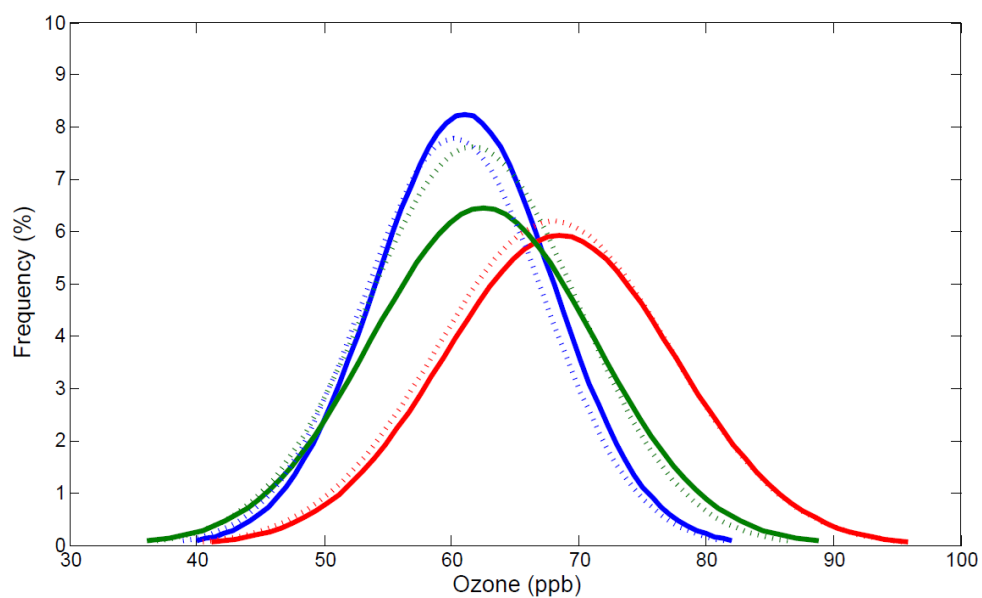


Figure 4.12. Frequency distributions of the simulated daily maximum 8-h  $O_3$  concentrations averaged over zone A (dashed lines) and zone B (solid lines) during August for BASE (blue), CL (green), and CL-LU (red) simulations.

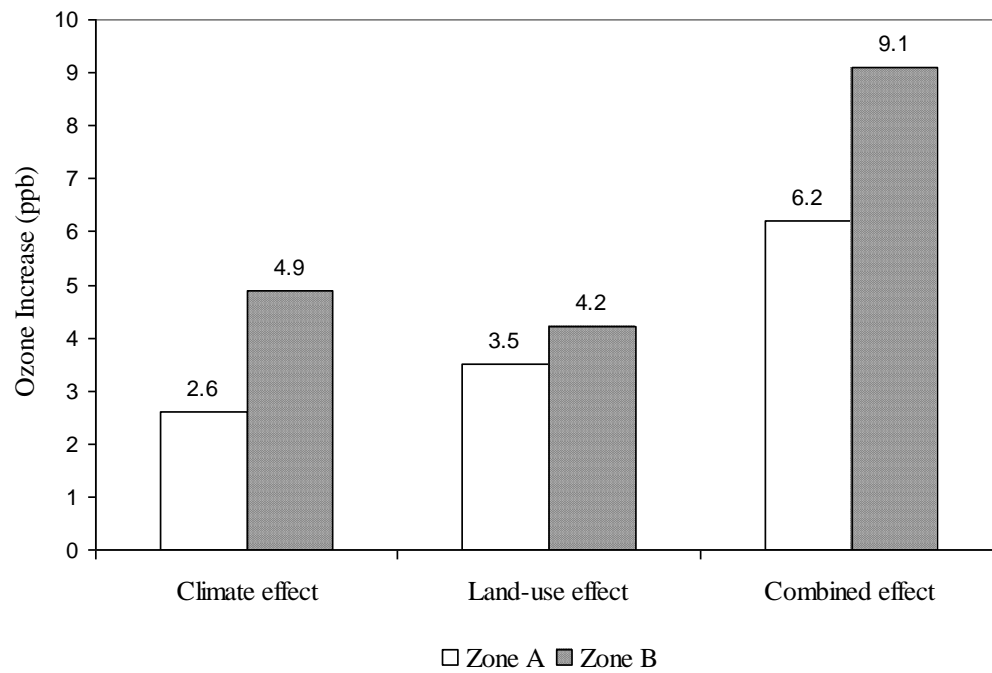


Figure 4.13. Spatially averaged contributions of climate-induced change, land use-induced change, and combined climate and land use change from the 2000s to the 2050s to changes in daily maximum 8-h  $O_3$  concentrations.

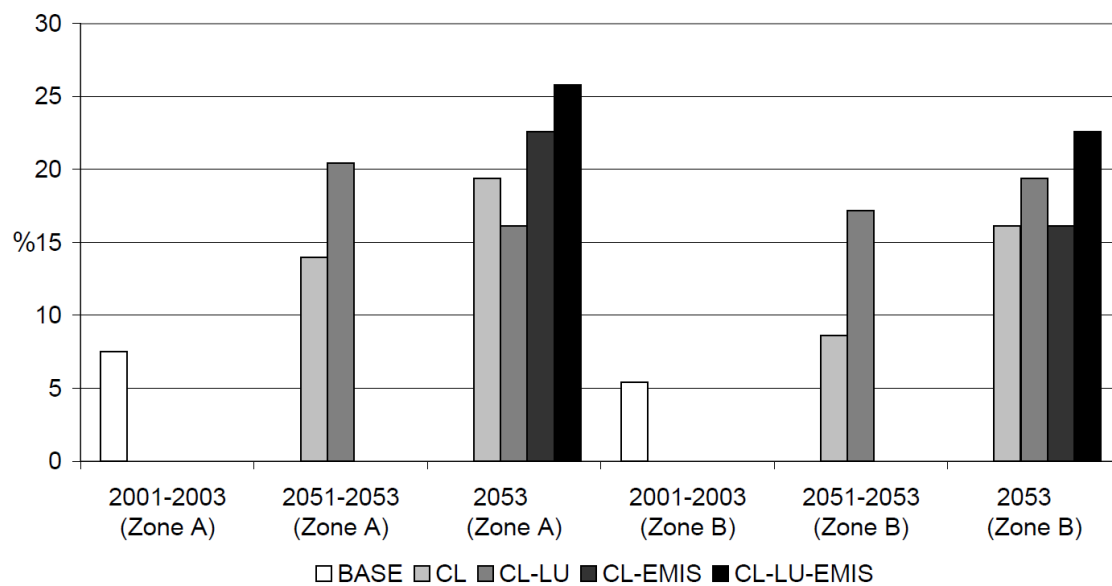


Figure 4.14. The percentage of the number of days with the daily maximum 8-h O<sub>3</sub> concentrations larger than 84 ppb over zone A and zone B. CL-LU-EMIS represents future year simulations with the consideration of future anthropogenic emissions change.

## Chapter 5: Sensitivity of Biogenic Secondary Organic Aerosols to Future Climate Change at Regional Scales<sup>3</sup>

### 5.1. ABSTRACT

Biogenic emissions and secondary organic aerosols (SOA) are strongly dependent on climatic conditions. To understand the SOA levels and their sensitivity to future climate change in the United States (U.S.), I present a modeling work with the consideration of SOA formation from the oxidation of biogenic emissions with atmospheric oxidants (e.g., OH, O<sub>3</sub>, and NO<sub>3</sub>). The model simulation for the present-day climate is evaluated against satellite and ground-based aerosol measurements. Although the model underestimates aerosol concentrations over the northwestern U.S. due to the lack of fire emissions in the model simulations, overall, the SOA results agree well with previous studies. Comparing with the available measurements of organic carbon (OC) concentrations, I found that the amount of SOA in OC is significant, with the ratio ranging from 0.1 to 0.5/0.6. The enhanced modeling system driven by global climate model output was also applied for two three-year one-month simulations (July 2001–2003 and 2051–2053) to examine the sensitivity of SOA to future climate change. Under the future two emissions scenarios (A1B and A2), future temperature changes are predicted to increase everywhere in the U.S., but with different degrees of increase in different regions. As a result of climate change in the future, biogenic emissions are predicted to increase everywhere, with the largest increase (~20%) found in the

---

<sup>3</sup>Significant portions of this chapter were first published as:

Jiang, X., Z.-L. Yang, H. Liao, and C. Wiedinmyer (2010), Sensitivity of biogenic secondary organic aerosols to future climate change at regional scales: An online coupled simulation, *Atmos. Environ.*, 44, 4891–4907, doi:10.1016/j.atmosenv.2010.08.032

Work cited here is referenced in the **References** section of this dissertation.

southeastern and northwestern U.S. under the A1B scenario. Changes in SOA are not identical with those in biogenic emissions. Under the A1B scenario, the biggest increase in SOA is found over Texas, with isoprene emissions being the major contributor to SOA formation. The range of change varies from 5% over the southeast region to 26% over Texas. The changes in either biogenic emissions or SOA under the two climate scenarios are different due to the differences in climatic conditions. The results also suggest that future SOA concentrations are also influenced by several other factors such as the partitioning coefficients, the atmospheric oxidative capability, primary organic carbon aerosols, and anthropogenic emissions.

## **5.2. INTRODUCTION**

Secondary organic aerosols (SOA) are formed in the atmosphere through oxidation with precursor volatile organic compounds (VOCs). They not only affect solar radiation reaching the Earth's surface (e.g., Chung and Seinfeld, 2002; Hoyle et al., 2009), but also play a very important role in the hydrological cycle through changing the amount of clouds in the atmosphere (e.g., Kanakidou et al., 2005; Barth et al., 2005). However, impacts of SOA on climate relative to other aerosols remain highly uncertain due to the lack of direct measurements on large scales and less understanding of their formation. SOA can be formed from the oxidation of anthropogenic VOCs and biogenic VOCs (BVOCs). On a large scale, BVOCs are estimated to be the predominant source (e.g., Andersson-Sköld and Simpson, 2001; Tsigaridis and Kanakidou, 2003; Kanakidou et al., 2005).



Thanks to recent progress achieved from laboratory experiments (e.g., Griffin et al., 1999; Kroll et al., 2006; Offenberg et al., 2006; Kroll and Seinfeld, 2008), and ambient measurements (e.g., Claeys et al., 2004; Pun and Seigneur, 2008), our understanding of SOA formation chemistry has recently improved. With knowledge obtained from laboratory experiments, SOA formation has been parameterized in models (e.g., Chung and Seinfeld, 2002; Donahue et al., 2006; Jimenez et al., 2009). Traditional SOA models (e.g., Chung and Seinfeld, 2002; Tsigaridis and Kanakidou, 2003; Heald et al., 2008) use a two-product absorptive partitioning scheme (Odum et al., 1997) that assumes that only two semi-volatile products are formed from the oxidation of a parent hydrocarbon by an oxidant. This approach has some limitations. It neglects the contributions from VOC oxidation products of high and intermediate volatility. It does not include second-generation chemistry to SOA formation, the importance of which was illustrated by Ng et al. (2006).

Several recent studies (e.g., Robinson et al., 2007; Donahue et al., 2006, 2009) have made efforts to improve SOA parameterizations. For instance, Donahue et al. (2006) presented a new framework for organic aerosol modeling. The volatility basis set in their study spans a larger range of atmospheric conditions than the two-product model does, and conveniently accounts for partitioning, dilution, and chemical aging of organic vapors. Robinson et al. (2007) proposed an organic aerosol model scheme based on lumping species into volatility bins of a basis set, and their results show a good agreement with ambient measurements. However, emission inventories for volatility basis set approach do not exist. Thus, in this study, I use the two-product approach. SOA

formation has also been included in regional (Griffin et al., 2002; Zhang, et al., 2008) and global (e.g., Tsigaridis and Kanakidou, 2003; Lack et al., 2004; Tsigaridis et al., 2005; Henze and Seinfeld, 2006; Liao et al, 2007; Heald et al., 2008) models to study SOA burden. At global scales, Tsigaridis et al. (2005) studied the variability of SOA distributions and budget to natural climate variability by incorporating a SOA scheme in a global three-dimensional chemistry transport model. Liao et al. (2007) included a SOA scheme in a global chemistry model and evaluated model performance with the available ground-based aerosol products over the U.S. Their results reveal that SOA contributes 5%–38% of fine particles with diameter less than 2.5  $\mu\text{m}$  ( $\text{PM}_{2.5}$ ) in different regions of the U. S..

Climate affects SOA concentrations in the atmosphere via temperature, precipitation, and changing the oxidative capacity of the atmosphere. In the meantime, changes in temperature also influence the amount of precursor emissions of SOA, in particular, biogenic emissions. The interest in the effects of potential future climate change on air quality including ozone and aerosols has risen during the past few years (e.g., Tagaris et al., 2007; Jiang et al., 2008; Jacob and Winner, 2009). Several studies (Liao et al., 2006; Tsigaridis and Kanakidou, 2007; Heald et al., 2008) have studied the sensitivity of SOA to future climate change; they found that increased biogenic emissions due to an increase in temperature account for most of the changes in SOA. The largest future increase in SOA from 2000 to 2100 is predicted by Tsigaridis and Kanakidou (2007). They also found that in 2100, SOA burden will exceed that of sulfate, suggesting the importance of SOA in the atmosphere. Heald et al. (2008) studied the sensitivity of

SOA to changes in future climate, anthropogenic emissions, and land use using a global climate model. They found that climate change alone does not change the global mean SOA, while the rising of biogenic emissions and anthropogenic emissions can result in an increase of 36% in SOA in 2100. Although their studies examined different factors in controlling SOA concentrations, the regional details are not well represented. On regional scales, Zhang et al. (2008) examined the sensitivity of air quality to potential regional climate change in the United States (U.S.) using downscaled climate output. They found that models underestimate by at least 20% of the responses of organic aerosols to future climate change if SOA formation is not included. These studies suggest that understanding the response of SOA change to climate change is important not only for air quality studies, but also for climatic effects.

In the current study, I mainly focus on biogenic SOA from BVOCs. It should be noted that anthropogenic VOCs contribute to SOA formation much more than previously assumed (e.g., Heald et al., 2008; Farina et al., 2010). An evaluation of the contribution of anthropogenic VOCs to SOA formation over the U.S. will be the subject of future studies. In addition, SOA from BVOC precursors and/or their oxidation products can also form via aqueous phase processing in cloud droplets and atmospheric particles (Carlton et al., 2006; Volkamer et al., 2009; El Haddad et al., 2009) or gas phase hydrolysis (Axson, et al., 2010). The omission of these processes may result in underestimation of SOA in the results. As our understanding on the aqueous phase aerosol improves, this needs to be considered in SOA formation.

The objectives of this study are: 1) to investigate detailed SOA levels over the contiguous U.S. using a coupled land–atmosphere–chemistry model; and 2) to understand how SOA levels will respond to future climate change under different emissions scenarios on a regional scale. I first include a SOA model in an existing coupled model to evaluate the model performance. I then employ this modified model to examine the sensitivity of SOA to different future climate change scenarios. I begin in section 5.3 with a description of the coupled model and SOA model. In section 5.4, I evaluate the model results against available satellite and ground-based measurements. Finally, I discuss the effects of future climate change on biogenic SOA formation.

### **5.3. MODEL DESCRIPTION**

#### **5.3.1. WRF/Chem model**

The chemistry version of the physically-based Weather Research and Forecasting (WRF) model (Skamarock et al., 2005)—referred as the WRF/Chem model (Grell, 2005) thereafter—is used in this study. In the WRF/Chem, both the meteorological and the air quality components are mutually consistent in that they employ the same transport scheme (mass and scalar preserving), grid (horizontal and vertical components), physics schemes for subgrid-scale transport, land surface models, and timestep. That means all transport of chemical species is done simultaneously with other meteorological variables. The dynamic core I use in this study is the mass coordinate version of the model, called Advanced Research WRF (ARW). The gas-phase chemistry used in this study is based on the CBM-Z mechanism (Zaveri and Peters, 1999). This scheme uses 67 prognostic species and 164 reactions in a lumped structure approach according to their internal bond

types. It is similar to the widely used carbon bond mechanism (CBM-IV), but is extended for use on different spatial and temporal scales. Fast-J photolytic reactions are used within CBM-Z (Wild et al., 2000; Barnard et al., 2004). The model for simulating aerosol interactions and chemistry (MOSAIC) (Zaveri et al., 2008) is used in this work to simulate aerosols. MOSAIC treats several major aerosol species including sulfate, methanesulfonate, nitrate, chloride, carbonate, ammonium, sodium, calcium, black carbon, primary organic mass and liquid water. Gas-phase species are allowed to partition into the particle phase. The size distributions of aerosols are represented using a sectional approach based on dry particle diameters. In this study, I use four discrete size bins. Dry deposition of trace gases from the atmosphere to the surface is calculated by multiplying concentrations in the lowest model by the spatially and temporally varying deposition velocity. The deposition velocity is proportional to the sum of three characteristic resistances (aerodynamic resistance, sublayer resistance, surface resistance). The surface resistance parameterization used in the dry deposition scheme is developed by Wesley (1989). Dry deposition of aerosol number and mass is based on Binkowski and Shankar (1995) and is calculated using the wet size of particles. Simplified wet deposition by convective parameterization with scavenging factor of 0.6 for aerosols is used in the current study. Wet deposition considering in-cloud and below-cloud wet removal will be used in future studies when the aerosol-cloud feedback is treated in the model.

### 5.3.2. Secondary organic aerosol model

The version of WRF/Chem used in this study is version 2.2, which does not include a SOA module with the selected gas-phase and aerosol schemes, thus I follow the idea of the two-product model approach to describe SOA formation in the WRF/Chem based on the method used in Chung and Seinfeld (2002) and Liao et al. (2007). As this is the simplest way to represent SOA formation, it could lead to some uncertainties in the modeling results. In addition, heterogeneous and aqueous phase reactions forming SOA are not included in the current model since the level of understanding is still low. Although it is important to represent all factors in the model accurately, all model results are subject to uncertainty. Rate constants and aerosol yield parameters determined from laboratory chamber results (Seinfeld and Pankow, 2003) are used in the SOA model. A complete implementation of SOA formation from monoterpenes and other reactive VOCs (ORVOCs) in a global model was described by Chung and Seinfeld (2002). Isoprene has recently been recognized to contribute to a significant amount of SOA in nature (e.g., Claeys et al., 2004; Zhang et al., 2007; Carlton et al., 2009; Karl et al., 2009). Some studies have started to include isoprene as a source of SOA in global and regional models (Henze and Seinfeld, 2006; Liao et al., 2007; Zhang et al., 2007, 2008; Heald et al., 2008).

Following their approaches, I implement a SOA module in the WRF/Chem with the consideration of oxidation of monoterpenes, isoprene and ORVOC emissions. I include oxidation of monoterpenes and ORVOC emissions with OH, O<sub>3</sub> and NO<sub>3</sub>, whereas considering oxidation of isoprene emissions with only OH. Formation of SOA from photooxidation of isoprene emissions in this work is based on the work of Henze and

Seinfeld (2006) in which they presented results of chamber experiments about reaction of isoprene emissions with OH at low NO<sub>x</sub> condition (Kroll et al., 2006). Though reaction with O<sub>3</sub> or NO<sub>3</sub> may also lead to SOA formation, the magnitudes of these sources are assumed to be minor (Calvert et al., 2000).

As in the work of Chung and Seinfeld (2002), monoterpenes and ORVOCs are divided into five hydrocarbon classes according to the values of their experimentally measured aerosol yield parameters (Griffin et al., 1999). In this work, biogenic emissions are calculated with the Biogenic Emissions Inventory System, version 3 (BEIS3) (Vukovich and Pierce, 2002) in the WRF/Chem. Species calculated in the BEIS3 model are different from those used in Chung and Seinfeld (2002). Thus, following their approach, I categorized monoterpenes and ORVOCs into four reactive biogenic hydrocarbon groups excluding sesquiterpenes due to the lack of emission estimates in the current model (BEIS3) (Table 5.1). Short-lived sesquiterpenes have been shown to produce a substantial amount of SOA, and the magnitude of formed SOA can be as large as that from monoterpenes (Sakulyanontvittaya et al., 2008), thus we need to be aware that the simulated SOA concentrations in the present study may be underestimated. Isoprene is included as hydrocarbon class V. The fraction of monoterpenes is from Table 4 of Griffin et al. (1999). For each of the first four reactive hydrocarbon classes, there are three oxidation products, two for combined O<sub>3</sub> and OH oxidation and one for NO<sub>3</sub> oxidation. Reaction of isoprene with oxidants generates two oxidation products. The mass-based stoichiometric coefficients ( $\alpha_i$ ) for all reactions are presented in Table 5.2. The partition coefficients  $K_i$  corresponding to  $\alpha_i$  are also listed in Table 5.2. All products

are semi-volatile, and they partition between the gas and aerosol phases. Thus, there are a total of 28 oxidation products. In the model, I use SOG1, SOG2, and SOG3 to represent lumped gas phase products from oxidation of hydrocarbon classes I, II and III, from hydrocarbon class IV and from hydrocarbon class V respectively (Table 5.3). SOA1, SOA2 and SOA3 are lumped aerosol phase products from oxidation of these five hydrocarbon classes (Table 5.3).

All products are semi-volatile and can partition between gas and aerosol phases. The partitioning of these products between gas phase ( $G_i$ ) and aerosol ( $A_i$ ) is represented by the partitioning theory (Pankow, 1994),

$$G_i = A_i / (K_i M_o), \quad (5.1)$$

in which  $K_i$  represents partitioning coefficient and  $M_o$  represents pre-existing absorptive organic matter. In the partitioning process, the effect of temperature is considered according to the temperature dependence of saturation concentrations derived from Clausius-Clapeyron equation:

$$K_i(T_{ref}) = K_i(T)(T_{ref}/T)\exp(\Delta H_{vap}/R(1/T_{ref} - 1/T)), \quad (5.2)$$

where  $T_{ref}$  is set at 295K for isoprene and 310K for others;  $R$  is ideal gas constant;  $T$  is temperature. The heat of vaporization for organic compounds is from the CRC Handbook of Chemistry and Physics (Lide, 2001),  $\Delta H_{vap} = 42 \text{ KJ mol}^{-1}$  is used for all compounds. Dry deposition of SOA follows the method used for gas-phase species, in which the surface resistance is defined by Wesley (1989). Simplified wet deposition by convective



parameterization with scavenging factor of 0.6 (Chin et al., 2000) is used for SOA in the current study.

### **5.3.3 Anthropogenic and biogenic emissions**

The anthropogenic emissions inventory of gas and aerosol species is the U.S. EPA's 1999 National Emissions Inventory (NEI-99, version 3) released in 2003 (<http://www.epa.gov/air/data/neidb.html>). The emissions are derived by temporal allocation factors specific to each source classification code provided by the EPA. They are representative of a typical summer day. This inventory has been successfully used in the WRF/Chem simulations (Jiang et al., 2008). A more detailed description of this anthropogenic emissions inventory can be found in Jiang et al. (2008). Biogenic emissions are very sensitive to changes in temperature and radiation. Emission rates of biogenic compounds at standard temperature and light conditions have been assigned to the model grid on the basis of BEIS3 and the Biogenic Emissions Landuse Database, version 3 (BELD3), which provides distributions of 230 vegetation classes at 1-km resolution over North America (Kinnee et al., 1997). Figure 5.1 shows the BVOCs emissions under standard climatic condition of light and temperature. Then, biogenic emissions in all simulations are calculated online using the temperature and light-dependence algorithms from the BEIS3 (Williams et al., 1992; Geron et al., 1994; Guenther et al., 1995). Emissions from biomass burning, sea-salt, and dusts are not considered in the current study.

## **5.4. EXPERIMENT DESIGN**

The first part of this study is to investigate the SOA levels over the U.S. for the present-day climate using the modified WRF/Chem model with the inclusion of SOA formation. The modeling domain covers the entire contiguous U.S. on a 32-km horizontal grid. There are a total of 28 vertical model layers, with finer vertical resolution in the lower troposphere to allow the model to simulate boundary-layer processes more realistically. The highest emissions of BVOCs from vegetation occur between June and August (Guenther et al., 1995), thus production of SOA from the oxidation of biogenic emissions will be most relevant during that period. To understand the SOA levels in the U.S., multiyear simulations are preferred. However, to run multiyear simulations with this fully coupled land–atmosphere–chemistry model demands a huge amount of computing time. Under this circumstance, I carefully selected one month, July 2002 to represent summer season to examine the model performance in terms of simulating BVOCs and SOA. The initial and lateral boundary meteorological conditions required by the WRF/Chem are from the NCEP’s North American Regional Reanalysis (NARR) data set, which has a domain covering the configured computational area (Mesinger et al., 2006). As aforementioned, anthropogenic emissions are from the NEI-99 and biogenic emissions are calculated online.

The second objective of this study is to understand the effects of potential future climate change on SOA concentrations on regional scales. A series of experiments using global climate model projections as initial and lateral meteorological boundary conditions are conducted. The output of global climate model—Community Climate System Model 3.0 (CCSM3)—is used to provide different future climate scenarios. The CCSM3 has

been used for the 4<sup>th</sup> Assessment Report of the Intergovernmental Panel on Climate Change (IPCC) (Collins et al., 2006), and the horizontal resolution is T85 (~1.41 °). Readers are referred to Meehl et al. (2006) for a full analysis of the CCSM3 future climate simulations. The greenhouse gas concentrations during the CCSM3 simulation period used in this study follow the IPCC Special Report on Emission Scenarios (SRES) A1B and A2. The emissions scenarios, built on storylines that link emissions to different driving forces, are described in detail in Nakicenovic et al. (2000). The A1B scenario is associated with increasing trace gases and aerosol concentrations from 2001 until 2050. It is a mid-line scenario for carbon dioxide output and economic growth. As an alternative, the A2 scenario, which is based on a world that is regionally organized economically, technological change, is fragmented, and population growth is high, is also selected to test the sensitivity of SOA formation to different climate scenarios.

The CCSM3 output has been successfully applied to WRF/Chem simulations on a relatively high spatial resolution (Jiang et al., 2008). Most previous studies about the impacts of future climate change on regional air quality or aerosol concentrations rely on downscaled regional climate model output (e.g., Hogrefe et al., 2004; Zhang et al., 2008; Avise et al, 2009). In this study, the WRF/Chem is a fully coupled regional model including online atmosphere and land surface models, thus, the regional downscaling of climate and SOA simulation are performed simultaneously with the WRF/Chem. For this part of study, I also selected July to represent summer situation. In previous studies of the impacts of climate change on O<sub>3</sub> (e.g., Hogrefe et al., 2004; Liao et al., 2006) and aerosols (e.g., Tagaris et al., 2007; Heald et al., 2008; Zhang et al., 2008), authors used

either a few (e.g., two) summer seasons or a few (e.g., one or two years) years to study the impacts. Thereby, I designed experiments for three consecutive Julys to represent the present and future scenarios respectively. I simulated a current period (2001–2003, denoted as “current”) and a future period (2051–2053, denoted as “future”). In future work, with increasingly available computational resource, multiyear runs would be the optimal way to statistically assess the changes. The differences between the future year and current year simulations are used to assess the impacts of climate change on SOA formation. The anthropogenic emissions for the present-day simulations are also applied for the future year simulations to avoid any impacts from changes in anthropogenic emissions on the results. Biogenic emissions for the future years are simulated online with the BEIS3 scheme.

To minimize the effect of initial conditions on model results, the initial two-day period (June 29 and 30) of each simulation was considered as a spin-up period to establish the initial conditions for several atmospheric concentrations of different emission species. In all simulations, I used the same set of gas-phase chemistry (CMB-Z) and aerosol scheme (MOSAIC). Other parameterizations used in all simulations include the Lin et al. (1983) microphysics scheme, the Kain-Fritsch Cumulus Parameterization scheme (Kain and Fritsch, 1990), the Yonsei University Planetary Boundary Layer (PBL) scheme (Hong and Pan, 1996), the Simple Cloud Interactive Radiation scheme (Dudhia, 1989), the Rapid Radiative Transfer Model Longwave Radiation scheme (Mlawer et al., 1997), and the Noah LSM.

## **5.5. PRESENT-DAY SIMULATION OF BIOGENIC SOA**

In this section, I first present the simulated distributions of biogenic emissions and SOA. Then I compare model results with available satellite and ground-based aerosol measurements to evaluate model performance.

### **5.5.1 Regional distributions of biogenic emissions and SOA**

Figure 5.2 shows the spatial plots of the online calculated total biogenic emissions, isoprene, monoterpenes, and ORVOCs in July 2002. Due to the lack of the measurements of biogenic emissions at a regional scale, simulated spatial pattern of total biogenic emissions is compared with previous studies. Over all, the pattern in July agrees with the patterns simulated by several previous studies (e.g., Guenther et al., 1995; Levis et al., 2003). High emissions occur where there is a significant amount of vegetation, such as the southeastern and northwestern U.S. The simulated spatial patterns of isoprene and monoterpenes are slightly different, which is attributed to the different emission capacities of different types of vegetation. Example trees emitting isoprene are deciduous trees (Kesselmeier and Staudt, 1999) such as oak trees, which are more dominant in the southern U.S. including Texas. Coniferous trees such as pines, cedars, and firs, which exist over the northwestern U.S., emit a significant amount of monoterpenes. Overall, the model shows reasonable skill in simulating the spatial patterns of biogenic emissions over the U.S.

Figure 5.3a shows the spatial pattern of model predicted mean surface concentrations of SOA in July 2002. The concentrations of SOA range up to  $1.6 \mu\text{g m}^{-3}$ , and the maximum values are found over the regions where there are high concentrations

of BVOC emissions (the northwestern and southeastern U.S.). Over the northwestern U.S., a majority of SOA comes from the oxidation of monoterpenes (Figure 5.3b), while over the southeastern U.S., the contribution of isoprene is dominant (Figure 5.3c). The results suggest the importance of including isoprene emissions in SOA formation. The simulated SOA concentrations of 0.4–1.6  $\mu\text{g m}^{-3}$  are predicted over the two major regions, and SOA levels predicted over other regions (e.g., northeast) are around 0.2–0.8  $\mu\text{g m}^{-3}$ . Comparing with other studies (e.g., Liao et al., 2007), the simulated SOA levels are reasonable, but more regional details are simulated in the present study.

### **5.5.2. Comparison with observations**

Model performance is the key to understanding SOA levels over the U.S. Measurements of organic aerosols under ambient atmospheric conditions generally do not distinguish between primary and secondary sources. One common way is to use other relevant aerosol products to evaluate model performance. In this subsection, spatial and temporal distributions of model simulated aerosol optical property and concentrations are compared with MODIS (Moderate Resolution Imaging Spectroradiometer) – derived aerosol optical depth (AOD), AOD from Aerosol Robotic Network (AERONET) and organic carbon aerosol concentrations from the ground-based measurement network of the Interagency Monitoring of Protected Visual Environments (IMPROVE) (<http://vista.cira.colostate.edu/improve/>) .

To compare with the available AOD measurements, I calculated AOD using Mie theory in the WRF/Chem. The details regarding the treatment of aerosol optical

properties can be found in Fast et al. (2006). The aerosol optical properties in the WRF/Chem are calculated at four wavelengths, 300, 400, 600, and 1000 nm. For the MODIS AOD product, monthly MOD04 level-2 product at 550 nm wavelength with a spatial resolution of 1-degree is used for model evaluation on a monthly basis. The AERONET measurements are site-specific with wavelengths up to eight wavelengths (1640, 1020, 870, 675, 500, 440, 380, and 340 nm). Level 2.0 (quality-assured) data are used in this study (Smirnov et al., 2000). MODIS AOD is directly retrieved at 550 nm, whereas model calculated AOD and AERONET AOD are not at 550 nm. As the three AOD data sets are at different wavelengths, the comparisons are made at 550 nm wavelength. I used Angstrom exponent relation ([http://disc.sci.gsfc.nasa.gov/data-holdings/PIP/aerosol\\_angstrom\\_exponent.shtml](http://disc.sci.gsfc.nasa.gov/data-holdings/PIP/aerosol_angstrom_exponent.shtml)) to derive AOD at 550 nm for both model output and AERONET data based on AOD at the near wavelengths. For instance, for the AERONET data, the Angstrom exponent between wavelengths 440 and 675 nm was used to derive AERONET AOD at 550 nm using the following equation:

$$\tau_2 = \tau_1 / \exp(-\alpha \ln(\lambda_1 / \lambda_2)) \quad (5.3)$$

where  $\tau_2$  is the AOD at 550 nm,  $\tau_1$  is the AOD at 500 nm,  $\alpha$  is the Angstrom exponent between 440 and 675 nm,  $\lambda_1$  is 500 nm, and  $\lambda_2$  is 550 nm. Similar method is applied to model simulated AOD output to derive AOD at 550 nm.

Figure 5.4 shows the spatial distributions of monthly mean MODIS-derived and model simulated AOD at 550 nm wavelength. With the largest amount of biogenic emissions occurring in the southeastern U.S. including Texas, an increase in AOD is

simulated in this region when considering SOA in the model. Over the northeast part of the country, there is also an increase in AOD. The default model underestimates AOD over much of the abovementioned areas by 0.1–0.5, in particular, over the regions where the amount of biogenic emissions is significant. It should be noted that the model with or without SOA fails to capture the high AOD in the northwestern U.S. shown in Figure 5.4b and 5.4c. This could be attributed to the lack of fire and dust emissions in the current simulations. Liao et al., (2007) also found a large underprediction in organic matter over this region, which they attributed to some uncounted primary emissions from some sources such as wildfires over the U.S. My model does not include fire and dust emissions, so the calculated AOD values are subject to these uncertainties.

The comparison of model results with ground-based measurements cannot be done with all available data, because the model grid represents the mean concentration of rather large areas. From this perspective, it is good to select the measurements that could represent different land surface features. Figure 5.5 displays model simulated and AERONET measured daily mean AOD over three major sites (Figure 5.5d), where the landscapes are different. Comparison at site HJAndrews and site BSRN\_BAO\_Boulder shows a better agreement except for two high peaks. The measured and simulated AOD values at the two locations are relatively low, and the contribution of biogenic SOA to the total aerosol is small. The two peaks of AOD observed in the measurements at the two sites are identified to be due to local fire events. High AOD values on July 2, 2002 at site BSRN\_BAO\_Boulder (Figure 5.5b) are caused by a wildfire that occurred between June 8 and July 2, 2002. It is also true for site HJAndrews (Figure 5.5a), where high AOD



values resulted from a nearby fire event, which occurred on July 21, 2002 in the Sierra Nevada Mountains of California. Again, this is due to the lack of fire emissions in the model. It is recommended to include them in future studies. Prediction at site Stennis (Figure 5.5c) is quite promising, the simulated AOD values with SOA model included agree well with measurements. The results suggest that considering SOA in the current model is important for aerosol prediction.

Figure 5.6a compares simulated spatial distribution of monthly mean surface layer organic carbon (OC) concentrations in the presence of SOA with observations obtained from the IMPROVE network. Overall, the model reasonably replicates the observed spatial distribution of OC over the U.S., with higher concentrations over the southeast and northwest regions. The simulated OC concentrations over the southeastern and northwestern U.S. are very close to the IMPROVE measurements. Some exceptions do exist. For instance, over some sites in the eastern U.S., observed OC concentrations are higher than the model simulated. The high concentrations of OC in this region are mainly due to forest fires that occurred in Quebec, Canada during early July 2002 (DeBell et al., 2004). A few high spots in the western U.S. are also due to the fire events. Over the Rocky mountain region, model underestimates OC. This, again, suggests the importance of including fire and dust emissions in the model. Figures 5.6b and 5.6c mainly depict the primary organic carbon (POC) aerosols and the ratio of SOA in the total OC. The amount of SOA in OC ranges from 0.1 to 0.5/0.6, which agrees well with previous studies (Tsigaridis et al., 2005; Liao et al., 2007). Overall, comparisons between the simulated aerosol products and measurements suggest that the model has a relatively good

performance in terms of simulating SOA over the U.S. The evaluation of the model performance gives us confidence to examine the future climate effects.

## **5.6. PROJECTED FUTURE CHANGES**

This section presents changes in regional climate, biogenic emissions, and aerosols concentrations due to future climate change. The success of the WRF/Chem model simulations using CCSM model output has been evaluated in Jiang et al. (2008). Their results show that the WRF/Chem model when forced with the CCSM model output is able to simulate meteorological conditions reasonably well. Therefore, the following description mainly focuses on projected changes.

### **5.6.1. Projected changes in regional climate**

Climatic conditions not only affect the formation of SOA in a direct way through changing temperature, relative humidity, clouds, winds, PBLH, precipitation, and radiation, but also influence SOA levels by changing biogenic emissions in an indirect way. The calculation of biogenic emissions took into account the effects of temperature and radiation under different climates. Differences between the present-year simulations and future year simulations are calculated to estimate the projected regional climate change over the next 50 years.

Projected changes in regional climate are to some extent dependent on the projected global climate change, which is also scenario-dependent. Figure 5.7 shows the simulated changes in 2m temperature, wind speed, PBLH, and cloud fraction based on the present year and future year simulations. In response to increased greenhouse gases in 2050s, the

simulated surface warming under the A1B scenario occurs everywhere in the contiguous U.S., with the largest warming ( $>2\text{K}$ ) found over the Great Lakes region, the northwestern U.S., and Texas. The overall pattern of 2m temperature change is identical with that presented in Zhang et al. (2008) in which they used a regional climate model to downscale global climate model output, but the regional details are slightly different. Areas with more warming tend to have reduced near surface wind speed, enhanced PBLH, reduced cloud fraction, slightly reduced precipitation, and increased shortwave radiation at the surface. Over the central Great Plains, the warming is much less as compared to the abovementioned regions. This small warming is also associated with decreased PBLH, increased cloud fraction, increased precipitation, and slightly reduced shortwave radiation. Changes in these climate variables are intimately related.

In comparison with the A1B scenario, under the A2 emissions scenario, areas over the northern U.S. are expected to experience more warming, while the southern U.S. shows a relatively smaller warming. This is consistent with what presented in the IPCC report that if more greenhouse gases are put into the atmosphere, the mid-latitude and high-latitude regions would suffer more warming (IPCC, 2007). The changes in wind speed are also different from those observed under the A1B scenario. Over those areas with more warming, There is a slightly increase in wind speed. For the PBLH, the areas with more warming would still have higher PBLH. Cloud fraction always decreases under future warming climate. Warming is also associated with relatively increased shortwave radiation at the surface. Precipitation decreases over much of the modeling domain in response to future more warming. Comparing the two climate scenarios,

differences are most pronounced in temperature, wind speed, PBLH, precipitation, and shortwave radiation at the surface.

Quantitative changes in these climate variables under the two emissions scenarios (Table 5.4) are calculated over seven sub-regions (Figure 5.8) in the U.S. On average, the largest temperature increases are projected to occur in Texas where Pye et al. (2009) also found the largest temperature increase in summer, while the smallest increases in temperature occur in the northwest under the A1B scenario. Under the A2 scenario, the largest increases in temperature ( $>2\text{K}$ ) are found over the central U.S., and the smallest increase occurs over the southeastern U.S.. An increase of 1.5–1.9 K in temperature is seen in the other regions. Changes in near-surface wind speed are more pronounced in the northwest, central, southeast, and northeast, with the northeast experiencing the largest decrease under the A1B scenario. Under the A2 scenario, the regions which would experience more warming are projected to have strong near-surface wind. Over the eastern U.S. including the northeast and southeast, the near-surface wind speed is expected to decrease due to relatively small increase in temperature. Changes in PBLH are more identical to changes in temperature. However, percentage of changes in PBLH is not as significant as that of wind speeds. Changes in cloud fraction are highly related to temperature changes under the two scenarios. Over the regions where the temperature changes are the largest, there are decreases in cloud fraction correspondingly, such as the southeast region ( $-34.8\%$ ) under the A1B scenario, and the northwest ( $-28.4\%$ ) and the central region ( $-30.6\%$ ) under the A2 scenario. As presented in the IPCC 2007 report, on average, the regions with the largest temperature increases tend to have less cloud

coverage, thus a decrease in precipitation. As seen from Table 5.4, over the areas where I see more warming, there are significant decreases in precipitation, such as the southeast under the A1B scenario, the northwest and the central under the A2 scenario.

Overall, under the two climate scenarios, the projected warming and the related climate change, in particular winds and precipitation are variable everywhere. There are significant differences in regional details. Thus, I would expect these differences would attribute to differences in projected biogenic emissions, aerosols and SOA.

### **5.6.2. Projected changes in biogenic emissions and SOA**

Changes in climate, especially temperature changes, could affect biogenic emissions (e.g., Wiedinmyer et al., 2006). Figure 5.9 shows predicted changes in monthly mean isoprene, monoterpenes, ORVOCs, and total biogenic emissions at the surface. Changes in projected biogenic emissions are different under different climate scenarios, in particular, over the southeast and west regions. As the algorithm used to calculate biogenic emissions is temperature and radiation-dependent, the spatial patterns of changes in biogenic emissions are strongly influenced by these variables. On average, projected temperature changes have the largest impact on biogenic emissions over the southeast region and the western U.S.. Under the A1B scenario, more isoprene and monoterpenes are seen over the southeast region, whereas the amounts of isoprene and monoterpenes are slightly less under the A2 scenario. This is mainly due to the temperature differences under the two scenarios as seen from Figure 5.7a and 5.7b. In the

northeastern U.S., more biogenic emissions are projected under the A2 scenario, as the temperature increase is larger than that under the A1B scenario.

Changes in climate and biogenic emissions can further influence aerosol levels. Generally, warmer climate can influence aerosol burdens by changing aerosol wet deposition, altering climate-sensitive emissions, and shifting aerosol thermodynamic equilibrium. Figure 5.10 shows the projected changes in SOA under the two climate scenarios. The overall changes in the spatial patterns are not identical with those of biogenic emissions or temperature. Although biogenic emissions increase under the future warmer climate, changes in SOA because of climate change are various over the domain. As noted above, an increase in biogenic emissions is found over the southeast region, while over this area, I see a decrease and an increase in SOA. This can be explained that not only the amount of biogenic emissions could affect SOA formation, but also climate variables such as temperature, wind, and precipitation may play an important role in SOA formation and deposition. For example, since the model considers the effect of temperature on partitioning coefficients, the reduction in partitioning coefficients due to temperature increase in the future could lead to lower SOA concentrations near the surface. In addition to the effect of temperature on the partitioning coefficients, temperature increase could also affect the reaction rates of the gas-phase chemistry. Tsigaridis and Kanakidou (2007) studied the sensitivity of temperature on SOA formation, and they found lower SOA concentrations due to the effects on the partitioning coefficients and reaction rates of the gas-phase chemistry over some regions. Recent studies (Goldstein et al., 2009; Carlton et al., 2010) found that

biogenic SOA can be strongly affected by anthropogenic emissions. This can also explain why the future changes in SOA are not identical with those in biogenic emissions.

The preexisting POC aerosols could also play an important role in the SOA formation. The effects of future climate change on POC aerosols are shown in Figure 5.11. Decreases in POC concentrations are found over the regions (e.g., the southeastern U.S.) where I see a decrease in SOA. This could be another factor driving the reduction in SOA in the future. Comparing the changes in SOA under the A1B and A2 scenarios, although more warming is seen under the A1B scenario over the southeastern U.S., the increase in SOA over this region is smaller than that under the A2 scenario. The non-linearity in SOA formation and the involved chemical and physical feedbacks make it different to quantitatively address the contributions of changes in SOA due to different factors. A more comprehensive study considering the effects of different factors might be helpful in understanding SOA formation under the different climate conditions, which is beyond the scope of the current study.

Results for percentage changes in biogenic emissions and SOA are only listed for the three regions—Southwest, Texas, and Southeast—because these regions are experiencing pronounced changes. Figure 5.12 shows, on average, changes in biogenic emissions including isoprene and monoterpenes over the three regions are quite similar (around 20%), with Texas being the one having the largest increase in biogenic emissions under the A1B scenario in the future. If the climate scenario is A2, the biggest increase in biogenic emissions is seen over the southwest region (22%). Differences in biogenic

emissions under the two different emissions scenarios can be explained by the differences in temperature increase in the future. Again, changes in SOA concentrations due to future climate change are not consistent with those of biogenic emissions. Under the A1B scenario, the biggest increase in SOA is found over Texas, with isoprene emissions being the major contributor to SOA formation. The range of change varies from 5% over the southeast to 26% over Texas. As an alternative, the results about SOA changes in response to another climate scenario A2 show that SOA concentrations do not increase linearly with temperature increase. Using a global model, Heald et al. (2008) estimated a 26% increase due to the increase in biogenic emissions, a 6% increase due to the climate change, and a 35% increase due to the combined effect in 2010. On regional scales, Zhang et al. (2008) estimated an 18% decrease in predicted SOA concentrations due to the regional climate change by 2050s. These results suggest that there are uncertainties associated with different models. Future studies about the sensitivity of SOA to different factors are needed for a better understanding of effects of climate change and biogenic emissions on SOA.

## **5.7. CONCLUSIONS**

A regional coupled land–atmosphere–chemistry model has been extended to include SOA formation. As there is no direct measurement of SOA on a large scale, the model performance is evaluated with available ground-based and satellite aerosol measurements including AOD and OC concentrations. The overall simulated spatial pattern of SOA agrees with previous modeling studies. The contribution of SOA to AOD is more pronounced over the area where there is a significant amount of biogenic



emissions. The comparison also reveals that the model with the lack of aerosol sources from fire events and dusts underestimates AOD and OC over some regions, in particular in the northwestern U.S. Future studies with the model including fire and dust emissions are required to improve the model performance in terms of simulating aerosol concentrations.

The sensitivity of SOA to different climate scenarios is investigated with the model driven by global climate model output. Under the future A1B and A2 emissions scenarios, future temperature changes were predicted to increase everywhere in the U.S., but with different degrees of increase in different regions. More specifically, the largest temperature increases are projected to occur in Texas, while the smallest increases in temperature occur in the northwest under the A1B scenario. Under the A2 scenario, I found that the largest increases in temperature ( $>2\text{K}$ ) over the central U.S. and the smallest increases over the southeastern U.S. Over other regions, the temperature increase is around 1.5–1.9 K. Clearly, different climate scenarios lead to different temperature responses. These changes in temperature are also associated with changes in other climate variables such as wind speed, PBLH, precipitation and cloud fraction. As a result of climate change or temperature increase in the future, biogenic emissions are predicted to increase everywhere, with the largest increase found in the southeastern U.S. and the northwestern U.S. The increases under the two different climate scenarios are different due to the differences in temperature increases. Changes in SOA are not identical with those in biogenic emissions. Other factors such as partitioning coefficients, atmospheric oxidative capability, POC, and anthropogenic emissions also play a role in SOA

formation. Direct and in-direct impacts from climate change complicate the future SOA formation. In order to gain a more accurate understanding of how future climate will affect SOA, more detailed sensitivity analysis of SOA formation is required.

## **5.8. ACKNOWLEDGEMENTS**

This research is supported by NASA Headquarters under the NASA Earth and Space Science Fellowship (NESSF) Program grant NNX07AO28H and the Jackson School of Geosciences. Hong Liao acknowledges support from the National Science Foundation of China (grant 40825016). I thank the Texas Advanced Computing Center for computing resources. I acknowledge the AERONET, MODIS and IMPROVE teams for use of their data.

Table 5.1. Hydrocarbon classes of reactive biogenic emissions<sup>a</sup>

Hydrocarbon class	Composition
I	$\alpha$ -pinene, $\beta$ -pinene, sabinene, $\Delta^3$ -carene, terpenoid ketones
II	Limonene
III	$\alpha$ -terpinene, $\gamma$ -terpinene, terpinolene
IV	myrcene, terpenoid, alcohols, ocimene
V	isoprene
<sup>a</sup> based on the work of Chung and Seinfeld (2002)	

Table 5.2. Parameters used in the SOA model<sup>b</sup>

Hydrocarbon class	O <sub>3</sub> + OH oxidation		NO <sub>3</sub> oxidation	O <sub>3</sub> + OH oxidation		NO <sub>3</sub> oxidation
	$\alpha_1$	$\alpha_2$	$\alpha_3$	K <sub>1</sub>	K <sub>2</sub>	K <sub>3</sub>
I	0.0670	0.35425	1.0	0.1835	0.004275	0.0163
II	0.2390	0.3630	1.0	0.0550	0.0053	0.0163
III	0.06850	0.2005	1.0	0.1330	0.0035	0.0163
IV	0.06675	0.135	1.0	0.223750	0.0082	0.0163
V <sup>a</sup>	0.232	0.288	N/A	0.00862	1.62	N/A

$\alpha_i$ : stoichiometric coefficients;  
 $K_i$ : equilibrium gas-particle partition coefficients of semi-volatile compounds ( $\text{m}^3 \mu\text{g}^{-1}$ );  
<sup>a</sup>Only considered the reaction with OH;  
<sup>b</sup>Based on the work of Griffin et al. (1999), Chung and Seinfeld (2002), and Liao et al. (2007).

Table 5.3. Description of oxidation products<sup>a</sup>

Lumped products	Description
SOG1	lumped 9 gas-phase products from oxidation of hydrocarbon class I, II, and III
SOG2	lumped 3 gas-phase products from oxidation of hydrocarbon class IV
SOG3	lumped 2 gas-phase products from oxidation of hydrocarbon class V
SOA1	lumped 9 aerosol phase products from oxidation of hydrocarbon class I, II, and III
SOA2	lumped 3 aerosol phase products from oxidation of hydrocarbon class IV
SOA3	lumped 2 aerosol phase products from oxidation of hydrocarbon class V
<sup>a</sup> Based on the work of Liao et al.(2007)	

Table 5.4. Regional climate changes in seven sub-regions as shown in Figure 5.8

	Southwest	Northwest	Texas	Central	Midwest	Southeast	Northeast
A1B							
2 m Temperature (K)	1.52	1.56	2.13	1.65	1.74	1.86	1.24
10 m Wind Speed (%)	0.03	-3.96	-0.03	-4.28	-1.34	-8.72	-14.37
Planetary Boundary Layer Height (%)	-0.02	-0.04	0.04	-1.72	3.89	7.87	0.67
Cloud Fraction (%)	-18.69	-12.18	-0.11	-8.47	-4.41	-34.82	4.84
Precipitation (%)	-4.82	-9.35	0.88	15.09	17.60	-26.30	32.61
Net Shortwave Radiation at the Surface (%)	0.19	0.36	0.01	0.32	0.01	2.04	-1.90
A2							
2 m Temperature (K)	1.92	1.82	1.61	2.28	1.93	1.22	1.65
10 m Wind Speed (%)	0.23	17.44	-0.05	27.58	28.64	-5.96	-12.30
Planetary Boundary Layer Height (%)	1.03	3.00	0.01	6.53	3.13	4.99	-0.94
Cloud Fraction (%)	-8.55	-28.39	-0.02	-30.58	-18.95	-21.76	-15.85
Precipitation (%)	0.76	-39.22	0.43	-22.72	-2.67	-8.67	0.62
Net Shortwave Radiation at the Surface (%)	0.01	3.45	0.00	4.64	1.65	1.40	-0.41

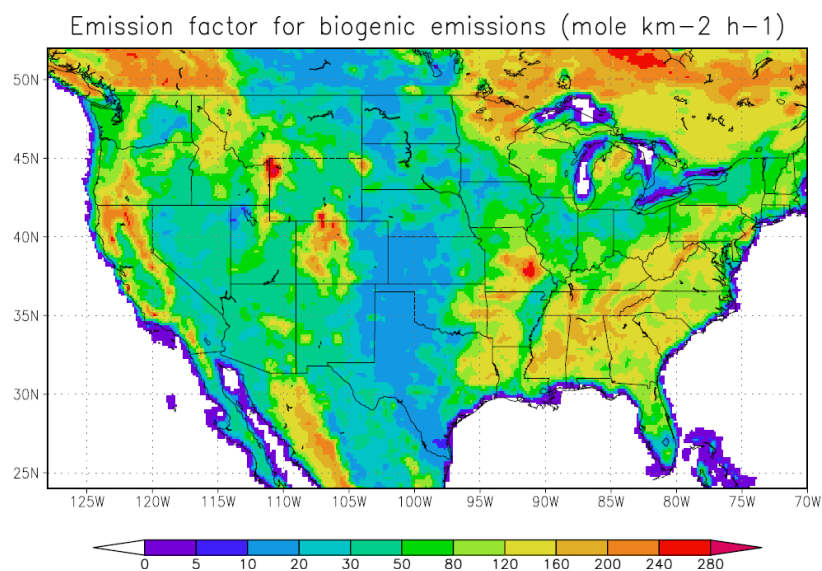


Figure 5.1. BVOC emissions under standard climatic condition of light and temperature ( $30\text{ }^{\circ}\text{C}$  and  $1000\text{ }\mu\text{mol}$  photosynthetically active radiation (PAR)). This is based on the work of Williams et al. (1992), Geron et al. (1994), and Guenther et al. (1995).

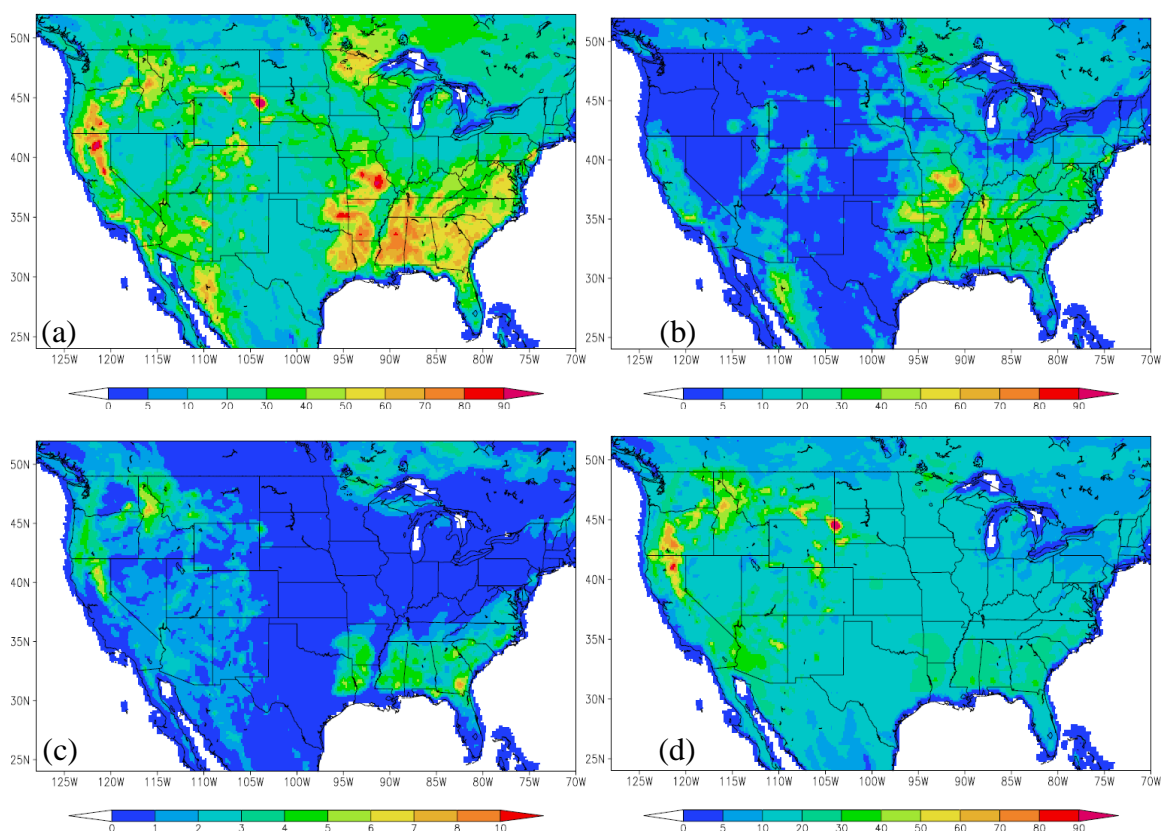


Figure 5.2. Model calculated BVOCs (a), Isoprene (b), Monoterpenes (c) and ORVOCs (d) in July 2002. ( $\text{mole km}^{-2} \text{h}^{-1}$ ).



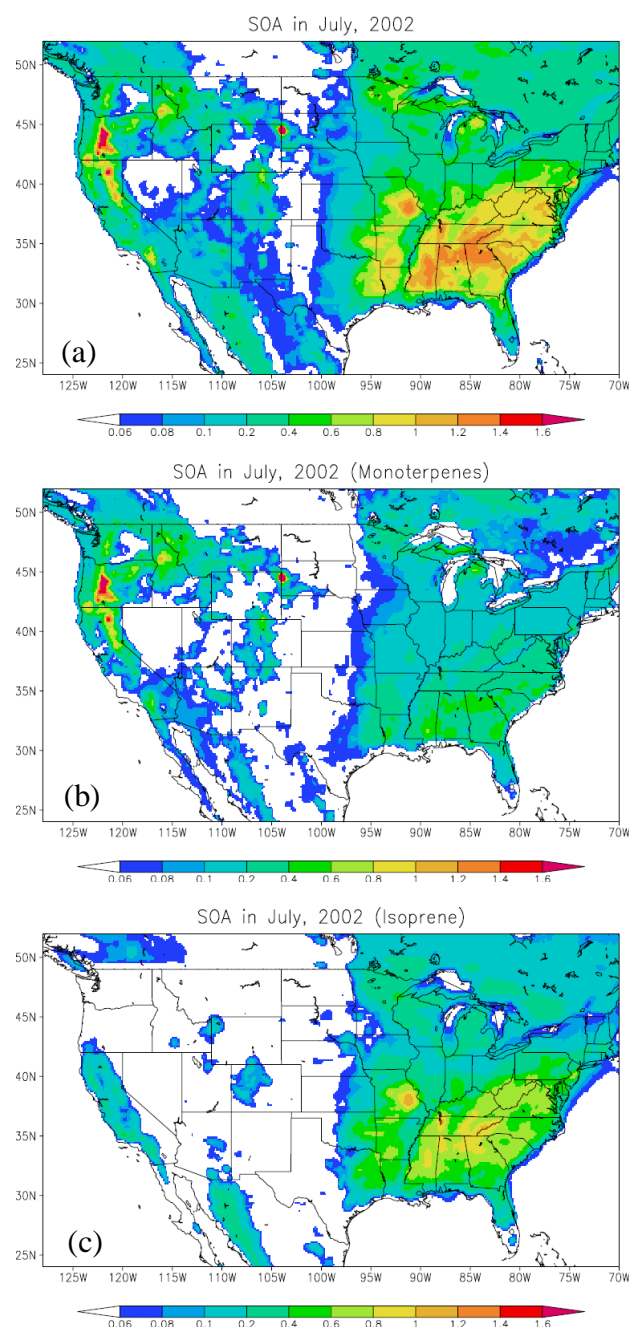


Figure 5.3. Model simulated concentrations of total SOA (a), SOA from monoterpenes (b) and SOA from isoprene (c) in July 2002. ( $\mu\text{g m}^{-3}$ ).

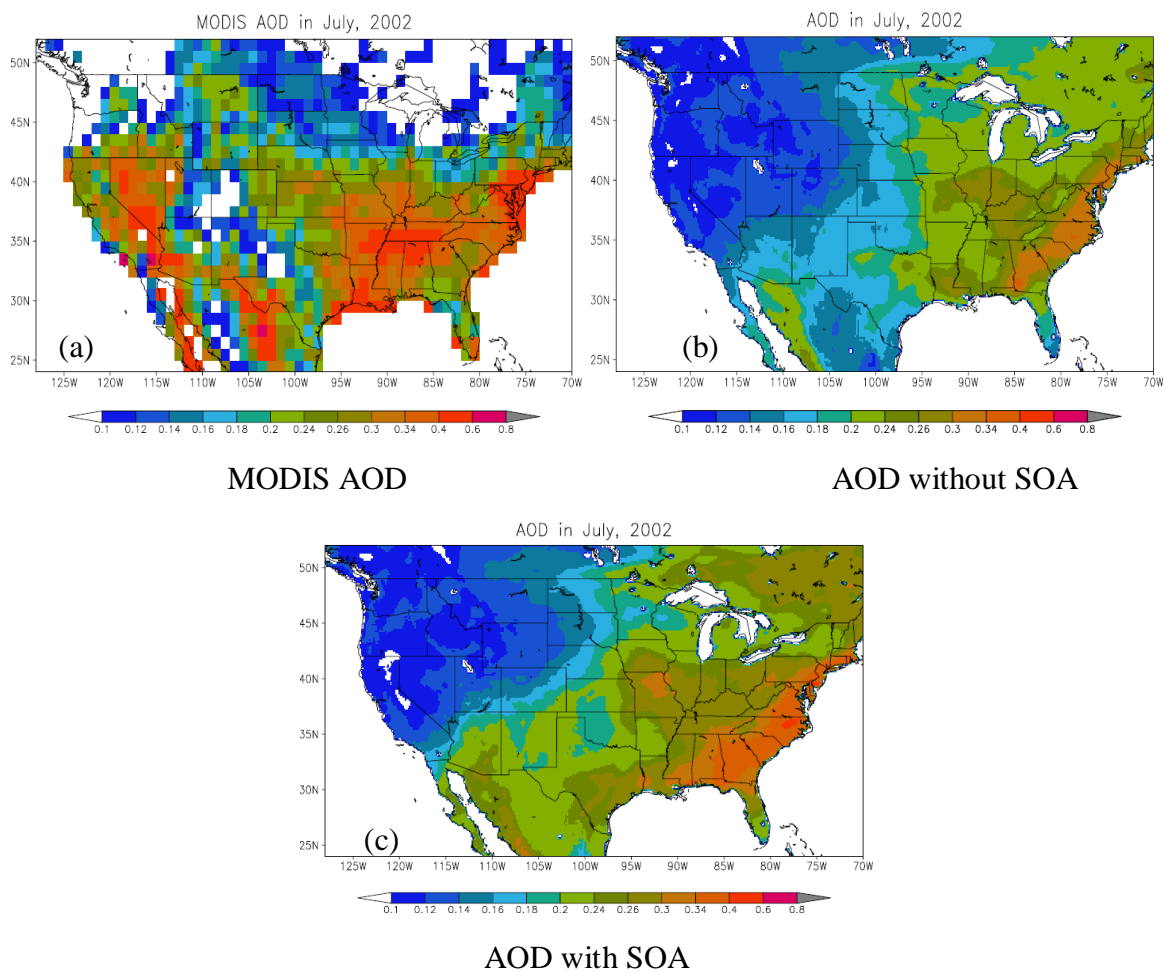


Figure 5.4. Aerosols optical depth (AOD): (a) MODIS derived monthly level 2 product, (b) Model simulated without SOA, and (c) Model simulated with SOA included.

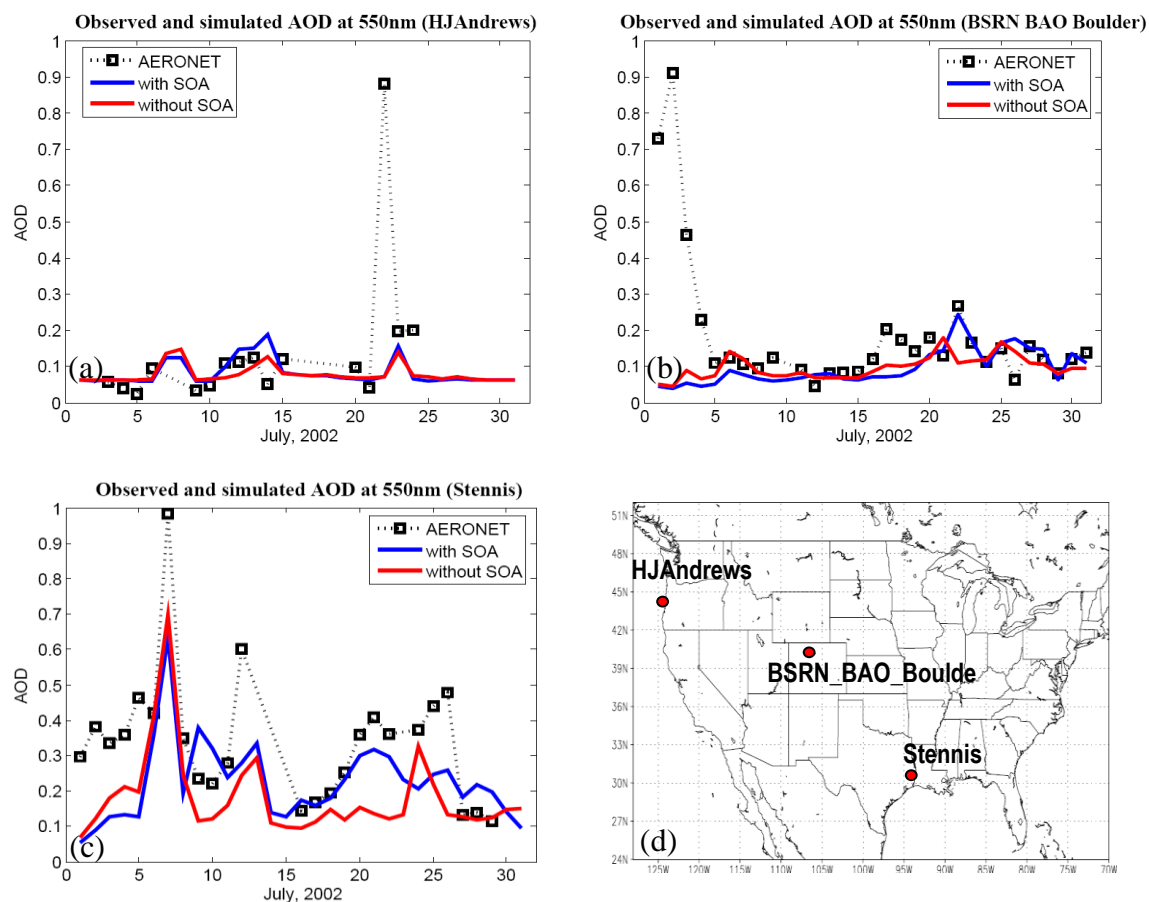


Figure 5.5. AERONET measured and model simulated AOD at three sites (a) HJAndrews, (b) BSRN\_BAO\_Boulder and (c) Stennis. (d) is a map showing the three locations.

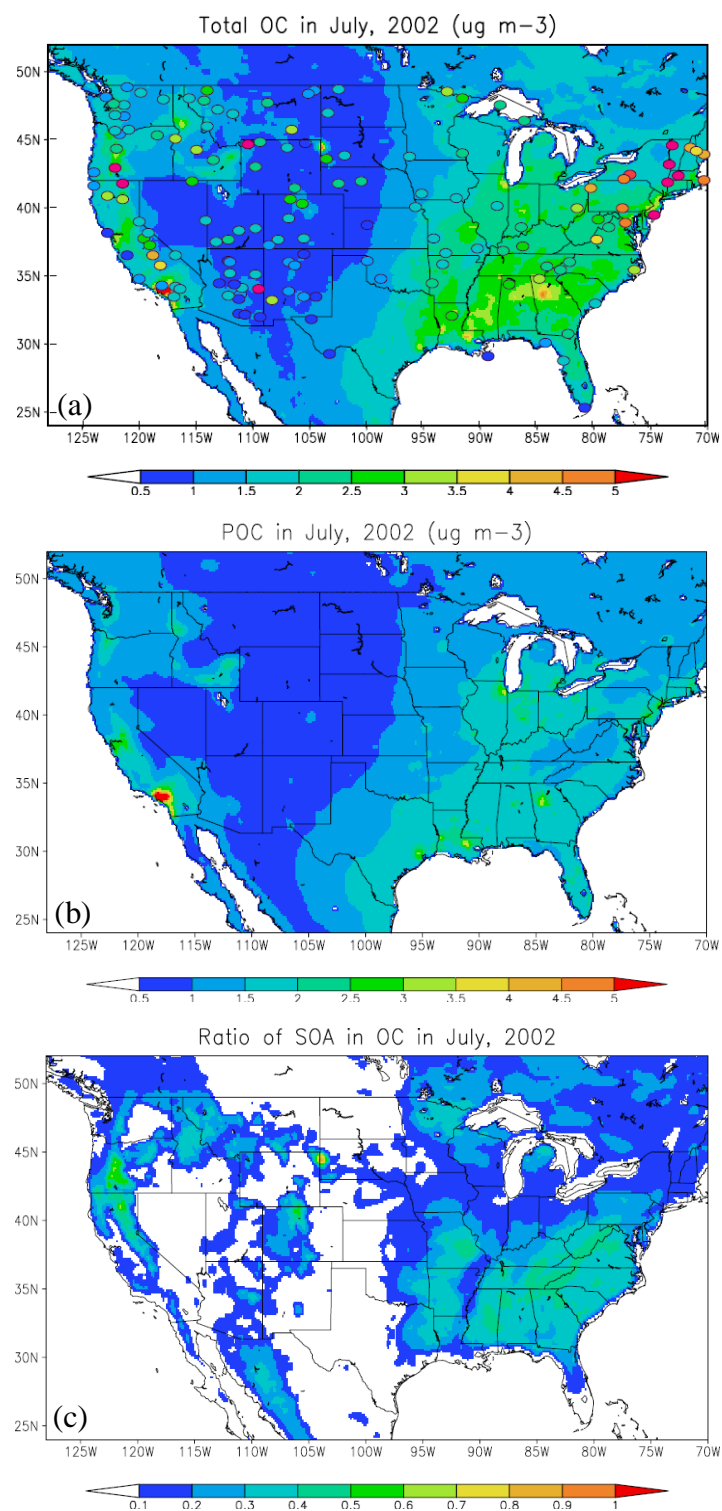
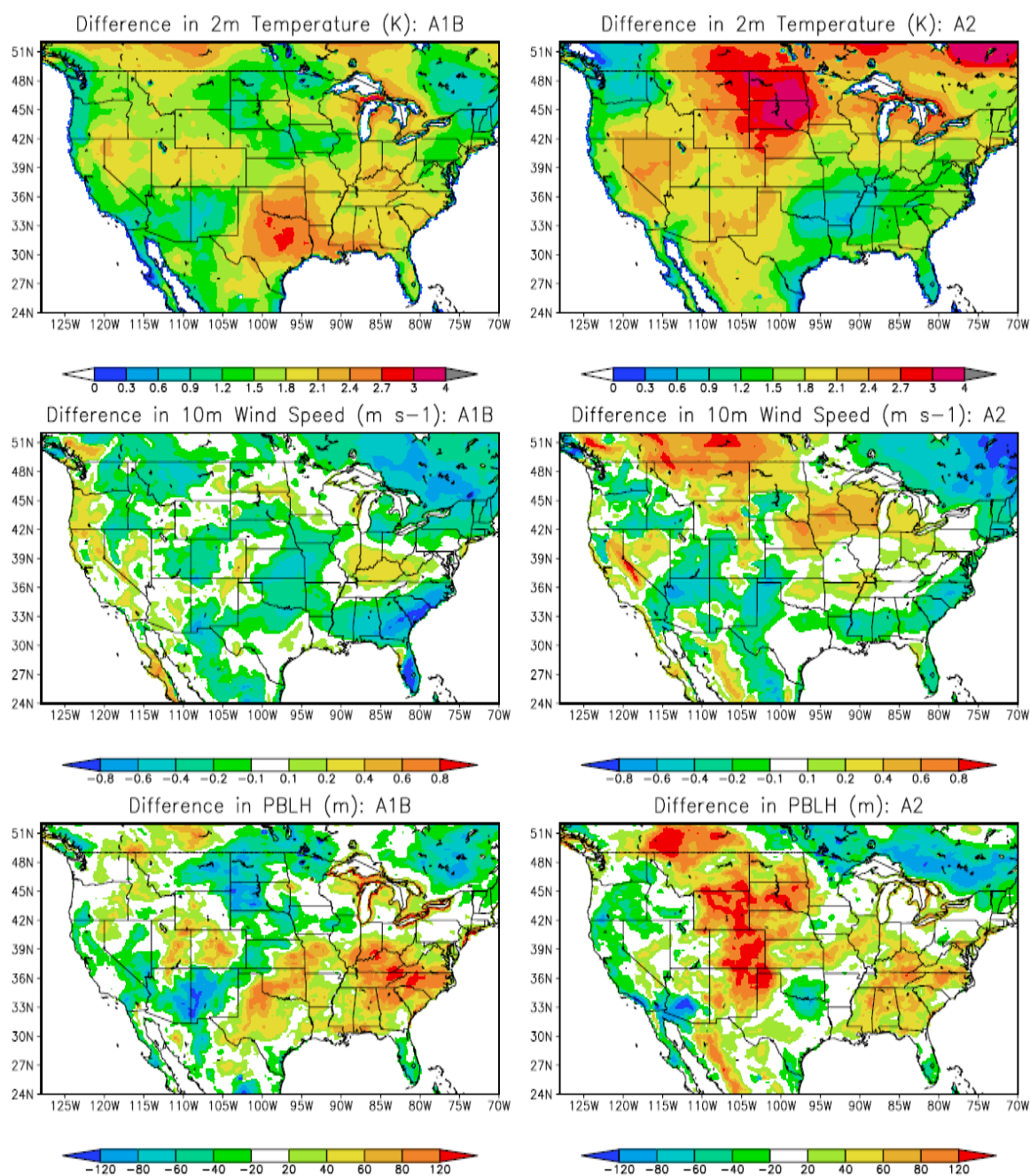


Figure 5.6. (a) Model simulated and measured (at IMPROVED sites) monthly mean surface layer OC (Primary OC (POC) + SOA) concentrations ( $\mu\text{g m}^{-3}$ ), (b) POC, and (c) ratio of SOA in OC in July 2002.





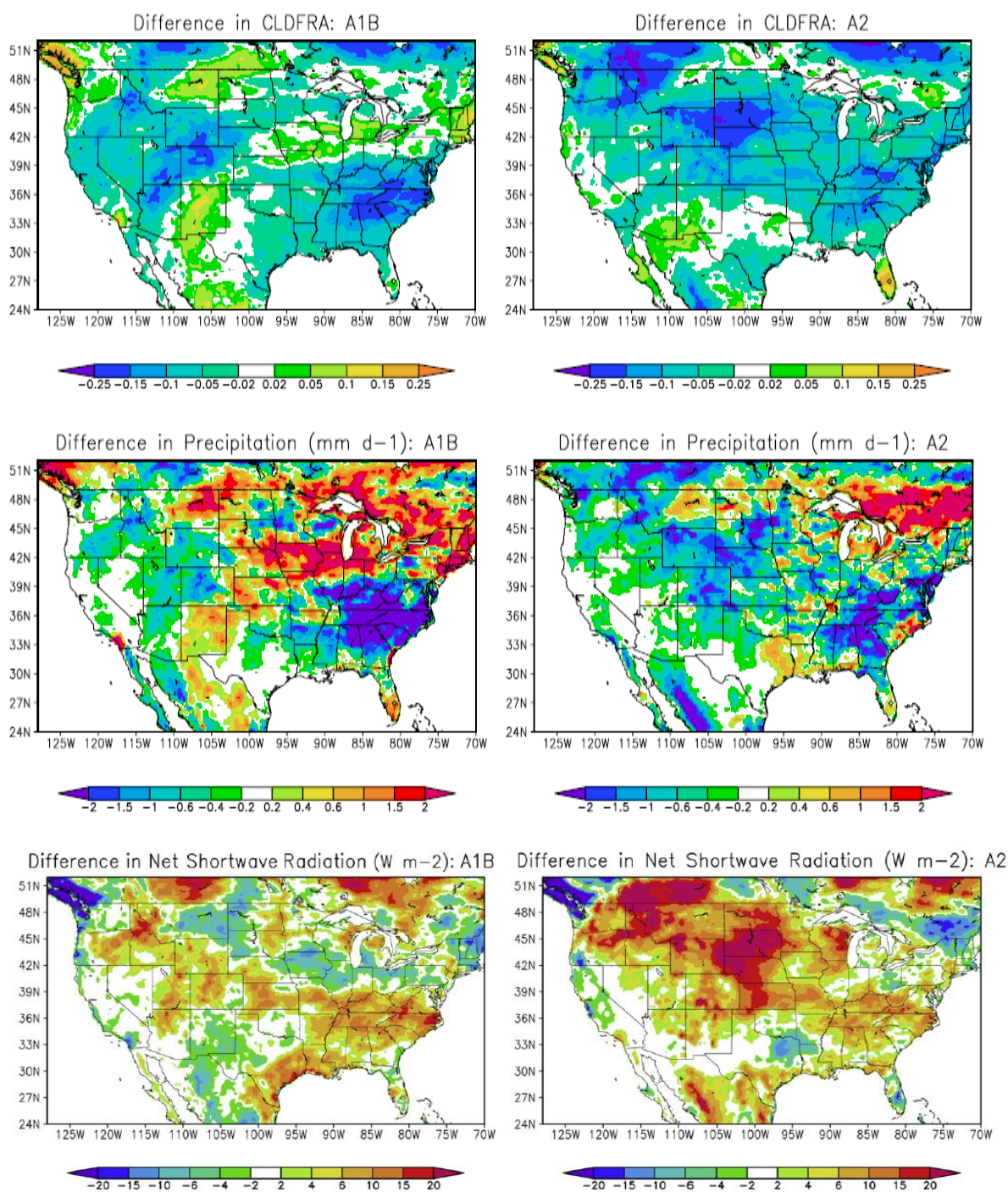


Figure 5.7. Differences in temperature, wind speed, PBLH, cloud fraction (CLDFRA), precipitation and net shortwave radiation in July between 2050s (2051–2053) and 2000s (2001–2003) under the A1B and A2 scenarios.

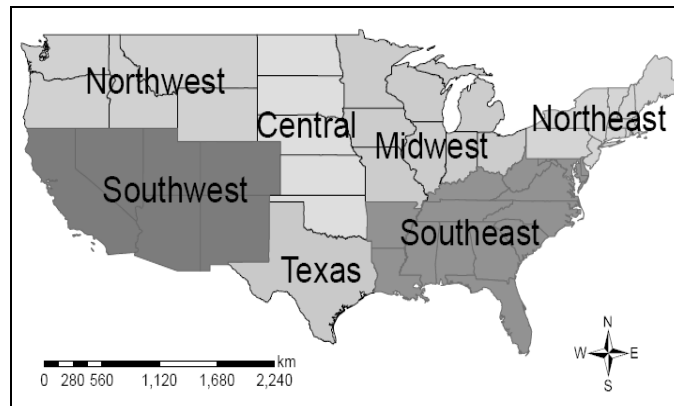


Figure 5.8. Seven sub-regions in the United States (U.S.).

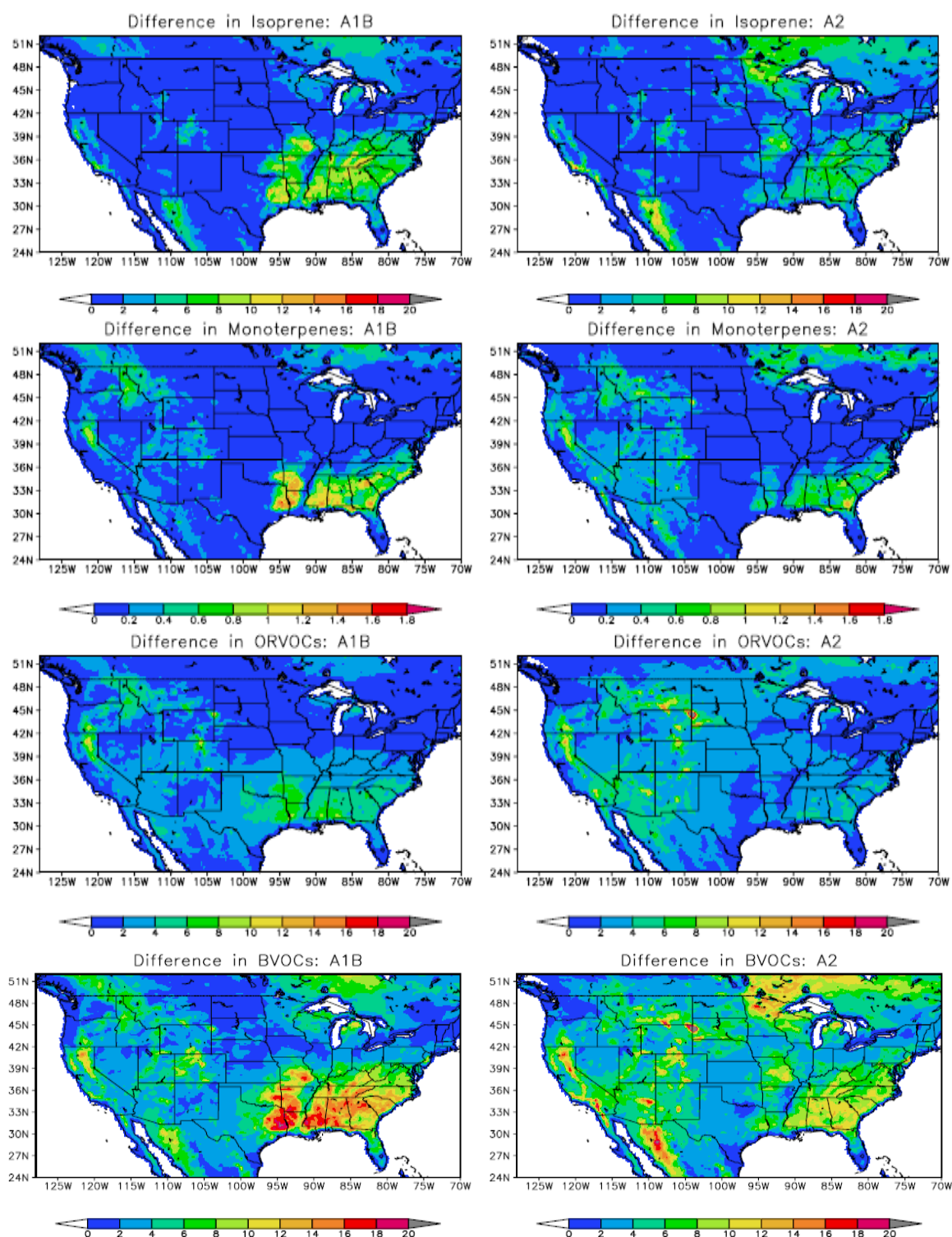


Figure 5.9. As in Figure 5.7, but for isoprene, monoterpenes, ORVOCs, and total biogenic emissions. (mol km<sup>-2</sup> h<sup>-1</sup>).



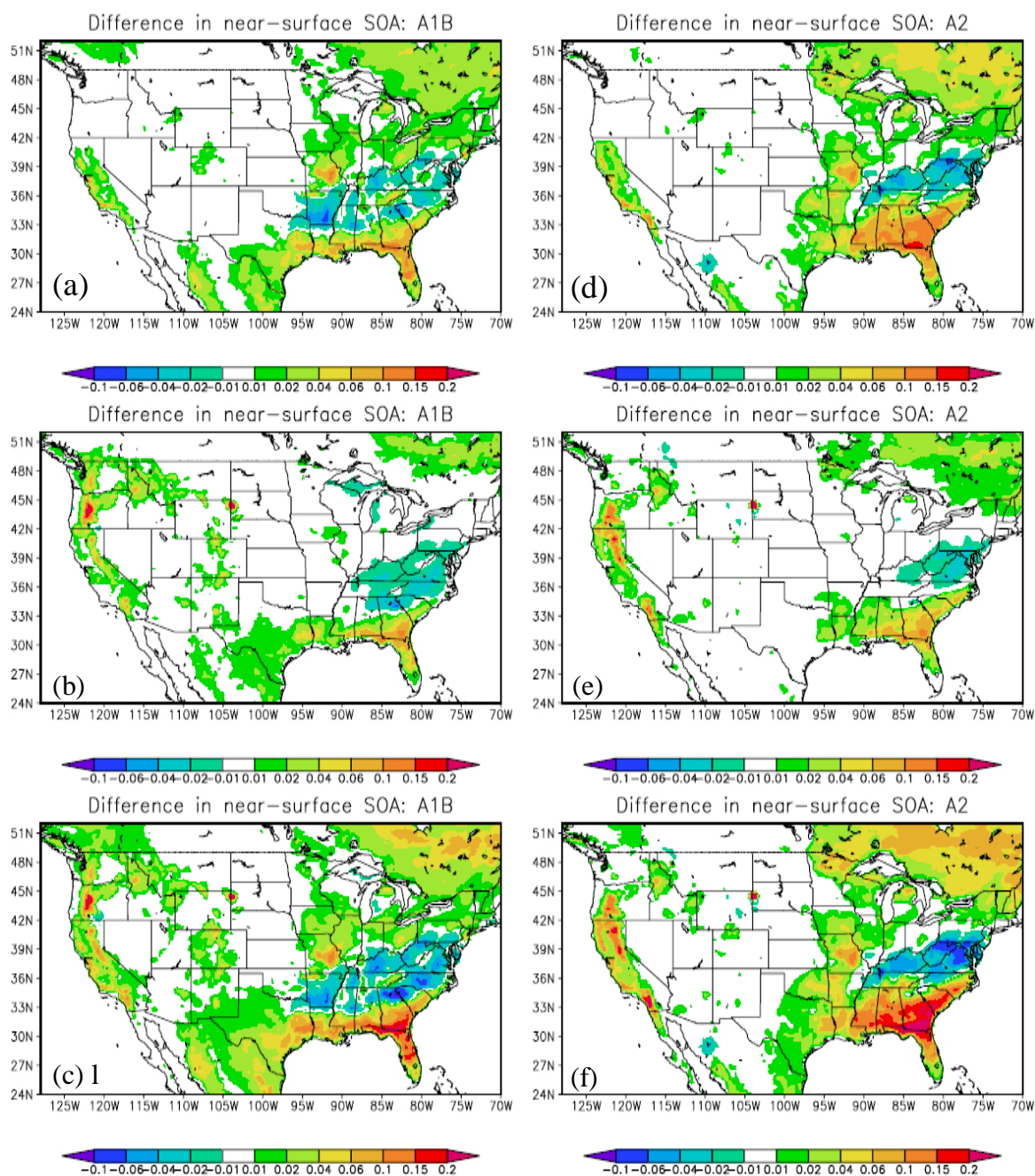


Figure 5.10. As in Figure 5.7, but for SOA concentrations ( $\mu\text{g m}^{-3}$ ). (a) and (d) are the contribution from isoprene, (b) and (e) are the contribution from monoterpenes, and (c) and (f) are the total concentrations.

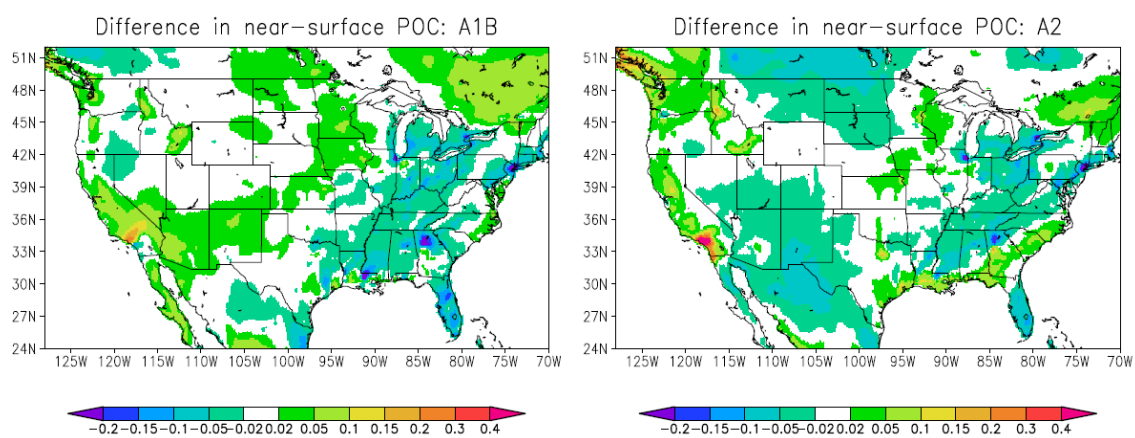


Figure 5.11. As in Figure 5.7, but for POC. ( $\mu\text{g m}^{-3}$ ).

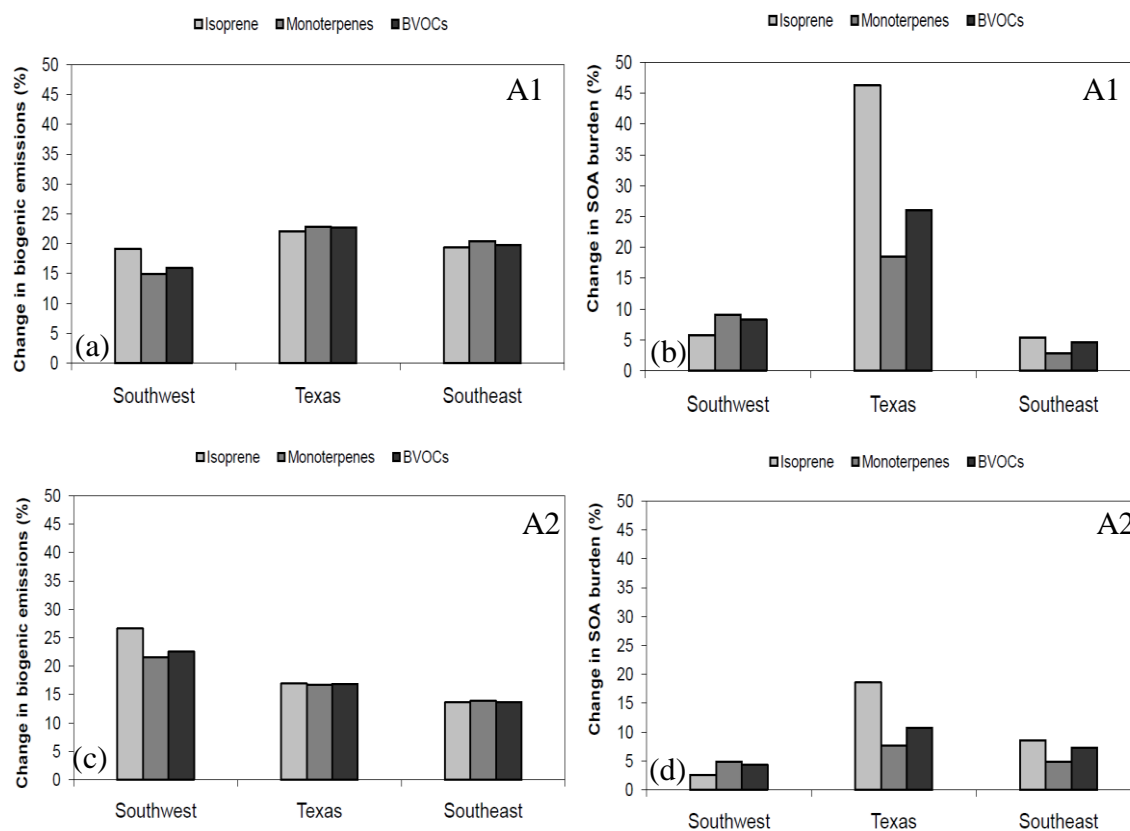


Figure 5.12. Percentage changes of biogenic emissions and SOA concentrations in three regions (Southwest, Texas and Southeast) under the A1B (a and b) and A2 (c and d) scenarios.

## **Chapter 6: Conclusions and Future Work**

This dissertation started with a set of research questions, and it has reached its objectives. It has also identified more new research questions related to land–climate interactions and their roles in the Earth system. Below I summarize the main accomplishment for each part of this dissertation. Contributions, limitations, and future research directions are presented at the end of this dissertation.

### **6.1. SUMMARY AND IMPLICATIONS**

The first part of this dissertation, Chapter 2, deals with land–climate interactions, and how land surface processes, particularly vegetation and groundwater processes, affect the overlying atmosphere. To achieve this goal, I performed a series of simulations with a regional coupled land–atmosphere model augmented with a vegetation phenology model and a simple groundwater model. A detailed analysis of modeling results suggests that the model with the considerations of vegetation growth and groundwater dynamics improves the simulations of summer precipitation over the transition zone, the Central U.S. The model, when considering vegetation growth, produces more rainfall (nearly 1 mm d<sup>-1</sup>) over the Central U.S. and northern parts of North American Monsoon regions (e.g., New Mexico and West Texas). Incorporating groundwater dynamics into the model adds 1–2 mm d<sup>-1</sup> increase in summer precipitation over the Central U.S. The comparisons of cumulative precipitation and monthly precipitation with observations over the Central U.S. suggest that the two new components play a very important role in enhancing the persistence of intraseasonal precipitation in regional climate models.

Moreover, the model with both vegetation growth and groundwater dynamics included improve the simulation of diurnal cycle of precipitation, a challenging issue in climate modeling research. The analysis of evapotranspiration (ET) and the relationship between Lifting Condensation Level (LCL) and Soil Moisture Index (SMI) indicates that vegetation and groundwater dynamics exert a strong role on land–climate coupling. The impact of groundwater is significant when soil moisture is relatively dry. Overall, this work suggests incorporating vegetation and groundwater dynamics into a regional climate model would be especially beneficial for seasonal precipitation forecast over the transition zones. The findings presented in Chapter 2 provide a greater understanding of the impacts of vegetation phenology on intraseasonal precipitation, and demonstrate the importance of groundwater dynamics on precipitation, which was traditionally ignored in climate models.

Chapter 3 provides an overview of the importance of land–climate interactions in future air quality projections. It describes how the interactions might affect surface ozone ( $O_3$ ) and secondary organic aerosols (SOA) in both direct and in-direct ways. Results of detailed case studies are presented in Chapters 4 and 5. In these two chapters, I addressed application of an integrated land–atmosphere–chemistry modeling system in understanding the impacts of land and climate interactions on regional air quality in a future changing climate.

In Chapter 4, the role of land–climate interactions in future changes in surface ozone ( $O_3$ ) and other related chemical species is explored through the sensitivity

experiments taking into account the future changes in urban land use and climate. The role of changes in land surface conditions was explored with the use of a coupled land–atmosphere–chemistry model augmented with an urban canopy model. To understand future O<sub>3</sub> changes due to land use and climate change in the Houston area, the coupled model with the utilization of projected future land use data was driven by the global climate model output. The modeling results suggest that the impact of land use change is at least equally important with that of climate change on future changes in O<sub>3</sub> air quality. Climate change induces about an 8% increase in the extreme O<sub>3</sub> days and land use change adds an additional 4% increase over the Houston area. The increase is found near the urban area, but not exactly in the urban center. The impacts of land use change and climate change on surface ozone concentrations differ across the various areas of the modeling domain. The core urban area is highly influenced by land use change, while the suburban areas are more likely affected by climate change. Additional sensitivity experiment investigating the relative impacts of anthropogenic emissions change on extreme O<sub>3</sub> days suggest that future anthropogenic emissions change also play an important role. This work indicates that urban land use extension and climate change will worsen O<sub>3</sub> pollution in the Houston area.

The findings about possible changes in future air quality have some implications. As the world moves forward, policies aimed at mitigating climate change and improving air quality should be made. For instance, energy policy offers an opportunity to improve air quality through the utilization non-polluting energy sources. Urban extension should be taken into account in air quality management. The results presented in this dissertation

could also help policy makers set future national air quality standards such as the National Ambient Air Quality Standard (NAAQS) in the United States

Chapter 5 addressed the sensitivity of biogenic emissions from vegetation and SOA formed through the oxidation of biogenic emissions to different climate change scenarios. Vegetation on land can regulate climate through not only biophysical pathways, but also biogeochemical pathways. In this part of the dissertation, I explored how vegetation could affect biogenic emissions and, thus, SOA. A simple two-product SOA model was incorporated into the coupled land–atmosphere–chemistry model to simulate SOA concentrations. Satellite and ground-based aerosol measurements were used to evaluate the model performance. Comparison of model simulated AOD with MODIS derived AOD shows that the model without the consideration of SOA underestimates aerosol optical depth (AOD) by 0.1–0.5 over the region where the amount of biogenic emissions is significant (e.g., southeastern U.S.). Evaluation of simulated organic carbon OC against ground-based measurements shows a very good agreement over much of the modeling domain. However, some exceptions do exist. For example, the model with or without SOA fails to capture the high AOD or OC in the northwestern and eastern U.S., which is attributed to the lack of fire and dust emissions in the current simulations. The modeling results show that high concentrations of biogenic emissions are mainly located over the areas where there is a significant amount of vegetation. Vegetation contributes to the formation of SOA to a large extent. The modeled SOA in OC is significant, with the ratio ranging from 0.1 to 0.5/0.6. .

The sensitivity of SOA to different climate change scenarios is investigated with the model driven by global climate model output. Changes in regional climate, biogenic emissions and SOA under different future climate scenarios are analyzed. I found that projected changes in regional climate are to some extent dependent on the projected global climate changes, which are scenario-dependent. Under the A1B scenario, the largest temperature increases ( $>2\text{K}$ ) are projected to occur in Texas, while the smallest increases in temperature occur in the northwest. Under the A2 scenario, the largest increases are seen over the central U.S., and the smallest increases occur over the southeastern U.S. As a result of climate change in the future, biogenic emissions are predicted to increase everywhere, with the largest increase found in the southeastern and northwestern U.S. under the two scenarios. The spatial variations in biogenic emissions change do exist because of differences in future temperature increases. The overall changes in the spatial patterns in SOA are not identical with those in temperature and biogenic emissions. Other factors including primary organic aerosols and anthropogenic emissions could also influence SOA formation.

The findings from this part of research suggest the importance of vegetation in the formation of biogenic emissions and SOA. It is of great importance to represent the vegetation conditions in the coupled model more precisely to improve the simulations of atmospheric composition including BVOCs and SOA. Although there are several previous studies that have examined different factors in controlling SOA concentrations in the future climate, the regional details are not well represented. This work provided the regional-scale details and assessed how different climate scenarios would influence BVOCs and SOA.



## **6.2. CONTRIBUTIONS, LIMITATIONS, AND FUTURE DIRECTIONS**

The Earth's climate system is fully coupled involving many interactions and feedbacks among different subsystems. Our ability to predict future changes in climate is strongly influenced by our ability to simulate conditions in each subsystem and feedbacks between them. This work made a number of contributions. Overall, conclusions drawn from the research conducted for this dissertation improve our understanding of land–climate interactions and their impacts on air quality. The developed integrated regional land–atmosphere–chemistry modeling system can be used to further investigate the roles of land surface in the climate system, to better understand the interactions between climate and atmospheric chemistry, and to provide better regional air quality and climate predictions. There has been a strong need to develop a regional Earth system model including all the components and feedbacks. This work increases our knowledge in building such a system.

With regard to the roles of vegetation and groundwater in regional climate, the work conducted in this dissertation demonstrated the importance of vegetation phenology and groundwater dynamics in simulating summer precipitation and land–climate coupling in a regional climate model. The developed modeling framework can be used to study the impacts of vegetation and subsurface processes on precipitation over the timescales of months to decades. The framework can also be applied to other places of the world. However, in this part of work, I did not include the effects of horizontal exchange of water between grid cells, which has been shown to play an important role in soil moisture and precipitation on local scales (Maxwell and Kollet, 2008). The simple groundwater

model used in this dissertation research needs to be improved to take into account of this feature. For the vegetation model, there is only one layer; a multi-layer canopy model is preferred in future studies.

The work on understanding the impacts on future O<sub>3</sub> air quality has important implications for air quality management. The results reveal that future O<sub>3</sub> air quality is very sensitive to future climate change. Model projections of future climate change are crucial for projecting future regional air quality changes. In addition, urban land use change could also contribute to O<sub>3</sub> increase, reflecting the importance of accounting for the effects of human disturbance on air quality forecasting. While previous studies have studied the potential contribution of climate change and land use change to O<sub>3</sub> air quality separately, this work compared and quantified the impacts of climate change and land use change on O<sub>3</sub> air quality. It also utilized an urban canopy model in air quality modeling, which was not used in previous studies that examined land use impacts on air quality. The work also suggests that future changes in biogenic emissions could affect future O<sub>3</sub> air quality. However, simulations of biogenic emissions in this work are only dependent on radiation and temperature. Future work should take into account of the effects of carbon dioxide, soil moisture, and vegetation phenology on biogenic emissions as suggested by other studies (e.g., Guenther et al., 2006; Heald et al., 2009; Wilkinson et al., 2009). Moreover, the results of this work are under one climate and land use change scenario, more sensitivity experiments accounting for the effects of different factors including anthropogenic emissions, biogenic emissions, land use/land cover change, and

climate change are needed to investigate and quantify the relative impacts on air quality in a comprehensive manner for a range of different scenarios.

The implementation of SOA formation in the current version of WRF/Chem represents an important step towards understanding the roles of BVOCs and SOA in air quality and climate on regional scales. The feedbacks of BVOCs to climate through the formation of SOA are still less certain. The development of the integrated land–atmosphere–chemistry model with SOA included allows us to examine their roles in the climate system. Although there are uncertainties in the SOA formation mechanism, the work presented in this dissertation on the effects of climate change on future changes in biogenic emissions and SOA under the different emissions scenarios at least provides us with some ideas about how climate change would matter in projecting future levels of BVOCs and SOA on regional scales. Further improvements in SOA formation (i.e., the consideration of the impacts of isoprene inhibition on SOA formation, and more realistic values of heat of vaporization, and the inclusion of more SOA precursors) and the biogenic emissions model as aforementioned, are particularly important for us to investigate the roles of BVOCs and SOA in climate change. My research findings also suggest the importance of including fire and dust emissions in the model. They need be considered in future studies.

## Appendix: Acronyms and Terms

2-m temperature	Air temperature at the level that is 2 meters above the surface
A1B	A midline scenario describes a future world of very rapid economic growth and global population that peaks in mid-century and declines thereafter, and the rapid introduction of new and more efficient technologies. Balanced is defined as not relying too heavily on one particular energy source, on the assumption that similar improvement rates apply to all energy supply and end-use technologies. (IPCC, 2001) A scenario describes a very heterogeneous world. The underlying theme is self-reliance and preservation of local identities. Fertility patterns across regions converge very slowly, which results in continuously increasing population. Economic development is primarily regionally oriented and per capita economic growth and technological change more fragmented and slower than other storylines. (IPCC, 2001)
A2	
AERONET	AErosol RObotic NETwork
AOD	Aerosol Optical Depth
AR4	Fourth Assessment Report
AVHRR	Advanced Very High Resolution Radiometer
BEIS3	Biogenic Emissions Inventory System, version 3
BELD3	Biogenic Emissions Land use Database, version 3
BVOCs	Biogenic Volatile Organic Compounds
CBM	Carbon Bond Mechanism
CCSM	Community Climate System Model
CH <sub>4</sub>	Methane
CO	Carbon Monoxide
CPC	Climate Prediction Center
EPA	Environmental Protection Agency
ET	Evapotranspiration
GCM	General Circulation Model
HCHO	Formaldehyde
HNO <sub>3</sub>	Nitric Acid
IGBP	International Geosphere–Biosphere Programme
IMPROVE	Interagency Monitoring of Protected Visual Environments
IPCC	Intergovernmental Panel on Climate Change
LAI	Leaf Area Index
LCL	Lifting Condensation Level
LSM	Land Surface Model
MODIS	Moderate Resolution Imaging Spectroradiometer
MOSAIC	Model for Simulating Aerosol Interactions and Chemistry

NAAQS	National Ambient Air Quality Standards
NARR	North American Regional Reanalysis
NASA	National Aeronautics and Space Administration
NCAR	National Center for Atmospheric Research
NCEP	National Centers for Environment Prediction
NDVI	Normalized Difference Vegetation Index
NEI-99	1999 National Emission Inventory
NH <sub>3</sub>	Ammonia
NLCD	National Land Cover Database
NMVOCs	Non-Methane Volatile Organic Compounds
NO	Nitrogen Oxide
NO <sub>3</sub>	Nitrate
NOAA	National Oceanic and Atmospheric Administration
NO <sub>x</sub>	Nitrogen Oxides
O <sub>3</sub>	Ozone
OC	Organic Carbon
OH	Hydroxyl Radical
ORVOCs	Other Reactive Volatile Organic Compounds
PAN	Peroxyacetyl Nitrate
PBL	Planetary Boundary Layer
PBLH	Planetary Boundary Layer Height
PM <sub>2.5</sub>	Particular Matter with diameter less than 2.5 μm
POA	Primary Organic Aerosols
POC	Primary Organic Carbon
RADM2	Regional Acid Deposition Model version 2
SIMGM	SIMple Groundwater Model
SMI	Soil Moisture Index
SO <sub>2</sub>	Sulfur Dioxide
SOA	Secondary Organic Aerosols
SRES	Special Report on Emission Scenarios
SST	Sea Surface Temperature
T85	Spatial resolution of global climate model, and represents a 256 by 128 regular longitude/latitude global horizontal grid (~1.41 °)
TCEQ	Texas Commission on Environmental Quality
TOPMODEL	Watershed hydrology model
UCM	Urban Canopy Model
USGS	United States Geological Survey
VGf	Vegetation Greenness Fraction
VOCs	Volatile Organic Compounds
WRF	Weather Research and Forecasting

## References

- Andersson-Skold Y. and D. Simpson (2001), Secondary organic aerosol formation in northern Europe: A model study, *J. Geophys. Res.*, 106(D7), 7357–7374.
- Andreae, M. O. and P. J. Crutzen (1997), Atmospheric aerosols: biogeochemical sources and role in atmospheric chemistry, *Science*, 276, 1052–1058, 1997.
- Anyah, R. O., C. P. Weaver, G. Miguez-Macho, Y. Fan, and A. Robock (2008), Incorporating water table dynamics in climate modeling: 3. Simulated groundwater influence on coupled land–atmosphere variability, *J. Geophys. Res.*, 113, D07103, doi:10.1029/2007JD009087.
- Avise, J., J. Chen, B. Lamb, C. Wiedinmyer, A. B. Guenther, E. Salathe, and C. Mass (2009), Attribution of projected changes in summertime US ozone and PM<sub>2.5</sub> concentrations to global changes, *Atmos. Chem. Phys.*, 9, 1111–1124.
- Aw, J., and M. J. Kleeman (2003), Evaluating the first-order effect of intraannual temperature variability on urban air pollution, *J. Geophys. Res.*, 108(D12), 4365, doi:10.1029/2002JD002688.
- Axson, J. L., K. Takahashi, D. DeHaan, and V. Vaida (2010), Gas-phase water-mediated equilibrium between methylglyoxal and its geminal diol, *Proc. Natl. Acad. Sci., U.S.A.*, (107)15: 6687–6692.
- Barnard, J. C., E. G. Chapman, J. D. Fast, J. R. Schmelzer, J. R. Slusser, and R. E. Shetter (2004), An evaluation of the FAST-J photolysis algorithm for predicting nitrogen dioxide photolysis rates under clear and cloudy sky conditions, *Atmos. Environ.*, 38, 3393–3403.
- Barth, M., J. McFadden, J. Sun, et al. (2005), Coupling between land ecosystems and the atmospheric hydrologic cycle through biogenic aerosol pathways, *Bull. Amer. Meteorol. Soc.*, 86, 1738–1742.
- Baudena, M., F. D’Andrea, and A. Provenzale (2008), A model for soil-vegetation-atmosphere interactions in water-limited ecosystems, *Water Resour. Res.*, 44, W12429, doi:10.1029/2008WR007172.
- Beljaars, A. C. M., P. Viterbo, M. J. Miller, and A. K. Betts (1996), The anomalous rainfall over the United States during July 1993—Sensitivity to land-surface parameterization and soil moisture, *Mon. Wea. Rev.*, 124, 362 – 383.
- Betts, A. K. (1997), The parameterization of deep convection, in *The Physics and Parameterization of Moist Atmospheric Convection*, edited by R. K. Smith, chap. 10, NATO ASI Ser. C, 505, 255–279.
- Betts, A. K. (2004), Understanding hydrometeorology using global models, *Bull. Am.*

- Meteorol. Soc., 85, 1673–1688.
- Betts, A. K., and P. Viterbo (2005), Land-surface, boundary layer and cloud-field coupling over the south-western Amazon in ERA-40, *J. Geophys. Res.*, 110, D14108, doi:10.1029/2004JD005702.
- Betts, A. K. (2007), Coupling of water vapor convergence, clouds, precipitation, and land-surface processes, *J. Geophys. Res.*, 112, D10108, doi:10.1029/2006JD008191.
- Beven, K. J., and M. J. Kirkby (1979), A physically based, variable contributing model of basin hydrology, *Hydrol. Sci. Bull.*, 24, 43–69.
- Bierkens, M. F. P., and B. J. J. M. van den Hurk (2007), Groundwater convergence as a possible mechanism for multi-year persistence in rainfall, *Geophys. Res. Lett.*, 34, L02402, doi:10.1029/2006GL028396.
- Binkowski, F.S. and U. Shankar (1995), The regional particulate matter model: 1. Model description and preliminary results, *J. Geophys. Res.*, 100, 26 191–26 209.
- Bonan, G. B., et al. (2002), The land surface climatology of the Community Land Model coupled to the NCAR Community Climate Model, *J. Clim.*, 15, 3123–3149.
- Bonan, G. B., et al. (2003), A dynamic global vegetation model for use with climate models: Concepts and description of simulated vegetation dynamics, *Global Change Biol.*, 9(11), 1543–1566, doi:10.1046/j.1365-2486.2003.00681.x.
- Bonan, G. B. (2008), *Ecological climatology*, Cambridge Univ. Press, Cambridge, ed. 2.
- Bonan, G. B. (2008), Forests and climate change: Forcings, feedbacks, and the climate benefits of forests, *Science*, 320, 1444–1449, doi:10.1126/science.1155121.
- Bossioli, E., M. Tombrou, A. Dandou, and N. Soula-kellis (2007), Simulation of the effects of critical factors on ozone formation and accumulation in the greater Athens area, *J. Geophys. Res.*, 112, D02309, doi:10.1029/2006JD007185.
- Byun, D.W., S. Kim, B. Czader, et al. (2005), Estimation of biogenic emissions with satellite-derived land use and land cover data for air quality modeling of Houston-Galveston ozone nonattainment area, *J. Environ. Manage.*, 75(4), 285–301.
- Calvert, J. G., R. Atkinson, J. A. Kerr, S. Madronich, G. K. Moortgat, T. J. Wallington, and G. Yarwood (2000), *The mechanisms of the atmospheric oxidation of the alkenes*, Oxford University Press, Oxford, pp552.
- Carlton, A. G., B. J. Turpin, H.-J. Lim, K. E. Altieri, and S. Seitzinger (2006), Link between isoprene and secondary organic aerosol (SOA): Pyruvic acid oxidation yields low volatility organic acids in clouds, *Geophys. Res. Lett.*, 33, L06822,

doi:10.1029/2005GL025374.

- Carlton, A. G., C. Wiedinmyer, and J. H. Kroll (2009), A review of Secondary Organic Aerosol (SOA) formation from isoprene, *Atmos. Chem. Phys.*, 9, 4987–5005.
- Carlton, A. G., R. W. Pinder, P. V. Bhawe, and G. A. Pouliot (2010), To What Extent Can Biogenic SOA be Controlled?, *Environ. Sci. Technol.*, 44:3376–3380.
- Carslaw, K. S., O. Boucher, D. V. Spracklen, G. W. Mann, J. G. L. Rae, S. Woodward, and M. Kulmala (2010), A review of natural aerosol interactions and feedbacks within the Earth system, *Atmos. Chem. Phys.*, 10, 1701–1737, doi:10.5194/acp-10-1701-2010.
- Chase, T. N., R. A. Pielke, T. G. F. Kittel, R. Nemani, and S. W. Running (1996), Sensitivity of a general circulation model to global changes in leaf area index, *J. Geophys. Res.*, 101(D3), 7393–7408.
- Chase, T. N., R. A. Pielke, T. G. F. Kittel, R. R. Nemani, and S. W. Running (2000), Simulated impacts of historical land cover changes on global climate in northern winter, *Climate Dyn.*, 16, 93–105.
- Chen, F., and J. Dudhia (2001), Coupling an advanced land-surface/hydrology model with the Penn State/ NCAR MM5 modeling system. Part I: Model description and implementation, *Mon. Wea. Rev.*, 129, 569–585.
- Chen, F., H. Kusaka, M. Tewari, J.-W. Bao, and H. Hirakuchi (2004), Utilizing the coupled WRF/LSM/Urban modeling system with detailed urban classification to simulate the urban heat island phenomena over the Greater Houston area, Fifth Conference on Urban Environment, Vancouver, BC, Canada, Amer. Meteorol. Soc., CD-ROM. 9.11.
- Chen, F., M. Tewari, H. Kusaka, and T. T. Warner (2006), Current status of urban modeling in the community Weather Research and Forecast (WRF) model, Joint with Sixth Symposium on the Urban Environment and AMS Forum: Managing our Physical and Natural Resources: Successes and Challenges, Atlanta, GA, USA, Amer. Meteorol. Soc., CD-ROM. J1.4.
- Chen, J., J. Avise, A. Guenther, C. Wiedinmyer, E. Salathe, R.B. Jackson, and B. Lamb (2009), Future land use and land cover influences on regional biogenic emissions and air quality in the United States, *Atmos. Environ.*, 43, 5771–5780.
- Chin, M., R. B. Rood, S.-J. Lin, J.-F. Müller, and A. M. Thompson (2000), Atmospheric sulfur cycle simulated in the global model GOCART: Model description and global properties, *J. Geophys. Res.*, 105(D20), 24,671–24,687.
- Christensen J. H., et al. (2007), Regional Climate Projections. In: *Climate Change 2007: The Physical Science Basis. Contribution of Working Group I to the Fourth*



- Assessment Report of the Intergovernmental Panel on Climate Change [Solomon, S., D. Qin, M. Manning, Z. Chen, M. Marquis, K.B. Averyt, M. Tignor and H.L. Miller (eds.)]. Cambridge University Press, Cambridge, United Kingdom and New York, NY, USA.
- Chung, S. H., and J. H. Seinfeld (2002), Global distribution and climate forcing of carbonaceous aerosols, *J. Geophys. Res.*, 107(D19), 4407, doi:10.1029/2001JD001397.
- Civerolo, K. L., G. Sistla, S. T. Rao, and D. J. Nowak (2000), The effects of land use in meteorological modeling: implications for assessment of future air quality scenarios, *Atmos. Environ.*, 34(10), 1615–1621.
- Civerolo, K. L., et al. (2007), Estimating the effects of increased urbanization on surface meteorology and ozone concentrations in the New York City metropolitan region, *Atmos. Environ.*, 41, 1803–1818.
- Claeys, M., et al. (2004), Formation of secondary organic aerosols through photooxidation of isoprene, *Science*, 303, 1173–1176.
- Collatz, G.J., J.T. Ball, C. Grivet, and J. A. Berry (1991), Physiological and environmental regulation of stomatal conductance, photosynthesis and transpiration—a model that includes a laminar boundary layer, *Agric. For. Meteorol.*, 54 (2–4), 107–136.
- Collins, W. D., et al. (2006), Radiative forcing by well-mixed greenhouse gases: Estimates from climate models in the Intergovernmental Panel on Climate Change (IPCC) Fourth Assessment Report (AR4), *J. Geophys. Res.*, 111, D14317, doi:10.1029/2005JD006713.
- Dabberdt, W. F., et al. (2004), Meteorological research needs for improved air quality forecasting: Report of the 11th Prospectus Development Team of the U.S. Weather Research Program, *Bull. Amer. Meteorol. Soc.*, 85(4), 563–586.
- Dai, A. and K. Trenberth (2004), The diurnal cycle and its depiction in the community climate system model, *J. Clim.*, 17, 930–951.
- Dawson J. P., P. J. Adams, and S. N. Pandis (2006), Sensitivity of ozone to summertime climate in the eastern USA: A modeling case study, *Atmos. Environ.*, 41, 1494–1511.
- Dawson, J. P., P. N. Racherla, B. H. Lynn, P. J. Adams, and S. N. Pandis (2009), Impacts of climate change on regional and urban air quality in the eastern United States: Role of meteorology, *J. Geophys. Res.*, 114, D05308, doi:10.1029/2008JD009849.
- de Gouw, J. A., et al. (2005), Budget of organic carbon in a polluted atmosphere: Results

- from the New England Air Quality Study in 2002, *J. Geophys. Res.*, 110, D16305, doi:10.1029/2004JD005623.
- DeBell, L. J., R.W. Talbot, J. E. Dibb, J. W. Munger, E. W. Fischer, and S. E. Frolking (2004), A major regional air pollution event in the northeastern United States caused by extensive forest fires in Quebec, Canada, *J. Geophys. Res.*, 109, D19305, doi:10.1029/2004JD004840.
- Dekker, S. C., M. Pietkerk, and M. F. P. Bierkens (2007), Coupling microscale vegetation-soil water and macroscale vegetation-precipitation feedbacks in semiarid ecosystems, *Global Change Biol.*, 13(3), 671–678.
- Dickinson R. E., M. Shaikh, R. Bryant, and L. Graumlich (1998), Interactive canopies for a climate model, *J. Clim.*, 11, 2823–2836.
- Dirmeyer, P. A. (2006), The hydrologic feedback pathway for land–climate coupling, *J. Hydrometeorol.*, 7, 857–867.
- Donahue, N., A. Robinson, C. Stanier, and S. Pandis (2006), Coupled partitioning, dilution, and chemical aging of semivolatile organics, *Environ. Sci. Technol.*, 40(8), 2635–2643, doi:10.1021/es052297c.
- Donahue, N. M., A. L. Robinson, and S. N. Pandis (2009), Atmospheric organic particulate matter: from smoke to secondary organic aerosol, *Atmos. Environ.*, 43 (1), 94e106. doi:10.1016/j.atmosenv.2008.09.055.
- Dong, J., W. Ni-Meister, and P. R. Houser (2007), Impacts of vegetation and cold season processes on soil moisture and climate relationships over Eurasia, *J. Geophys. Res.*, 112, D09106, doi:10.1029/2006JD007774.
- Dudhia, J. (1989), Numerical study of convection observed during the winter monsoon experiment using a mesoscale two-dimensional model, *J. Atmos. Sci.*, 46, 3077–3107.
- Eastman, J. L., M. B. Coughenour, and R. A. Pielke Sr. (2001), The effects of CO<sub>2</sub> and landscape change using a coupled plant and meteorological model, *Global Change Biol.*, 7, 797–815.
- Ek, M. B., K. E. Mitchell, Y. Lin, E. Rogers, P. Grunmann, V. Koren, G. Gayno, and J. D. Tarpley (2003), Implementation of Noah land surface model advances in the National Centers for Environmental Prediction operational mesoscale Eta model, *J. Geophys. Res.*, 108(D22), 8851, doi:10.1029/2002JD003296.
- El Haddad, I., Y. Liu, L. Nieto-Gligorovski, V. Michaud, B. Temime-Roussel, E. Quivet, N. Marchand, K. Sellegri, and A. Monod (2009), In-cloud processes of methacrolein under simulated conditions – Part 2: Formation of secondary organic aerosol, *Atmos. Chem. Phys.*, 9, 5107–5117.

- Famiglietti, J. S., and E. F. Wood (1994), Multiscale modeling of spatially variable water and energy balance processes, *Water Resour. Res.*, 30(11), 3061–3078.
- Fan, Y., G. Miguez-Macho, C. P. Weaver, R. Walko, and A. Robock (2007), Incorporating water table dynamics in climate modeling: 1. Water table observations and the equilibrium water table, *J. Geophys. Res.*, 112, D10125, doi:10.1029/2006JD008111.
- Farina, S. C., P. J. Adams, and S. N. Pandis (2010), Modeling global secondary organic aerosol formation and processing with the volatility basis set: Implications for anthropogenic secondary organic aerosol, *J. Geophys. Res.*, 115, D09202, doi:10.1029/2009JD013046.
- Fast, J. D. and W. E. Heilman (2005), Simulated sensitivity of seasonal ozone exposure in the Great Lakes region to changes in anthropogenic emissions in the presence of interannual variability, *Atmos. Environ.*, 39 (29), 5291–5306.
- Fast, J. D., W. I. Gustafson Jr., R. C. Easter, R. A. Zaveri, J. C. Barnard, E. G. Chapman, G. A. Grell, and S. E. Peckham (2006), Evolution of ozone, particulates, and aerosol direct radiative forcing in the vicinity of Houston using a fully coupled meteorology-chemistry-aerosol model, *J. Geophys. Res.*, 111, D21305, doi:10.1029/2005JD006721.
- Ferguson, I. M., and R. M. Maxwell (2010), Role of groundwater in watershed response and land surface feedbacks under climate change, *Water Resour. Res.*, 46, W00F02, doi:10.1029/2009WR008616.
- Fiore, A. M., D. J. Jacob, I. Bey, R. M. Yantosca, B. D. Field, A. C. Fusco, and J. G. Wilkinson (2002), Background ozone over the United States in summer: Origin, trend, and contribution to pollution episodes, *J. Geophys. Res.*, 107(D15), 4275, doi:10.1029/2001JD000982.
- Fiore, A. M., L. W. Horowitz, D. W. Purves, et al. (2005), Evaluating the contribution of changes in isoprene emissions to surface ozone trends over the eastern United States, *J. Geophys. Res.*, 110, D12303, doi:10.1029/2004JD005485.
- Foley, J. A., C. I. Prentice, N. Ramankutty, S. Levis, D. Pollard, S. Sitch, and A. Haxeltine (1996), An integrated biosphere model of land surface processes, terrestrial carbon balance, and vegetation dynamics, *Global Biogeochem. Cycles*, 10, 603–628.
- Foley, J. A., et al. (2005), Global consequences of land use, *Science*, 309(5734), 570–574.
- Foley, J. A., S. Levis, I. C. Prentice, D. Pollard, and S. L. Thompson (1998), Coupling dynamic models of climate and vegetation, *Global Change Biol.*, 4, 561–579.

- Foley, J. A., S. Levis, M. H. Costa, W. Cramer, and D. Pollard (2000), Incorporating dynamic vegetation cover within global climate models, *Ecol. Appl.*, 10, 1620–1632.
- Forkel, R., and R. Knoche (2006), Regional climate change and its impact on photooxidant concentrations in southern Germany: Simulations with a coupled regional climate-chemistry model, *J. Geophys. Res.*, 111, D12302, doi:10.1029/2005JD006748.
- Friedl, M. A., D. K. McIver, J. C. F. Hodges, et al. (2002), Global land cover mapping from MODIS: algorithms and early results, *Remote Sens. Environ.*, 83, 287–302.
- Frost, G. J., et al. (2006), Effects of changing power plant NO<sub>x</sub> emissions on ozone in the eastern United States: Proof of concept, *J. Geophys. Res.*, 111, D12306, doi:10.1029/2005JD006354.
- Gallo, K., L. Ji, B. Reed, J. Dwyer, and J. Eidenshink (2004), Comparison of MODIS and AVHRR 16-day normalized difference vegetation index composite data, *Geophys. Res. Lett.*, 31, L07502, doi:10.1029/2003GL019385.
- Geron, C. D., A. B. Guenther, and T. E. Pierce (1994), An improved model for estimating emissions of volatile organic compounds from forests in the eastern United States, *J. Geophys. Res.*, 99(D6), 12,773–12,792.
- Goldstein, A. H., C. D. Koven, C. L. Heald, and I. Y. Fung (2009), Biogenic carbon and anthropogenic pollutants combine to form a cooling haze over the southeastern United States, *Proc. Natl. Acad. Sci.*, 106, 8835–8840, doi:10.1073/pnas.0904128106.
- Grell, G. A., J. Dudhia, and D. R. Stauffer (1994), A description of the fifth-generation Penn State/NCAR mesoscale model (MM5), NCAR Technical Note, NCAR/TN-398+STR, 117pp.
- Grell, G. A., S. E. Peckham, R. Schmitz, S. A. McKeen, G. Frost, W. C. Skamarock, and B. Eder (2005), Fully coupled “online” chemistry within the WRF model, *Atmos. Environ.*, 39, 6957–6975.
- Griffin, R. J., D. R. Cocker III, J. H. Seinfeld, and D. Dabdub (1999), Estimate of global atmospheric organic aerosol from oxidation of biogenic hydrocarbons, *Geophys. Res. Lett.*, 26(17), 2721–2724.
- Griffin, R. J., D. Dabdub, M. J. Kleeman, M. P. Fraser, G. R. Cass, and J. H. Seinfeld (2002), Secondary organic aerosol: III. Urban/Regional scale model of size- and composition-resolved aerosols, *J. Geophys. Res.*, 107(D17), 4334, doi:10.1029/2001JD000544.
- Grossman-Clarke, S., J. A. Zehnder, W. L. Stefanov, et al. (2005), Urban modifications

- in a mesoscale meteorological model and the effects on near-surface variables in an arid metropolitan region, *J. Appl. Meteorol.*, 44 (9), 1281–1297.
- Grote, R., E. Lehmann, C. Brümmer, N. Brüggemann, J. Szarzynski, and H. Kunstmann (2009), Modelling and observation of biosphere-atmosphere interactions in natural savannah in Burkina Faso, West Africa, *Phys. Chem. Earth*, 34, 251–260.
- Guenther, A., et al. (1995), A global model of natural volatile organic compound emissions, *J. Geophys. Res.*, 100(D5), 8873–8892, doi:10.1029/94JD02950.
- Gulden, L. E., Z.-L. Yang, and G.-Y. Niu (2007), Interannual variation in biogenic emissions on a regional scale, *J. Geophys. Res.*, 112, D14103, doi:10.1029/2006JD008231.
- Guo, Z., P. A. Dirmeyer, R. D. Koster, et al. (2006), GLACE: The global land–atmosphere coupling experiment. Part II: Analysis, *J. Hydrometeorol.*, 7(4), 611–625.
- Gutman, G. and A. Ignatov (1998), Derivation of green vegetation fraction from NOAA/AVHRR for use in numerical weather prediction models, *Int. J. Remote Sens.*, 19, 1533–1543.
- Gutowski, W. J., Jr., C. J. Vörösmarty, M. Person, Z. Ötles, B. Fekete, and J. York (2002), A Coupled Land–Atmosphere Simulation Program (CLASP): Calibration and validation, *J. Geophys. Res.*, 107(D16), 4283, doi:10.1029/2001JD000392.
- Heald, C. L., D. J. Jacob, R. J. Park, L. M. Russell, B. J. Huebert, J. H. Seinfeld, H. Liao, and R. J. Weber (2005), A large organic aerosol source in the free troposphere missing from current models, *Geophys. Res. Lett.*, 32, L18809, doi:10.1029/2005GL023831.
- Heald, C. L., et al. (2008), Predicted change in global secondary organic aerosol concentrations in response to future climate, emissions, and land use change, *J. Geophys. Res.*, 113, D05211, doi:10.1029/2007JD009092.
- Heald, C. L., M. J. Wilkinson, R. K. Monson, C. A. Alo, G. Wang, and A. Guenther (2009), Response of isoprene emission to ambient CO<sub>2</sub> changes and implications for global budgets, *Glob. Cha. Bio.*, 15, 4, 1127–1140.
- Henze, D. K. and J. H. Seinfeld (2006), Global secondary organic aerosol from isoprene oxidation, *Geophys. Res. Lett.*, 33, L09812, doi:10.1029/2006GL025976.
- Higgins, R.W., W. Shi, E. Yarosh and R. Joyce (2000), Improved United States Precipitation Quality Control System and Analysis. NCEP/Climate Prediction Center ATLAS No. 7, 40 pp., Camp Springs, MD 20746, USA.

- Hoffmann, W. A., and R. B. Jackson (2000), Vegetation-climate feedbacks in the conversion of tropical savanna to grassland, *J. Clim.*, 13, 1593–1602.
- Hogrefe, C., et al. (2004), Simulating changes in regional air pollution over the eastern United States due to changes in global and regional climate and emissions, *J. Geophys. Res.*, 109, D22301, doi:10.1029/2004JD004690.
- Hogrefe, C., Lynn, B., Solecki, B., et al. (2007), Air quality in future decades - Determining the relative impacts of changes in climate, emissions, global atmospheric composition, and regional land use, *Air Pollution Modeling and Its Applications XVII*, 217–226.
- Holt, T. R., D. Niyogi, F. Chen, K. Manning, M. A. LeMone, and A. Qureshi (2006), Effect of land-atmosphere interactions on the IHOP 24–25 May 2002 convection case, *Mon. Wea. Rev.*, 134, 113–133.
- Holt, T, Author, Reprint Author Holt Teddy Holt, Teddy, Pullen, J, et al. (2007), Urban canopy modeling of the New York City metropolitan area: A comparison and validation of single- and multilayer parameterizations, *Mon. Wea. Rev.*, 135(5), 1906–1930.
- Hong, S.Y., and H. L. Pan (1996), Nonlocal boundary layer vertical diffusion in a medium-range forecast model, *Mon. Wea. Rev.*, 124, 2322–2339.
- Hong, S.-Y., J. Dudhia, and S.-H Chen (2004), A revised approach to ice microphysical processes for the bulk parameterization of clouds and precipitation, *Mon. Wea. Rev.*, 132, 103–120.
- Horowitz, L. W., A. M. Fiore, G. P. Milly, R. C. Cohen, A. Perring, P. J. Wooldridge, P. G. Hess, L. K. Emmons, and J.-F. Lamarque (2007), Observational constraints on the chemistry of isoprene nitrates over the eastern United States, *J. Geophys. Res.*, 112, D12S08, doi:10.1029/2006JD007747.
- Houghton, J. T., Y. Ding, D. J. Griggs, M. Noguer, P. J. van der Linden, X. Dai, K. Maskell, and C. A. Johnson (2001), *Climate Change 2001: The Scientific Basis—Contribution of Working Group I to the Third Assessment Report of the Intergovernmental Panel on Climate Change*, 881 pp., Cambridge Univ. Press, New York.
- Hoyle, C. R., G. Myhre, T. K. Berntsen, and I. S. A. Isaksen (2009), Anthropogenic influence on SOA and the resulting radiative forcing, *Atmos. Chem. Phys.*, 9, 2715–2728.
- Inoue, E. (1963), On the turbulent structure of air flow within crop canopies, *J. Met. Soc. Japan*, 41(6), 317–326.
- Intergovernmental Panel on Climate Change (IPCC) (2001), in Houghton, J. T., Y. Ding,

- D. J. Griggs, M. Noguer, van der Linden, P. J., X. Dai, K. Maskell, C. A. Johnson (eds.), *Climate Change 2001: The Scientific Basis*, Cambridge University Press, U.K. Cambridge.
- Intergovernmental Panel on Climate Change (IPCC) (2007), *Climate Change 2007: The Scientific Basis. Contribution of Working Group I to the Fourth Assessment Report of the Intergovernmental Panel on Climate Change*, edited by S. Solomon et al., Cambridge Univ. Press, New York.
- Jacob, D. J., and D. A. Winner (2009), Effect of climate change on air quality, *Atmos. Environ.*, 43(1), 51–63, doi:10.1016/j.ATMOSENV.2008.09.051.
- Jiang, G. F., and J. D. Fast (2004), Modeling the effects of VOC and NOX emission sources on ozone formation in Houston during the TexAQS 2000 field campaign, *Atmos. Environ.*, 38(30), 5071–5085.
- Jiang, X., C. Wiedinmyer, F. Chen, Z.-L. Yang, and J. C.-F. Lo (2008), Predicted impacts of climate and land use change on surface ozone in the Houston, Texas, area, *J. Geophys. Res.*, 113, D20312, doi:10.1029/2008JD009820.
- Jiang, X., G.-Y. Niu, and Z.-L. Yang (2009), Impacts of vegetation and groundwater dynamics on warm season precipitation over the Central United States, *J. Geophys. Res.*, 114, D06109, doi:10.1029/2008JD010756.
- Jiang, X., Z.-L. Yang, H. Liao, and C. Wiedinmyer (2010), Sensitivity of biogenic secondary organic aerosols to future climate change at regional scales: An online coupled simulation, *Atmos. Environ.*, 44, 4891–4907, doi:10.1016/j.atmosenv.2010.08.032
- Jimenez, J. L., et al. (2009), Evolution of organic aerosols in the atmosphere, *Science*, 326, 1525–1529, DOI: 10.1126/science.1180353.
- Jimenez, P., O. Jorba, et al. (2006), Evaluation of MM5-EMICAT2000-CMAQ performance and sensitivity in complex terrain: High-resolution application to the northeastern Iberian Peninsula, *Atmos. Environ.*, 40(26), 5056–5072.
- Kain J. S. and M. Fritsch (1990), A one-dimensional entraining/detraining plume model and its application in convective parameterization, *J. Atmos. Sci.*, 47, 2784–2802.
- Kanakidou, M., et al. (2005), Organic aerosol and global climate modelling: A review, *Atmos. Chem. Phys.*, 5, 1053–1123.
- Karl, M., K. Tsigaridis, E. Vignati, and F. Dentener (2009), Formation of secondary organic aerosol from isoprene oxidation over Europe, *Atmos. Chem. Phys.*, 9, 7003–7030, doi:10.5194/acp-9-7003-2009 .
- Kesselmeier, J. and M. Staudt (1999), Biogenic Volatile Organic Compounds (VOC): an

- overview on emission, physiology and ecology, *J. Atmos. Chem.*, 33, 23–28.
- Kim, Y., and G. Wang (2005), Modeling seasonal vegetation variation and its validation against Moderate Resolution Imaging Spectroradiometer (MODIS) observations over North America, *J. Geophys. Res.*, 110, D04106, doi:10.1029/2004JD005436.
- Kim, Y. J. and G. L. Wang (2007), Impact of vegetation feedback on the response of precipitation to antecedent soil moisture anomalies over North America. *J. Hydrometeorol.*, 8(3), 534–550.
- Kinnee, E., C. Geron, and T. Pierce (1997), United States land use inventory for estimation biogenic ozone precursor emissions, *Ecolog. Appl.*, 7, 46–58.
- Kollet, S. J., and R. M. Maxwell (2008), Capturing the influence of groundwater dynamics on land surface processes using an integrated, distributed watershed model, *Water Resour. Res.*, 44, W02402, doi:10.1029/2007WR006004.
- Koster, R. and M. J. Suarez (2000), Soil moisture memory in climate models, *J. Hydrometeorol.*, 2, 558–570.
- Koster, R. D., M. J. Suarez, A. Ducharne, M. Stieglitz, and P. Kumar (2000), A catchment-based approach to modeling land surface processes in a general circulation model: 1. Model structure, *J. Geophys. Res.*, 105, 24,809–24,822.
- Koster, R.D., P. A. Dirmeyer, Z. Guo, et al. (2004), Regions of strong coupling between soil moisture and precipitation, *Science*, 305, 1138–1140.
- Krinner, G., et al. (2005), A dynamic global vegetation model for studies of the coupled atmosphere-biosphere system, *Global Biogeochem. Cycles*, 19, GB1015, doi:10.1029/2003GB002199.
- Kroll, J. H., N. L. Ng, S. M. Murphy, R. C. Flagan, and J. H. Seinfeld (2006), Secondary organic aerosol formation from isoprene photooxidation, *Environ. Sci. Technol.*, 40, 1869–1877, doi:10.1021/es0524301.
- Kroll, J. H., and J. H. Seinfeld (2008), Chemistry of secondary organic aerosol: Formation and evolution of low-volatility organics in the atmosphere, *Atmos. Environ.*, 42: 3593–3624.
- Kusaka, H. and F. Kimura (2004a), Thermal effects of urban canyon structure on the nocturnal heat island: Numerical experiment using a mesoscale model coupled with an urban canopy model, *J. Appl. Meteorol.*, 43, 1899–1910.
- Kusaka, H. and F. Kimura (2004b), Coupling a single-layer urban canopy model with a simple atmospheric model: Impact of urban heat island simulation for an idealized case, *J. Meteorol. Soc. Japan*, 82, 67–80.
- Kusaka, H., H. Kondo, Y. Kikegawa, and F. Kimura (2001), A simple single-layer urban



- canopy model for atmospheric models: Comparison with multi-layer and slab models, *Bound.-Layer Meteorol.*, 101, 157–182.
- Lack, D.A., X. X. Tie, N. D. Bofinger, A. N. Wiegand, and S. Madronich (2004), Seasonal variability of secondary organic aerosol: A global modelling study, *J. Geophys. Res.*, 109, D03203 doi:10.1029/2003JD003418.
- Lamb, R.G. (1988), Diagnostic studies of ozone in the northeastern United States based on application of the Regional Oxidant Model (ROM), in : *The Scientific and Technical Issues Facing Post – 1987 Ozone Control Strategies*, G. T. Wolff, J. L. Hanisch, and K. Schere, eds., Air Waste Manag. Assoc., Pittsburgh, Pennsylvania.
- Leung, L. R., and W. I. Gustafson Jr. (2005), Potential regional climate change and implications to U.S. air quality, *Geophys. Res. Lett.*, 32, L16711, doi:10.1029/2005GL022911.
- Levis, S., C. Wiedinmyer, G. B. Bonan, and A. B. Guenther (2003), Simulating biogenic volatile organic compound emissions in the Community Climate System Model, *J. Geophys. Res.*, 108(D21), 4659, doi:10.1029/2002JD003203.
- Li, G., R. Zhang, J. Fan, and X. Tie (2007), Impacts of biogenic emissions on photochemical ozone production in Houston, Texas, *J. Geophys. Res.*, 112, D10309, doi:10.1029/2006JD007924.
- Liang X., Z. Xie, and M. Huang (2003), A new parameterization for surface and groundwater interactions and its impact on water budgets with the variable infiltration capacity (VIC) land surface model, *J. Geophys. Res.*, 108, 8613, doi:10.1029/2002JD003090.
- Liao, H., W.-T. Chen, and J. H. Seinfeld (2006), Role of climate change in global predictions of future tropospheric ozone and aerosols, *J. Geophys. Res.*, 111, D12304, doi:10.1029/2005JD006852.
- Liao, H., D. K. Henze, J. H. Seinfeld, S. Wu, and L. J. Mickley (2007), Biogenic secondary organic aerosol over the United States: Comparison of climatological simulations with observations, *J. Geophys. Res.*, 112, D06201, doi:10.1029/2006JD007813.
- Lide, D. R., (Ed.) (2001), *CRC Handbook of Chemistry and Physics*, CRC Press, Boca Raton, Fla..
- Lin, W. S., C. H. Sui, et al. (2007), A numerical study of the influence of urban expansion on monthly climate in dry autumn over the Pearl River Delta, China, *Theor. Appl. Climatol.* 89 (1-2), 63–72.
- Lin, Y.-L., R. D. Rarley, and H. D. Orville (1983), Bulk parameterization of the snow

- field in a cloud model, *J. Appl. Meteorol.*, 22, 1065–1092.
- Liu, Y., F. Chen, T. Warner, and J. Basara (2006), Verification of a mesoscale data-assimilation and forecasting system for the Oklahoma City area during the Joint Urban 2003 field project, *J. Appl. Meteorol. Climatol.*, 45, 912–929.
- Liu, Z., M. Notaro, J. Kutzbach, and N. Liu (2006), Assessing global vegetation-climate feedbacks from observations, *J. Clim.*, 19 (5), 787–814.
- Lo, J. C. F., A. K. H. Lau, F. Chen, J. C. H. Fung, and K. K. M. Leung (2007), Urban Modification in a Mesoscale Model and the Effects on the Local Circulation in the Pearl River Delta Region, *J. Appl. Meteorol. Climatol.*, 46, 457–476.
- Lo, J. C.-F., Z.-L. Yang, and R. A. Pielke Sr. (2008), Assessment of three dynamical climate downscaling methods using the Weather Research and Forecasting (WRF) model, *J. Geophys. Res.*, 113, D09112, doi:10.1029/2007JD009216.
- Lorenz, E. N. (1963), The predictability of hydrodynamic flow. *Trans. New York Acad. Sci.*, 25B, 409–432.
- Lorenz, E. N. (1969), The predictability of a flow which possesses many scales of motion. *Tellus*, 21, 289–307.
- Madronich, S. (1987), Photodissociation in the atmosphere. I - Actinic flux and the effects of ground reflections and clouds, *J. Geophys. Res.*, 92, 9740–9752.
- Martin, R. V., D. J. Jacob, R. M. Yantosca, M. Chin, and P. Ginoux (2003), Global and regional decreases in tropospheric oxidants from photochemical effects of aerosols, *J. Geophys. Res.*, 108(D3), 4097, doi:10.1029/2002JD002622.
- Matsui, T., V. Lakshmi, and E. E. Small (2005), The effects of satellite-derived vegetation cover variability on simulated land–atmosphere interactions in the NAMS, *J. Clim.*, 18(1), 21–40.
- Maxwell, R. M., and N. L. Miller (2005), Development of a Coupled Land Surface and Groundwater Model, *J. Hydrometeorol.*, 6, 233–247.
- Maxwell, R. M., F. K. Chow, and S. J. Kollet (2007), The groundwater-land-surface-atmosphere connection: Soil moisture effects on the atmospheric boundary layer in fully-coupled simulations, *Adv. Wat. Resour.*, 30, 2447–2466.
- Maxwell, R. M. and S. J. Kollet (2008), Interdependence of groundwater dynamics and land-energy feedbacks under climate change, *Nat. Geosci.*, 1, 665–669.
- McKeen, S. A., et al. (2002), Ozone production from Canadian wildfires during June and July of 1995, *J. Geophys. Res.*, 107(D14), 4192, doi:10.1029/2001JD000697, 2002.

- Meehl, G. A., et al. (2006), Climate change projections for the twenty-first century and climate change commitment in the CCSM3, *J. Clim.*, 19(11), 2597–2616.
- Méndez-Barroso, L. A., E. R. Vivoni, C. J. Watts, and J. C. Rodríguez (2009), Seasonal and interannual relations between precipitation, surface soil moisture and vegetation dynamics in the North American monsoon region, *J. Hydrol.*, 377, 59–70, doi:10.1016/j.jhydrol.2009.08.009.
- Mesinger, F., et al. (2006), North American Regional Reanalysis, *Bull. Amer. Meteorol. Soc.*, 87, 343–360.
- Mickley, L. J., D. J. Jacob, B. D. Field, and D. Rind (2004), Effects of future climate change on regional air pollution episodes in the United States, *Geophys. Res. Lett.*, 31, L24103, doi:10.1029/2004GL021216.
- Mlawer, E. J., S. J. Taubman, P. D. Brown, M. J. Iacono, and S. A. Clough (1997), Radiative transfer for inhomogeneous atmospheres: RRTM, a validated correlated-k model for the longwave, *J. Geophys. Res.*, 102(D14), 16,663–16,682.
- Mödders, N. and W. Rühnack (2002), On the impact of explicitly predicted runoff on the simulated atmospheric response to small-scale land-use changes-an integrated modeling approach, *Atmos. Res.*, 63, 3–38.
- Murazaki, K., and P. Hess (2006), How does climate change contribute to surface ozone change over the United States?, *J. Geophys. Res.*, 111, D05301, doi:10.1029/2005JD005873.
- Nakicenovic, N., et al. (2000), *IPCC Special Report on Emissions Scenarios*. Cambridge University Press, Cambridge, United Kingdom and New York, NY, USA. 599pp.
- Nam, J., Y. Kimura, W. Vizuete, C. Murphy C., and D. T. Allen (2006), Modeling the impacts of emission events on ozone formation in Houston, Texas, *Atmos. Environ.*, 40, 5329–5341.
- NASA (2007), MODIS 16-day Composite MOD44C, Collection 4, The Global Land Cover Facility, University of Maryland, College Park, Maryland.
- Ng, N. L., et al. (2006), Contribution of first- versus second-generation products to secondary organic aerosols formed in the oxidation of biogenic hydrocarbons, *Environ. Sci. & Tech.*, 40(7), 2283–2297, doi:10.1021/es052269u.
- Niu, G.-Y., Z.-L. Yang, R. E. Dickinson, and L. E. Gulden (2005), A simple TOPMODEL-based runoff parameterization (SIMTOP) for use in global climate models, *J. Geophys. Res.*, 110, D21106, doi:10.1029/2005JD006111.
- Niu, G.-Y., Z.-L. Yang, R. E. Dickinson, L. E. Gulden, and H. Su (2007), Development of a simple groundwater model for use in climate models and evaluation with

- Gravity Recovery and Climate Experiment data, *J. Geophys. Res.*, 112, D07103, doi:10.1029/2006JD007522.
- Notaro, M., S. Vavrus, and Z. Liu (2007), Global Vegetation and Climate Change due to Future Increases in CO<sub>2</sub> as Projected by a Fully Coupled Model with Dynamic Vegetation, *J. Clim.*, 20(1), 70–90.
- Odum, J. R., T. P. W. Jungkamp, R. J. Griffin, H. J. L. Forstner, R. C. Flagan, and J. H. Seinfeld (1997), Aromatics, reformulated gasoline, and atmospheric organic aerosol formation, *Environ. Sci. Technol.*, 31(7), 1890–1897.
- Offenberg, J. H., T. E. Kleindienst, M. Jaoui, M. Lewandowski, and E. O. Edney (2006), Thermal properties of secondary organic aerosols, *Geophys. Res. Lett.*, 33, L03816, doi:10.1029/2005GL024623.
- Ordóñez, C., H. Methis, M. Furger, S. Henne, C. Huglin, J. Staehelin, and A. S. H. Prevot (2005), Changes of daily surface ozone maxima in Switzerland in all seasons from 1992 to 2002 and discussion of summer 2003, *Atmos. Chem. Phys.*, 5, 1187–1203.
- Pal, J. S. and E. A. B. Eltahir (2001), Pathways Relating Soil Moisture Conditions to Future Summer Rainfall within a Model of the Land–Atmosphere System, *J. Clim.*, 14, 1227–1242.
- Pankow, J. F. (1994), An absorption model of gas/particle partitioning involved in the formation of secondary organic aerosol, *Atmos. Environ.*, 28, 189–193.
- Peñuelas, J., T. Rutishauher, and I. Filella (2009), Phenology feedbacks on climate change, *Science*, 327, 887–888, doi:10.1126/science.1173004.
- Pielke, R. A., Sr., G. E. Liston, J. L. Eastman, L. Lu, and M. Coughenour (1999), Seasonal weather prediction as an initial value problem, *J. Geophys. Res.*, 104(D16), 19,463–19,480.
- Prather, M., et al. (2003), Fresh air in the 21st century?, *Geophys. Res. Lett.*, 30(2), 1100, doi:10.1029/2002GL016285.
- Pun, B. and C. Seigneur, C. (2008), Organic aerosol spatial/temporal patterns: Perspective of measurements and model, *Environ. Sci. Technol.*, 42, 7287–7293.
- Putaud, J. P., et al (2004), A European aerosol phenomenology 2: chemical characteristics of particulate matter at kerbside, urban, rural and background sites in Europe, *Atmos. Environ.*, 38, 2579–2595.
- Pye, H. O. T., et al. (2009), Effect of changes in climate and emissions on future sulfate-nitrate-ammonium aerosol levels in the United States, *J. Geophys. Res.*, 114, D01205, doi:10.1029/2008JD010701.

- Racherla, P. N., and P. J. Adams (2006), Sensitivity of global tropospheric ozone and fine particulate matter concentrations to climate change, *J. Geophys. Res.*, 111, D24103, doi:10.1029/2005JD006939.
- Rao, S. T., J. Y. Ku, S. Berman, D. Zhang, and H. Mao (2003), Summertime characteristics of the atmospheric boundary layer and relationships to ozone levels over the eastern United States, *Pure Appl. Geophys.*, 160, 21–55.
- Roberts, G. C., M. O. Andreae, J. Zhou, and P. Artaxo (2001), Cloud condensation nuclei in the Amazon Basin: “Marine” conditions over a continent?, *Geophys. Res. Lett.*, 28(14), 2807–2810, 2001.
- Robinson, A. L., N. M. Donahue, M. K. Shrivastava, et al. (2007), Rethinking organic aerosols: Semivolatile emissions and photochemical aging, *Science*, 315, 1259–1262.
- Rodriguez-Iturbe, I., and A. Porporato (2004), *Ecohydrology of Water Controlled Ecosystems: Soil Moisture and Plant Dynamics*, Cambridge Univ. Press, New York, doi:10.2277/0521819431.
- Ropelewski, C. F., and E. S. Yarosh (1998), The observed mean annual cycle of moisture budgets over the central United States (1973–92), *J. Clim.*, 11, 2180 – 2190.
- Ruiz-Barradas, A. and S. Nigam (2006), Great Plains hydroclimate variability: the view from North American Regional Reanalysis, *J. Clim.*, 19, 3004–3010.
- Sakulyanontvittaya, T., A. Guenther, D. Helmig, J. Milford, and C. Wiedinmyer (2008), Secondary organic aerosol from sesquiterpene and monoterpene emissions in the United States, *Environ. Sci. Technol.*, 42 (23), 8784–8790.
- Schär, C., D. Lüthi, U. Beyerle, and E. Heise (1999), The soil–precipitation feedback: A process study with a regional climate model, *J. Clim.*, 12, 722–741.
- Schere, K. L. and R. A. Wayland (1989), EPA Regional Oxidant Model (ROM2.0): Evaluation on 1980 NEROS Data Bases, Report EPA – 600/3-89/057, Research Triangle Park, North Carolina.
- Seinfeld, J. H. and J. F. Pankow (2003), Organic atmospheric particulate material, *Ann. Rev. Phys. Chem.*, 54, 121–140.
- Seneviratne, S. I., D. Luethi, M. Litschi, and C. Schär (2006), Land–atmosphere coupling and climate change in Europe, *Nature*, 443, 205–209.
- Senna, M. C. A., M. H. Costa, and G. F. Pires (2009), Vegetation-atmosphere-soil nutrient feedbacks in the Amazon for different deforestation scenarios, *J. Geophys. Res.*, 114, D04104, doi:10.1029/2008JD010401.

- Seuffert, G., P. Gross, C. Simmer, and E. F. Wood (2002), The Influence of Hydrologic Modeling on the Predicted Local Weather: Two-Way Coupling of a Mesoscale Weather Prediction Model and a Land Surface Hydrologic Model, *J. Hydrometeorol.*, 3, 505–523.
- Sillman, S., and P. J. Samson (1995), Impact of temperature on oxidant photochemistry in urban, polluted rural and remote environments, *J. Geophys. Res.*, 100(D6), 11,497–11,508.
- Singh, H. B., et al. (1985), Relationship between peroxyacetyl nitrate and nitrogen oxides in the clean troposphere. *Nature*, 318, 346–349.
- Sitch S., et al (2003), Evaluation of ecosystem dynamics, plant geography and terrestrial carbon cycling in the LPJ dynamic global vegetation model, *Global Chang Biol.* 9: 161–185.
- Skamarock, W. C., J. B. Klemp, J. Dudhia, D. O. Gill, D. M. Barker, W. Wang, and J. D. Powers (2005), A description of the Advanced Research WRF version 2. Technical report, National Center for Atmospheric Research, TN-468+STR, 88p.
- Smirnov, A., B. N. Holben, T. F. Eck, O. Dubovik, and I. Slutsker (2000), Cloud-screening and quality control algorithms for the AERONET database, *Rem. Sens. Environ.*, 73, 337–349.
- Sotiropoulou, R. E. P., E. Tagaris, C. Pilinis and et al. (2004), The BOND project: Biogenic aerosols and air quality in Athens and Marseille greater areas, *J. Geophys. Res.*, 109, D05205, doi: 10.1029/2003JD003955.
- Steiner A. L., J. S. Pal, S.A. Rauscher, J.L. Bell, N.S. Diffenbaugh, L.C. Sloan, and F. Giorgi (2008), Land surface coupling in regional climate simulations of the West African monsoon, *Clim. Dyn. Obs. Theor. Comput. Res. Clim. Syst.* doi:10.1007/s00382-009-0543-6.
- Stockwell, W. R., P. Middleton, J. S. Chang, and X. Tang (1990), The second generation regional acid deposition model chemical mechanism for regional air quality modeling, *J. Geophys. Res.*, 95(D10), 16343–16367.
- Sud Y. C., W. C. Chao and Walker G. K. (1993), Dependence of rainfall on vegetation: theoretical considerations, simulation experiments, observations, and inferences from simulated atmospheric soundings, *J. Arid Environments*, 25, 5–18.
- Tagaris, E., et al. (2007), Impacts of global climate change and emissions on regional ozone and fine particulate matter concentrations over, *J. Geophys. Res.*, 112, D14312, doi:10.1029/2006JD008262.
- Taha, H. (1996), Modeling the impacts of increased urban vegetation on the ozone air

- quality in the South Coast Air Basin, *Atmos. Environ.*, 30 (20), 3423–3430.
- Taha, H., S. Konopacki, and H. Akbari (1998), Impacts of lowered urban air temperatures on precursor emission and ozone air quality, *J. Air Waste Manag. Assoc.*, 48, 860–865.
- Tao, Z. N., S. M. Larson, A. Williams, et al. (2004), Sensitivity of regional ozone concentrations to temporal distribution of emissions, *Atmos. Environ.*, 38(37), 6279–6285.
- Tao, Z., A. Williams, H.-C. Huang, M. Caughey, and X.-Z. Liang (2007), Sensitivity of U.S. surface ozone to future emissions and climate changes, *Geophys. Res. Lett.*, 34, L08811, doi:10.1029/2007GL029455.
- Theobald, D. (2005), Landscape patterns of exurban growth in the USA from 1980 to 2020, *Ecol. Soc.*, 10(1), 32.
- Thornton, P. E. and N. E. Zimmermann (2007), An improved canopy integration scheme for a land surface model with prognostic canopy structure, *J. Clim.*, 20, 3902–3923. doi: 10.1175/JCLI4222.1.
- Tie, X., G. Brasseur, L. Emmons, L. Horowitz, and D. Kinnison (2001), Effects of aerosols on tropospheric oxidants: A global model study, *J. Geophys. Res.*, 106(D19), 22,931–22,964.
- Tokairin, T., H. Kondo, H. Yoshikado, Y. Genchi, and T. Ihara (2006), Numerical study on the effect of buildings on temperature variation in urban and suburban areas in Tokyo, *J. Meteorol. Soc. Japan*, 84(5), 921–937.
- Tsigaridis, K., and M. Kanakidou (2003), Global modelling of secondary organic aerosol in the troposphere: A sensitivity analysis, *Atmos. Chem. Phys.*, 3, 1849–1869.
- Tsigaridis, K., J. Lathiere, M. Kanakidou, and D. A. Hauglustaine (2005), Naturally driven variability in the global secondary organic aerosol over a decade, *Atmos. Chem. Phys. Discuss.*, 5, 1255–1283.
- Tsigaridis, K. and M. Kanakidou (2007), Secondary organic aerosol importance in the future atmosphere, *Atmos. Environ.*, 41, 4682–4692.
- van den Hurk, Bart J. J. M., and Erik van Meijgaard (2010), Diagnosing land–atmosphere interaction from a regional climate model simulation over West Africa, *J. Hydrometeorol.*, 11, 467–481. doi: 10.1175/2009JHM1173.1.
- Volkamer, R., et al. (2006), Secondary organic aerosol formation from anthropogenic air pollution: Rapid and higher than expected, *Geophys. Res. Lett.*, 33, L17811, doi:10.1029/2006GL026899.
- Volkamer, R., P. J. Ziemann, and M. J. Molina (2009), Secondary Organic Aerosol

- Formation from Acetylene (C<sub>2</sub>H<sub>2</sub>): seed effect on SOA yields due to organic photochemistry in the aerosol aqueous phase, *Atmos. Chem. Phys.*, 9, 1907–1928.
- Vukovich, J. and T. Pierce (2002), The Implementation of BEIS3 within the SMOKE modeling framework. Proc. 11th International Emission Inventory Conference: Emission Inventories - Partnering for the Future, Atlanta, GA, US EPA, CD-ROM, 10.7 .
- Wallace, J. M., E. M. Rasmusson, T. P. Mitchell, V. E. Kousky, E. S. Sarachik, and H. von Storch (1998), On the structure and evolution of ENSO-related climate variability in the tropical Pacific: Lessons from TOGA, *J. Geophys. Res.*, 103(C7), 14,241–14,259.
- Wang, W., B. T. Anderson, D. Entekhabi, D. Huang, R. K. Kaufmann, C. Potter, and R. B. Myneni, 2006, Feedbacks of vegetation on summertime climate variability over the North American grasslands. Part II: A Coupled Stochastic Model, *Earth Interact.*, 10, 1–30.
- Wang, W., B. T. Anderson, N. Phillips, R. K. Kaufmann, C. Potter, and R. B. Myneni (2006), Feedbacks of vegetation on summertime climate variability over the North American grasslands. Part I: Statistical Analysis, *Earth Interact.*, 10, 1 – 27.
- Wang, X. M., W. S. Lin, L. M. Yang, R. R. Deng, and H. Lin (2007), A numerical study of influences of urban land-use change on ozone distribution over the Pearl River Delta region, China, *Tellus B*, 59 (3), 633–641.
- Wei, J., P. A. Dirmeyer, Z. Guo, L. Zhang, and V. Misra (2010), How much do Different land models matter for climate simulation? Part I: climatology and variability, *J. Clim.*, 23, 3120–3134. doi: 10.1175/2010JCLI3177.1.
- Weng, Q., S. H. Yang, et al. (2006), Urban air pollution patterns, land use, and thermal landscape: An examination of the linkage using GIS, *Environ. Monit. Assess.*, 117(1–3), 463–489.
- Wert, B. P., et al. (2003), Signatures of terminal alkene oxidation in airborne formaldehyde measurements during TexAQS 2000, *J. Geophys. Res.*, 108(D3), 4104, doi:10.1029/2002JD002502.
- Wesley, M. L. (1989), Parameterization of surface resistance to gaseous dry deposition in regional numerical models, *Atmos. Environ.*, 16, 1293–1304.
- Wiedinmyer, C., X. X. Tie, A. Guenther, R. Neilson, and C. Granier (2006), Future changes in biogenic isoprene emissions: How might they affect regional and global atmospheric chemistry?, *Earth Intert.*, 10(3), 1–19.
- Wigley, T. M. L., S. J. Smith, and M. J. Prather (2002), Radiative forcing due to reactive gas emissions, *J. Clim.*, 15(18), 2690–2696.



- Wild, O., X. Zhu, and M. J. Prather (2000), Fast-J: Accurate simulation of in- and below-cloud photolysis in tropospheric chemical models, *J. Atmos. Chem.*, 37, 245–282.
- Wilkinson, M.J., R. K. Monson, N. Trahan, S. Lee., E. Brown, R. B. Jackson, H.W. Polley, P. Fay, and R. Fall (2009), Leaf isoprene emission rate as a function of atmospheric CO<sub>2</sub> concentration, *Glob. Cha. Bio.*, 15, 1189–1200.
- Williams, E. J., A. Guenther, and F. C. Fehsenfeld (1992), An inventory of nitric oxide emissions from solids in the United States, *J. Geophys. Res.*, 97(D7), 7511–7519.
- Wu, S., L. J. Mickley, E. M. Leibensperger, D. J. Jacob, D. Rind, and D. G. Streets (2008), Effects of 2000–2050 global change on ozone air quality in the United States, *J. Geophys. Res.*, 113, D06302, doi:10.1029/2007JD008917.
- Xue, Y., F. De Sales, W. Li, C. R. Mechoso, C. Nobre, and H.-M. H. Juang (2006), Role of land surface processes in South American monsoon development, *J. Clim.*, 19, 741–762.
- Yang, Z.-L., R. E. Dickinson, A. Henderson-Sellers, and A. J. Pitman (1995), Preliminary study of spin-up processes in land surface models with the first stage data of Project for Intercomparison of Land Surface Parameterization Schemes Phase 1(a), *J. Geophys. Res.*, 100(D8), 16,553–16,578.
- Yang, Z.-L. and G.-Y. Niu (2003), The Versatile Integrator of Surface and Atmosphere Processes (VISA). Part 1: model description, global and planetary change, 38, 175–189.
- Yeh, P. J.-F., and E. A. B. Eltahir (2005), Representation of water table dynamics in a land-surface scheme. Part I: Model development, *J. Clim.*, 18, 1861–1880.
- York, J. P., M. Person, W. J. Gutowski, et al. (2002), Putting aquifers into atmospheric simulation models: An example from the Mill Creek Watershed, northeastern Kansas, *Adv. Water Resour.*, 25(2), 221–238.
- Yuan, X., Z. Xie, J. Zheng, X. Tian, and Z. Yang (2008), Effects of water table dynamics on regional climate: A case study over east Asian monsoon area, *J. Geophys. Res.*, 113, D21112, doi:10.1029/2008JD010180.
- Zaveri, R. A., and L. K. Peters (1999), A new lumped structure photochemical mechanism for large-scale applications, *J. Geophys. Res.*, 104, 30387–30415.
- Zaveri, R. A., R. C. Easter, J. D. Fast, and L. K. Peters (2008), Model for Simulating Aerosol Interactions and Chemistry (MOSAIC), *J. Geophys. Res.*, 113, D13204, doi:10.1029/2007JD008782.
- Zhang, F., N. Bei, J. W. Nielsen-Gammon, G. Li, R. Zhang, A. Stuart, and A. Aksoy

- (2007), Impacts of meteorological uncertainties on ozone pollution predictability estimated through meteorological and photochemical ensemble forecasts, *J. Geophys. Res.*, 112, D04304, doi:10.1029/2006JD007429.
- Zhang, Y., J.-P. Huang, D. K. Henze, and J. H. Seinfeld (2007), Role of isoprene in secondary organic aerosol formation on a regional scale, *J. Geophys. Res.*, 112, D20207, doi:10.1029/2007JD008675.
- Zhang, Y., X.-M. Hu, L. R. Leung, and W. I. Gustafson Jr. (2008), Impacts of regional climate change on biogenic emissions and air quality, *J. Geophys. Res.*, 113, D18310, doi:10.1029/2008JD009965.

## **Vita**

Xiaoyan Jiang was born in Changzhou, Jiangsu, China. She earned her bachelor's and master's degrees at Nanjing University, Nanjing, China, in 2001 and 2004 respectively. Before she entered the Graduate School at the University of Texas at Austin in 2006, she worked as a research assistant in an urban meteorological institute in Beijing, China.

Permanent Address: No. 12 Jinfeng Cun, Hengshan Qiao Town,

Changzhou, Jiangsu, China, 213119

This report was typed by author.